



ADAPTIVE ILLUMINATION PATTERNS
FOR RADAR APPLICATIONS

DISSERTATION

Phillip M. Corbell, Captain, USAF

AFIT/DS/ENG/06-02

DEPARTMENT OF THE AIR FORCE
AIR UNIVERSITY

AIR FORCE INSTITUTE OF TECHNOLOGY

Wright-Patterson Air Force Base, Ohio

APPROVED FOR PUBLIC RELEASE; DISTRIBUTION UNLIMITED.

The views expressed in this dissertation are those of the author and do not reflect the official policy or position of the United States Air Force, Department of Defense, or the United States Government.

ADAPTIVE ILLUMINATION PATTERNS
FOR RADAR APPLICATIONS

DISSERTATION

Presented to the Faculty
Department of Electrical and Computer Engineering
Graduate School of Engineering and Management
Air Force Institute of Technology
Air University
Air Education and Training Command
In Partial Fulfillment of the Requirements for the
Degree of Doctor of Philosophy

Phillip M. Corbell, B.S.E.E., M.S.E.E.
Captain, USAF

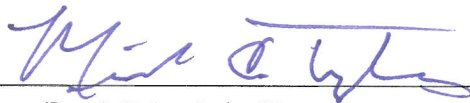
March 2006

ADAPTIVE ILLUMINATION PATTERNS
FOR RADAR APPLICATIONS

Phillip M. Corbell, B.S.E.E., M.S.E.E.

Captain, USAF

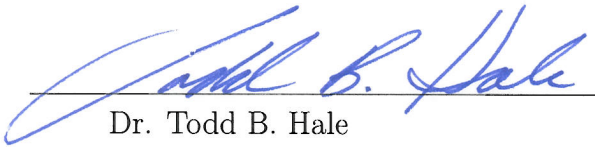
Approved:



Dr. Michael A. Temple
Dissertation Advisor

15 Mar 06

date



Dr. Todd B. Hale
Committee Member

15 MAR 06

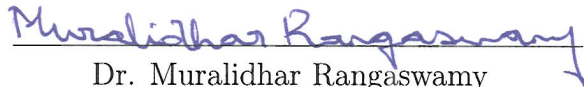
date



Dr. William P. Baker
Committee Member

15 Mar 06

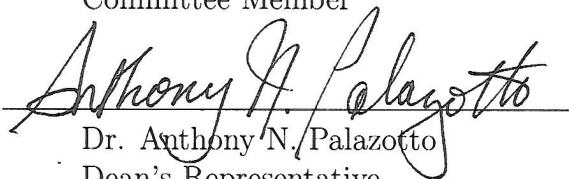
date



Dr. Muralidhar Rangaswamy
Committee Member

15 Mar 06

date



Dr. Anthony N. Palazotto
Dean's Representative

15 Mar 06

date

Accepted:



Marlin U. Thomas
Dean, Graduate School of Engineering and Management

17 Mar 06

Date

Abstract

Adaptive transmit architectures are envisioned as dominating the radar research of the next century, and are key components of the Fully Adaptive Radar (FAR) paradigm. The fundamental FAR goal involves full exploitation of the joint, synergistic adaptivity of the radar's transmitter and receiver. While phased array *receive processing* techniques jointly adapt over spatial and temporal Degrees-of-Freedom (DOF), little work has been done to exploit the same DOF available during the radar's *transmit illumination* cycle. This research introduces Adaptive Illumination Patterns (AIP) as a means for exploiting the previously untapped transmit DOF made available by modern Active Electronically Steered Arrays (AESAs).

A fundamental challenge to effective airborne radar surveillance lies in suppressing signal dependent interference, i.e., clutter responses which are inherently created and shaped by the illumination pattern. This research investigates ways to mitigate clutter interference effects by adapting the illumination pattern on transmit. Two types of illumination pattern adaptivity were explored. Space time "beamforming" on *transmit* has been demonstrated by allowing the antenna illumination pattern (spatial filter) to vary on a pulse-by-pulse (temporal) basis, a technique described as Space Time Illumination Patterns (STIP). Using clairvoyant knowledge, STIP demonstrates the ability to remove sidelobe clutter at user specified Doppler frequencies, resulting in optimum receiver performance using a *non-adaptive* receive processor. A customized partially adaptive STAP receive processor is shown to add robustness to the process while requiring only a fraction of the training data required under standard illumination conditions. Spatial-only adaptivity was also explored using a planar transmit array in a close-in sensing application. In this case, the ability to reduce training data heterogeneity was demonstrated in dense target environments, thereby greatly improving the minimum discernable velocity achieved through STAP processing.

Acknowledgements

“In all your ways acknowledge him, and he will make your paths straight.”

Proverbs 3:6

First and foremost, and with great joy I give thanks and praise to my Creator, Lord, and Savior Jesus Christ, from whom comes all wisdom, knowledge, and abundant grace. As the ultimate provider in my life, he has blessed me deeply through my beautiful bride, whose love, respect, and unending support has sustained me throughout this rigorous process. The journey was not easy, but we fought and conquered it *together*, and what I treasure most was having you by my side the whole way. This degree’s value is measured more by your abundant, willing sacrifices than by my efforts, and I dedicate it to you. To my kiddos, I can’t express the joy you brought to my heart throughout this long endeavor. I hope to spend my days catching up on “daddy time” and trying to enrich your lives as much as you have enriched mine. I also wish to thank my parents for their unconditional love and support. The skills that greatly contributed to the success of this process—hard work, tenacity, integrity, and perseverance—I learned from you.

I am also indebted to *many* at AFIT who have done so much to grow me, pray for me, and educate me throughout my time(s) here. I especially want to thank my advisor, Dr. Temple, for shepherding me through this process with his keen wit, positive attitude, superb advice and comprehensive technical prowess. Many thanks also goes to my research committee for their support and feedback. Thank you, Maj. Hale, for introducing me to radar, providing a solid STAP foundation, and for your thorough, thoughtful feedback. I am also very grateful for the encouragement, extensive knowledge, and support of my research sponsor, Dr. Muralidhar Rangaswamy. Finally, I want to thank those who believed in me and encouraged my return to AFIT for a PhD. I am extremely grateful for the instruction of many fine professors over the years, whom I hope to honor by applying their teachings throughout my career.

Phillip M. Corbell

Table of Contents

	Page
Abstract	iv
Acknowledgements	v
List of Figures	ix
List of Tables	xi
List of Symbols	xii
List of Abbreviations	xv
I. Introduction	1
1.1 Adaptive Radar Fundamentals	1
1.2 Interference Suppression: Methods and Challenges	3
1.2.1 Space Time Adaptive Processing (STAP)	4
1.2.2 Training Data Deficiencies	5
1.3 Recent Adaptive Radar Research Thrusts	7
1.3.1 Knowledge-Aided STAP	7
1.3.2 Fully Adaptive Radar (FAR)	8
1.4 New Idea: Adaptive Illumination Patterns	10
1.4.1 Space Time Illumination Patterns	12
1.4.2 Scene Adaptive Illumination Patterns	13
1.4.3 Approach and Methodology	15
1.5 Contributions and Document Overview	16
II. Adaptive Illumination Patterns for Planar Array Radar	21
2.1 Target Response Model	23
2.1.1 Radar Signal Model	23
2.1.2 Transmit Antenna Model	24
2.1.3 Transmitted Signal	25
2.1.4 Reflected Signal	25
2.1.5 Received Signal	26
2.1.6 Received Voltage Model	27
2.1.7 Spatial Frequency Modeling	28
2.1.8 Received Signal at Baseband	28
2.2 Matched Filtering	29

	Page
2.3 Amplitude Validation	32
2.4 Data Formatting	33
2.4.1 Incorporating TIPD	34
2.5 TIPD Target Space Time Snapshot	35
2.6 Modeling Antenna Subarrays	35
2.7 Clutter Response Model	40
2.7.1 TIPD Clutter Space Time Snapshot	40
2.7.2 TIPD Clutter Covariance	43
2.8 Simulation of Clutter Voltage Models	44
2.8.1 Incorporating Other Statistical and Deterministic Clutter Models	45
2.8.2 Validity Of Covariance Model For An Arbitrary Clutter Reflectivity Function	47
2.9 Training Data Modeling	50
2.10 Modeling Subarrays in the Clutter Model	51
2.11 Noise Model	52
2.12 Summary	53
III. Overview of STAP Processors	55
3.1 STAP Framework	55
3.2 Non-Adaptive Signal Match (SM) Processor	56
3.3 Fully Adaptive Processors	57
3.3.1 Optimal Matched Filter (MF) Processor	57
3.3.2 Adaptive Matched Filter (AMF) Processor	59
3.4 Partially Adaptive Processors	61
3.4.1 Factored Space Time (FST) Processor	61
3.5 STAP Performance Metrics	63
3.5.1 Output SINR	63
3.5.2 SINR Loss	63
3.6 Summary	64
IV. Space Time Illumination Patterns (STIP)	65
4.1 Motivation for STIP	65
4.1.1 A Deeper Look At Space-Time Processing	66
4.1.2 STAP Weights, AESA Weights, and Array Factors	68
4.1.3 Space-Time Filtering With <i>Real</i> Array Factors	75
4.2 Defining STIP	76
4.2.1 Standard Illumination Patterns (SIP)	77
4.2.2 Space-Time Illumination Patterns (STIP)	78
4.3 STIP vs. STAP: Understanding Differences	80

	Page
4.4 Illumination Pattern Synthesis	82
4.4.1 Pattern Synthesis: Optimum STAP MF Weights	83
4.4.2 Pattern Synthesis: Using Previous CPI Data	85
4.4.3 Pattern Synthesis: Knowledge-Aided Processing	87
4.5 Fully Adaptive Radar: Joint STIP-STAP Operation	89
4.5.1 FAR: Baseline Results for Joint STIP-STAP Processing	89
4.5.2 Clutter Covariance Eigenvalue Analysis	95
4.5.3 SINR Results	96
4.5.4 Transmit Power Assumptions	97
4.5.5 Factored Space Time (FST) Processing Under STIP	99
4.5.6 Multi-constraint weight vector synthesis	102
4.6 Summary	108
V. Scene Adaptive Illumination Patterns (SAIP)	110
5.1 Introduction	110
5.2 Site-Specific Adaptive Illumination	112
5.3 Site Specific Target Modeling	114
5.4 STAP Considerations for Planar Array Close-in Sensing	118
5.5 Adaptive Illumination Pattern Synthesis	122
5.6 Simulation Results	125
5.7 Summary	130
VI. Conclusions	131
6.1 Adaptive Illumination Patterns	131
6.1.1 Space Time Illumination Patterns (STIP)	132
6.1.2 Scene Adaptive Illumination Patterns (SAIP)	133
6.2 Research Contribution Summary	135
6.3 Future Research	138
6.3.1 Radar Modeling Research	138
6.3.2 Space Time Illumination Patterns	138
6.3.3 Scene Adaptive Illumination Patterns	139
6.4 Closing Thoughts	139
Bibliography	141

List of Figures

Figure		Page
1.1.	Graphic Illustration of the Airborne GMTI detection problem .	2
1.2.	Targets and Clutter projected into the azimuth-Doppler space .	2
1.3.	Research organization and technical contribution areas	17
2.1.	Phased array coordinate system and geometry	22
2.2.	Airborne array geometry for the planar array clutter model. .	41
4.1.	Minimum Variance (MV) spectrum of airborne clutter using SIP	66
4.2.	Azimuth-Doppler response of an optimum MF, $M = 4$	67
4.3.	Example Phaser diagram	69
4.4.	Phaser diagram of optimum MF weights $M = 4$	69
4.5.	Uniform weights array factor magnitude response	70
4.6.	Uniform weights array factor in cartesian coordinates	70
4.7.	Optimum MF array factor magnitude responses $M = 4$	71
4.8.	Optimum MF array factor phase response $M = 4$	72
4.9.	Uniform weights array factor phase response	73
4.10.	Optimum MF array factor magnitude and phase azimuth patterns	74
4.11.	Phaser diagram of uniform SIP weights	78
4.12.	Uniform weights array factor magnitude and phase azimuth cuts	79
4.13.	STIP weight synthesis procedure using optimal MF weights . .	84
4.14.	Azimuth-Doppler response of SIP transmit weights.	91
4.15.	Clutter PSD resulting from SIP transmit weights	91
4.16.	Azimuth-Doppler response of an optimum MF, $M = 10$	91
4.17.	Phaser Diagram of optimum MF weights $M = 10$	92
4.18.	Optimum MF array factor magnitude and phase plots $M = 10$	92
4.19.	Phaser Diagram of STIP weights	93
4.20.	STIP weights array factor magnitude and phase cuts	93

Figure		Page
4.21.	Azimuth-Doppler response of STIP weights	94
4.22.	Clutter PSD resulting from STIP transmit weights	94
4.23.	Azimuth-Doppler response of MF under STIP/AIP	95
4.24.	Clutter Eigenvalue analysis comparing SIP and AIP results . .	96
4.25.	MF and SM Output SINR results under SIP and AIP conditions	97
4.26.	Weight magnitude plot given different normalization assumptions	99
4.27.	Output SINR results under maximum element power assumption	100
4.28.	MF, SM, and FST Output SINR Results under SIP and AIP .	101
4.29.	Artificially synthesized clutter interference MV PSD	103
4.30.	Phaser Diagram of STIP weights using synthesized constraints	104
4.31.	Array factor magnitude and phase responses of Fig. 4.30 weights	104
4.32.	Azimuth-Doppler response of STIP weights in Fig. 4.30	105
4.33.	Clutter PSD resulting from STIP weights in Fig. 4.30	105
4.34.	MF, SM, and FST Output SINR results over wider Doppler span	105
4.35.	Output SINR results assuming maximum element power	106
5.1.	Map of site-specific simulated roads and targets	115
5.2.	Simulated targets projected into the azimuth-Doppler domain .	117
5.3.	Simulated targets projected into the range-Doppler domain . .	117
5.4.	Histogram of simulated targets per range bin	118
5.5.	Constraint map used to synthesize adaptive illumination patterns	124
5.6.	Projection of SIP onto the radar scene with target overlay . . .	126
5.7.	Projection of SAIP onto the radar scene with target overlay . .	126
5.8.	GIP test applied to TD under SIP and SAIP with and without TTD	128
5.9.	MF and AMF SINR Loss comparison under SI and AI	129
6.1.	Summary of research structure and technical contribution areas	136

List of Tables

Table		Page
4.1.	Simulation parameters for STIP illustration.	90
5.1.	Radar simulation parameters.	116

List of Symbols

Symbol		Page
M	Number of pulses in a CPI	23
a_s	Peak transmit voltage	23
ω_0	Carrier frequency	23
γ	Arbitrary starting phase	23
T_r	Pulse Repetition Interval (PRI)	23
T_p	Pulse Width	23
$F_m(\theta, \phi)$	Far-field array (voltage) response of the m^{th} pulse	24
θ	Elevation angle	24
ϕ	Azimuth angle	24
$W_m(\theta, \phi)$	complex array factor used to transmit the m^{th} pulse	24
$f(\theta, \phi)$	complex voltage pattern factor	24
$\mathcal{W}(\theta, \phi, t)$	Time dependent array factor magnitude	24
$\zeta(\theta, \phi, t)$	Time dependent array factor phase	24
σ_{tgt}	Target radar Cross-Section (RCS)	25
ω_{tgt}	Target Doppler frequency	25
ψ_{tgt}	Target's random phase response	25
R_{tgt}	Target range relative to reference element	25
τ_{np}	Total target to (n^{th}, p^{th}) element propagation time	26
τ'_{np}	relative TOA from the (n^{th}, p^{th}) and $(0, 0)$ array elements	26
d_x	Horizontal array spacing between elements	28
d_z	Vertical array spacing between elements	28
$\vartheta_x(\theta, \phi)$	Horizontal spatial frequency	28
$\vartheta_z(\theta)$	Vertical spatial frequency	28
$\bar{\omega}_{\text{tgt}}$	Normalized target Doppler	31
ψ	Composite random phase term	31

Symbol		Page
ξ_m	SNR of the m^{th} received pulse	32
α_{tgt}	Final complex target amplitude	32
$\mathbf{a}[\vartheta_x(\theta, \phi)]$	Horizontal spatial steering vector	33
N	Horizontal array elements	33
$\mathbf{e}[\vartheta_z(\theta)]$	Vertical spatial steering vector	33
P	Vertical array elements	33
$\mathbf{b}(\bar{\omega}_{\text{tgt}})$	Doppler steering vector	34
$\mathbf{x}_{\text{vaf}}(\theta, \phi)$	$M \times 1$ Complex Transmit Array Factor For All M Pulses	34
$\mathbf{w}_{\text{TX}m}$	m^{th} Pulse $N \times 1$ Transmit Weight Vector	34
$\tilde{\mathbf{b}}(\theta, \phi, \bar{\omega}_{\text{tgt}})$	TIPD modified Doppler steering vector	35
χ_t	Target space time snapshot	35
$\tilde{\mathbf{v}}_{\text{tgt}}$	TIPD target space-time steering vector	35
N_r	Number of clutter rings	40
N_c	Number of clutter patches	40
ψ_{ik}	Received Pulse Train Random Phase	41
a_{ik}	Received Pulse Train Amplitude	41
h_a	Aircraft Altitude Above Ground Level	42
a_e	Effective Radius of the Earth	42
R_h	Range to the Horizon	42
R_u	Unambiguous range	42
T_r	Pulse Repetition Interval	42
v_a	Aircraft Velocity	42
ϕ_{crab}	Crab Angle	42
ξ_{ik}	Single (Tx/Rx) Element, Single Pulse Clutter-to-Noise Ratio	43
P_t	Transmit Power	43
$g_{\text{tx}}(\theta_i, \phi_k)$	Transmit Element Power Pattern	43
$g_{\text{rx}}(\theta_i, \phi_k)$	Receive Element Power Pattern	43
λ_0	Signal Wavelength	43

Symbol		Page
σ_{ik}	Radar Cross Section	43
N_0	Thermal Noise Power	44
B	System Bandwidth	44
N_{sub}	Receive Subarray Columns	44
P_{sub}	Receive Subarray Rows	44
L_s	System Losses	44
R_i	Range to the i^{th} range ring	44
\mathbf{R}	Signal-Dependent Clairvoyant Covariance Matrix	52

List of Abbreviations

Abbreviation		Page
ABL	AirBorne Laser	10
AESA	Active Electronic Scanned Array	8
AGL	Above Ground Level	42
AIP	Adaptive Illumination Patterns	11
AMF	Adaptive Matched Filter	59
AMTI	Airborne Moving Target Indication	131
ATX	Adaptive Transmit	83
CFAR	Constant FALSE Alarm Rate	57
CNR	Clutter-to-Noise Power Ratio	43
CPI	Coherent Processing Interval	7
DARPA	Defense Advanced Research Projects Agency	4
dBsm	dB square meters	123
DOF	Degrees-of-Freedom	4
DPCA	Displaced Phase Center Antenna	3
FAR	Fully Adaptive Radar	9
FST	Factored Space Time	61
FTS	Factored Time Space	61
GIP	Generalized Inner Product	125
GMTI	Ground Moving Target Indication	1
ICM	Internal Clutter Motion	88
KASSPER	Knowledge Aided Sensor Signal Processing and Expert Reasoning	7
KA-STAP	Knowledge-Aided STAP	14
MCARM	Multi-Channel Airborne Radar Measurements	15
MDV	Minimum Discernable Velocity	5

Abbreviation		Page
MF	Matched Filter	58
MIMO	Multiple-In Multiple-Out	9
NHD	Non-Homogeneity Detectors	5
PRF	Pulse Repetition Frequency	11
PRI	Pulse Repetition Interval	23
R/H	Range-to-Height Ratio	51
RMB	Reed Mallet and Brennan Rule	4
SAIP	Scene Adaptive Illumination Patterns	12
SAR	Synthetic Aperture Radar	1
SINR	Signal to Interference-Plus-Noise Ratio	19
SIP	Standard Illumination Patterns	77
SM	Signal Match	57
SMI	Sample Matrix Inversion	4
SNR	Signal-to-Noise Ratio	32
STAP	Space Time Adaptive Processing	3
STIP	Space Time Illumination Patterns	12
STX	Standard Transmit	77
TD	Training Data	4
TIPD	Transmit Interpulse Pattern Diversity	18
TTD	Targets in the Training Data	14

ADAPTIVE ILLUMINATION PATTERNS FOR RADAR APPLICATIONS

I. Introduction

Since its inception, Radio Detection And Ranging (RADAR) continues to play a prominent role in remote sensing applications given its unique ability to effectively detect objects day or night, at long ranges, and in adverse weather conditions (haze, fog, rain, snow, etc.) [90]. Airborne radar systems mobilize these critical capabilities to wherever the battlefield exists, providing critical situational awareness to the warfighter. Unfortunately, the task of detecting ground targets from a moving airborne platform is intrinsically difficult. The composite *ground* reflections are typically stronger than the ground *target* reflections and thus targets of interest are easily obscured by the surrounding terrain.

1.1 Adaptive Radar Fundamentals

For stationary ground targets, detection and/or identification is often accomplished using Synthetic Aperture Radar (SAR) techniques which involve synthesizing images from a collection of sequential radar returns. Stationary ground targets are not the main focus of this research and thus they are not examined beyond this point. If the target is moving, the radar can rely on Doppler filtering to separate the small moving target return from the larger clutter return. This radar function is typically classified as providing a Ground Moving Target Indication (GMTI) which is (generically) encompassed within the scope of this research. The GMTI problem is not easily solved. A typical GMTI scenario is depicted in Fig. 1.1. Airborne platform motion effectively spreads ground reflections collected through antenna sidelobes (represented by the yellow ovals in Fig. 1.1) across a wide band of Doppler frequencies, often rendering simple Doppler detection schemes ineffective. Figure 1.2 provides a notional example of this problem in the azimuth-Doppler domain, depicting the clutter re-

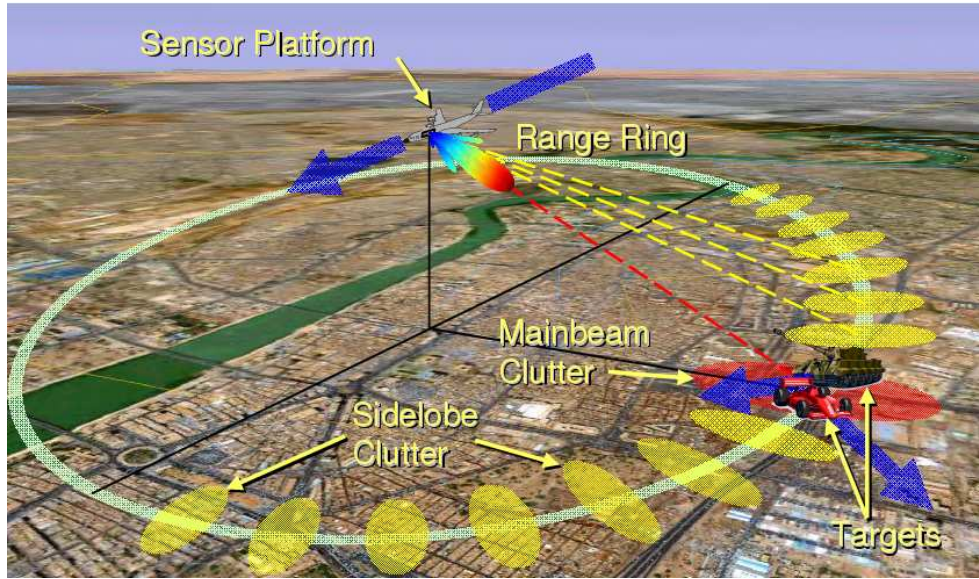


Figure 1.1: Graphic illustration of the airborne GMTI detection problem.

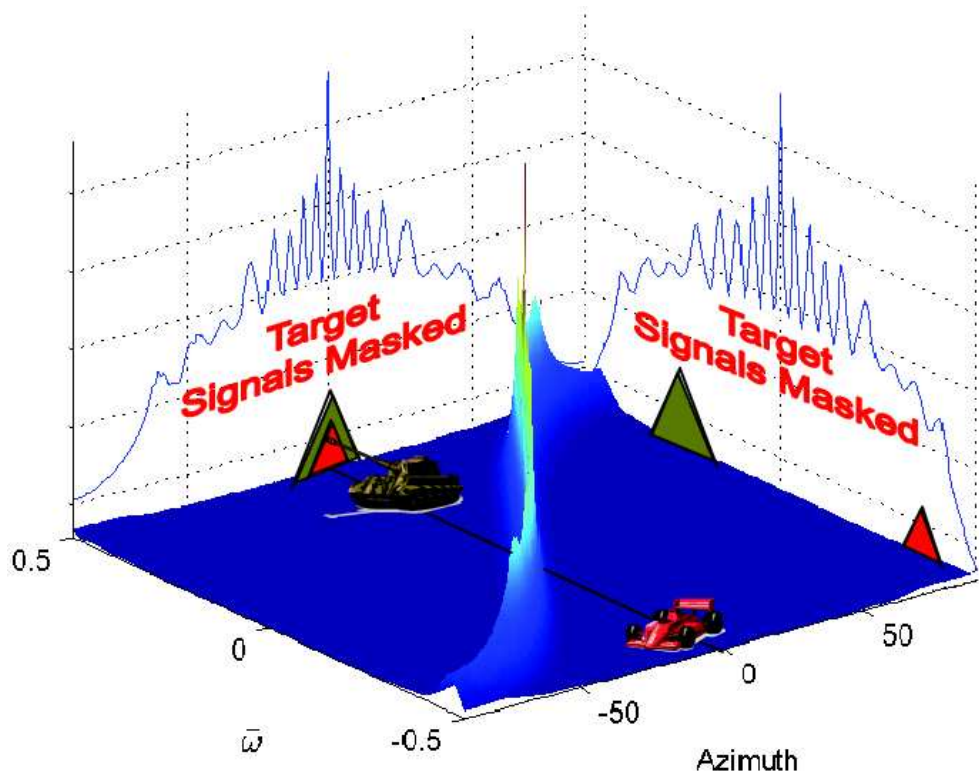


Figure 1.2: Graphic illustration of the targets and minimum variance clutter spectrum projected into the azimuth-Doppler space. The platform motion spreads the sidelobe clutter across Doppler, impeding target detection via Doppler filtering.

turns as a “wall” of interference which cuts across both space (azimuth) and time (Doppler) and masks the target signals. Adaptive radar [18] was largely invented to help address this problem. This research capitalizes on technological advancements to improve adaptive radar performance by adapting, diversifying, and generally exploiting a largely under-utilized resource: the transmit antenna pattern.

1.2 Interference Suppression: Methods and Challenges

The problem of mitigating airborne signal induced interference (clutter) has been extensively studied within the radar community. Most modern and classical interference mitigation techniques can usually be categorized as either Space Time Adaptive Processing (STAP) [43, 62, 63, 71, 81] or some form of Displaced Phase Center Antennas (DPCA) technique [43, 62, 94]. While there are some adaptive radar processing concepts and architectures suggested in the literature which don’t categorize neatly into either STAP or DPCA, an overview of the dominate techniques provides the necessary background upon which the contributions made in this research can be understood.

A thorough treatment of the most popular adaptive radar techniques can be found in [43, 62, 63], the details of which are not repeated here. Rather, a short summary of remaining challenges for current state-of-the-art adaptive interference suppression is instructive to provide a better understanding of research contributions. Furthermore, it is important to point out the distinction between signal-dependent interference, such as clutter returns due to radar transmission, and signal-independent interference, such as the interference caused by external radiation sources. The distinction between signal-dependent and signal-independent interference is important in the context of this research given the focus here is on modifying the transmit pattern illumination. Thus, the results presented herein only address, categorically, the problem of mitigating signal-dependent interference. However, this should not be viewed as a weakness given the techniques developed in no way hinder the ability of existing jammer mitigation methods. These methods, such as traditional STAP,

are easily augmented to incorporate the proposed architecture to provide overall improved radar performance. Thus, a fundamental understanding of traditional STAP is useful, to fully understand the synergistic relationships to be explained herein.

1.2.1 Space Time Adaptive Processing (STAP). Theoretical STAP-based GMTI radar performance is ultimately thwarted by the inability to have clairvoyant (perfect *a priori*) knowledge of the interference statistics. Given clairvoyance is not possible in practical applications, interference statistics are typically (historically) estimated from sampled radar data. The seminal paper by Reed, Mallet and Brennan (RMB) [86] in 1974 introduced a robust Sample Matrix Inversion (SMI) technique for estimating the interference covariance matrix from radar data collected from adjacent range bins. The data contained in the adjacent range bins is commonly referred to as Training Data (TD). The work in [86] also provides an important and commonly cited “RMB Rule” for SMI that relates, as a function of the STAP Degrees-of-Freedom (DOF), the average STAP performance to the number of independent and identically distributed (i.i.d.) target-free clutter samples (taken from adjacent range bins) used in forming the interference estimate. More often than not, the key assumption upon which SMI STAP is based (i.e., i.i.d. training data) is also the most questioned assumption in practice.

For example, consider Defense Advanced Research Projects Agency’s (DARPA) Mountain Top Radar [97], which can support the collection of 16 pulses through 14 receive antenna channels. In this case, STAP requires the estimation of a 224×224 covariance matrix and the RMB Rule estimates 448 range gates of training data are required to get within 3.0 dB of optimum performance. Since the instantaneous RF bandwidth of the Mountain Top Radar is only 200 kHz, the required 448 range gates span 672 km. This example highlights the fundamental challenge of full-DOF STAP processing, i.e., the need to obtain a sufficient *quantity of quality* training data. These two factors dictate how reliably the interference statistics can be estimated.

Getting good estimates of the interference statistics is crucial for STAP performance. With the exception of probability of detection and probability of false alarm, Minimum Discernable Velocity (MDV) is perhaps the most important performance parameter in a GMTI radar. Generally speaking, for STAP-GMTI radars the larger the Doppler frequency difference between the target and mainbeam clutter the easier it is to detect the target. Further, a lower MDV (target detection near the mainbeam clutter) results from lowering the bandwidth of the mainbeam clutter, which can be achieved through “higher” temporal and spatial DOF at the cost of increasing training data quantity (according to the RMB Rule [86]). Thus, from a practical perspective achieving a low MDV requires training data to be i.i.d. over a large range extent. Unfortunately, operating environments of interest are rarely i.i.d. (homogeneous) [70]. The reality of heterogeneous clutter returns makes STAP-based GMTI inherently difficult. Further, as the training data becomes less and less i.i.d., the resulting performance degradation (usually a result of over- or under-nulling the clutter) typically appears first near the mainbeam clutter Doppler frequency which directly impacts the radar’s MDV. Thus, mitigating heterogeneous clutter effects is one key to effectively lowering the MDV.

1.2.2 Training Data Deficiencies. For good reason, the vast majority of practical STAP research has focused on how to do more with less, i.e., how to derive the best performance possible from limited quantities of mediocre-quality training data. For example, to deal with the lack of TD quantity, much research has focused on partially adaptive STAP methods which reduce the TD required by reducing the adaptive DOF [43,62,63]. While this can sometimes improve overall TD homogeneity by reducing training range extent (e.g., in scenarios with range/elevation varying statistics), just reducing the training data extent does not directly address the issue of training data quality (homogeneity). Some researchers have reported improved STAP performance by using Non-Homogeneity Detectors (NHD) [63] to identify and remove highly heterogeneous samples from a TD set, improving overall TD homogeneity but

at the cost of reducing TD quantity. Unfortunately, such techniques tend to obey the law of diminishing returns when applied to highly heterogeneous clutter environments, which comprise most operating environments of interest [12, 93].

The causes and effects of many types of clutter heterogeneity have been reported in [63, 70, 71]. Experimentation with measured radar data has repeatedly confirmed the negative impact of heterogeneous clutter on STAP performance [12, 70] and much of the active STAP research can be linked to addressing the heterogeneous clutter problem. Remote sensing requirements drive the need to consider GMTI operation in multi-static, dense urban, and target-rich environments using antenna arrays which may be side-looking with a significant crab angle, forward-looking, space-based, conformal, sparse, non-uniform, and possibly damaged. Each of these array conditions induces a type of non-homogeneity into the training data along the range (training) dimension, whether it be amplitude, spectral, temporal, and/or a combination of all three [62, 63, 71, 81].

With today's challenging GMTI scenarios demanding increased radar resolution in range, Doppler, and azimuth (and better detection performance notwithstanding), the training data quantity and range extent increase as well and the problems of availability, heterogeneity, and non-stationary temporal-spatial clutter relationships are compounded. Dealing with these problems has framed, either directly or indirectly, the vast majority of adaptive radar research since its inception.

Though many remarkable STAP processors and techniques have been invented that ameliorate over the shortcomings of real world TD, it goes almost without saying that virtually any STAP technique incorporating training data as part of its algorithm benefits from increased training data quantity and/or quality. The use of intelligent transmit adaptivity and/or diversity, specifically the pattern adaptivity explored here, has demonstrated the ability to improve the quality of received training data (prior to any receive processing). By improving TD quality, any NHD process will remove less TD, resulting in a greater quantity of TD available as well. By restoring a degree

of homogeneity to the clutter, adaptive illumination patterns should bring about improved performance for many adaptive receiver processing algorithms.

1.3 Recent Adaptive Radar Research Thrusts

Many techniques have been developed to address the reality of limited and/or heterogeneous training data [63]. More recently, some success has been achieved using partially and fully adaptive methods which make extensive use of available knowledge sources. As mentioned previously, nearly all problems associated with STAP can be readily muted through clairvoyancy. Therefore, it is natural to expect that augmenting STAP with additional knowledge will result in improved performance. Fundamentally, this represents a Bayesian approach to radar processing whereby available *a priori* knowledge is used to reduce statistical uncertainty in quantities to be estimated. Extending the use of *a priori* knowledge into the radar transmitter has also been recently given much emphasis in the literature, with some at the DARPA claiming adaptive transmit architectures will dominate the radar research of the next century [44].

1.3.1 Knowledge-Aided STAP. Knowledge-Aided STAP has become a widely researched area in the radar community [2–4, 6–8, 12, 13, 15, 21, 31, 37, 41, 43, 48, 59, 64, 68, 69, 73–75, 89, 101]. Researchers have widely exploited the general structure of clutter (parametric methods), previously collected radar data (previous Coherent Pulse Intervals (CPI) and SAR imagery), as well as terrain and other geological databases (terrain elevation, reflectivity, etc). The DARPA funded Knowledge Aided Sensor Signal Processing and Expert Reasoning (KASSPER) program is one example of this type of research which has driven researchers toward employing *a-priori* information into radar signal processing methods to achieve better performance in very challenging clutter environments.

While the KASSPER program is representative of recent efforts to advance the state-of-the-art in knowledge-aided “adaptive” processing, a gap remains between

desired performance and what the current state-of-the-art provides. The KASSPER challenge dataset demonstrated that even with perfect statistical clairvoyancy (i.e., known covariance matrices), some targets remained undetected and false detections were prevalent even with optimum processing [37]. It is clear that signal *independent* interference (e.g., jamming), extreme heterogeneous clutter environments, and dense target fields remain a formidable challenge for the best *receiver processing* interference mitigation techniques. This has prompted some researchers to shift their focus toward modifying conventional *transmitter processing* to improve system performance [48].

This shift from a receiver centric processing paradigm to a synergistic adaptive transmitter and receiver paradigm is largely made possible by the development of knowledge-aided, knowledge-based methods. Aside from the required leaps in transmitter technology (specifically arbitrary waveform generation and Active Electronic Scanned Array (AESA) antennas) the obvious stumbling block to adaptive transmit is knowing what to adapt *to*. Knowledge-based and knowledge-aided receive processing techniques have pioneered the fusion of external, *a priori* knowledge into receiver processing, an arena formerly exclusively dependent on received data. Given the lack of received data prior to transmit, it is natural to investigate the exploitation of *a priori* knowledge on transmit.

1.3.2 Fully Adaptive Radar (FAR). Since the inception of adaptive radar processing [18], research predominantly followed a transmit–receive–adapt approach to interference mitigation. This widely-accepted *receiver centric* processing paradigm is intuitive, given the historical reliance on using received data to estimate interference statistics necessary for adaptive radar processing, such as done in STAP techniques. Knowledge-based and knowledge-aided receive processing techniques successfully pioneered the fusion of external, *a priori* knowledge into receiver processing. Given the lack of received data prior to transmit, it is natural to investigate the exploitation of *a priori* knowledge on transmit. However, relatively few adaptive radar techniques

have been proposed that attempt to optimize the *transmitted* energy characteristics (temporal, spectral, spatial or combination thereof) to improve system performance.

Systems that adapt transmit energy characteristics based on known environmental conditions may reduce the burden placed on receiver processing, thereby unlocking previously unreachable levels of performance by exploiting “priors” in a Bayesian paradigm during the *creation* of radar data. The combination of improved *a priori* knowledge data bases and recent improvements in arbitrary waveform synthesizers, low-noise linear amplifiers, and extremely agile Active Electronically Scanned Arrays (AESAs), is unlocking the door to an expanded paradigm involving an *adapt*–transmit–receive–adapt methodology.

Relatively few publications exist in the *radar* community which offer true *adaptive on transmit* approaches for enhancing radar system performance. A preliminary literature search indicates previous research in this area focused on the impact of pulse shaping [33–35, 48, 49, 76, 78, 79], waveform selection [91], and/or polarization matching [32] on target detection and/or identification. Adaptive pulse shaping is historically synonymous with “matched-illumination” as found in literature dating back to 1986 [32]. These works exploit *a priori* knowledge to generate an adaptive (sometimes optimal, sometimes multi-channel) transmit waveform/receive filter pair for detecting or identifying targets—a paradigm aptly described as “Fully Adaptive Radar” (FAR). It has been recently suggested that FAR will perhaps become the primary research focus of the 21st Century [44].

Adaptive transmit architectures are not unique to radar applications and are under investigation in related engineering disciplines. One example includes digital communication networks where much work has been done on using Multiple-In, Multiple-Out (MIMO) techniques which provide transmit adaptivity to boost channel capacity and signal-to-noise ratio in cellular networks [11, 28, 36, 65, 66, 80]. The proposed MIMO techniques take advantage of *a priori* channel information to improve system performance through spatially adapting transmit patterns within each

cell. Although the design problems and goals of a network centric communication system are somewhat different than that of a radar system, the cross-pollination of new communication “systems” or modulation techniques (such as spread spectrum architectures, orthogonal coding schemes, and stepped-frequency waveforms) into radar has often given birth to new radar system capabilities having increased performance.

There has been some work on MIMO based implementations for radar applications. In [5, 30], the authors propose work based on simultaneous broadcasts of orthogonal signals on different antenna elements where one signal is used to spatially mask the other signal in pattern sidelobe regions. The proposed system would deny a bistatic reference signal to an uncooperative sensor with the masking signal which could possibly double as a communications signal.

Another adaptive transmit example is found in the area of adaptive optics which is being used for the Airborne Laser (ABL) program. In this case, the deformable mirror shares a *conceptual* similarity to adaptive transmit patterns in that the transmit aperture (i.e., deformable mirror) adapts (changes the phase front) to the interference (atmospheric turbulence) prior to pulse transmission to increase performance (kill laser spot size/intensity) [92].

The aforementioned adaptive transmit techniques are based on optimizing the transmit pulse shape, polarization, or some other aspect of the transmit *signal*. Some methods take the target impulse response into account, as well as signal dependent interference, making them adaptive to the target and (in some cases) clutter. Having surveyed various applications of transmit adaptivity across multiple disciplines, the use of transmit *pattern* diversity as part of the fully adaptive radar paradigm stands out as a potentially rich and largely unexplored area of research.

1.4 New Idea: Adaptive Illumination Patterns

Modern waveform generator technology has enabled the development of a broad host of diverse and in some cases highly adaptive radar signal modulation and pulse

shaping techniques. The ability to precisely generate and modulate transmitted signals has given rise to countless advances in radar performance while providing the impetus for much advanced research. In a similar manner, the maturity of modern AESA technology could hold the key for unlocking a previously unexplorable concept in the era of fixed pattern, mechanically steered antennas.

With modern AESA technology, techniques involving rapid radar mode switching, transmit beam shaping, pattern dithering, and multi-beam search are becoming common place. Such capabilities are made possible through the creation of very agile and flexible antenna patterns. Although these patterns are currently flexible, configurable, and frequently updated in response to platform motion, relatively little research has been done on how to synthesize transmit (“illumination”) antenna patterns that are adaptive to specific operating environments or across the joint space-time domain for the purpose of improving radar performance.

Thus, the fundamental transmit diversity concept introduced in this research involves using Adaptive Illumination Patterns (AIP) to tailor scene illumination such that signal induced interference (i.e., clutter) is pre-structured for easier suppression on receive. Since the resulting illumination patterns are intended to be adaptive on transmit, AIP is viewed as an extension of the FAR paradigm, where the common goal is to pursue increased radar performance through knowledge-aided adaptive transmit.

As proposed, the AIP techniques include time-varying illumination patterns, where the capability for updating the transmit pattern on a CPI-to-CPI basis, or even more frequently on a pulse-to-pulse (interpulse basis), is assumed. Stimson [94] indicates that to stabilize the transmit beam in response to aircraft dynamics, an AESA must be able to update patterns at rates up to 2 kHz. Thus, it appears the technology exists to switch transmit antenna patterns on a pulse-to-pulse (interpulse) basis, at least at lower Pulse Repetition Frequencies (PRFs). Presuming this capability exists, and motivated by the power of STAP (i.e., joint space-time) processing, it is reasonable to investigate if some measure of system performance can be enhanced

by adaptively changing transmit pattern characteristics on a CPI-to-CPI or interpulse basis.

While this research uncovered no evidence that AIP will improve on the optimum (clairvoyant) receive STAP processor performance obtained under standard illumination conditions, this research suggests many detrimental real-world effects may be better addressed using a synergistic combination of AIP and STAP. In addition, implementing adaptive illumination via real transmit antenna patterns may induce new phenomenological effects into received data which could be further exploited to improve overall performance in a FAR architecture.

This research is divided into two major thrusts, which are distinctive in terms of their pattern update interval as well as their purpose. Illumination patterns *designed* to change on a pulse-by-pulse basis characterize the research area of Space Time Illumination Patterns (STIP), while those patterns which are adaptive but temporally constant for at least a CPI fall under the area termed Scene Adaptive Illumination Patterns (SAIP).

1.4.1 Space Time Illumination Patterns. The success of STAP at achieving interference suppression by *jointly* working across temporal and spatial domains motivates the investigation into the temporal variation of transmit/illumination antenna patterns. The temporal, *interpulse* pattern variation described here goes beyond the simple beampointing corrections described earlier, which are done in response to fast, dynamic changes in the sensor platform orientation. STIP involves the purposeful design of an entire time-varying weight set to achieve a joint space-time effect, not unlike the joint space-time advantage that STAP enjoys over factored space and/or Doppler processing. The use of pulse-varying AIP for this purpose is referred to throughout this document as Space-Time Illumination Patterns (STIP).

Viewing phased array antenna weights as digital filters applied to sampled radar returns, it is reasonable to consider what might be achieved through interpulse application of adaptive and/or diverse complex antenna weights applied during pulse

transmission. For example, it is later demonstrated that the use of changing antenna weights creates a spatially dependent Doppler response. This can have a key impact on the received clutter characteristics since the clutter *also* experiences a spatially dependent Doppler response. Additionally, these antenna weights could be generated adaptive to the environment using a-priori channel information, e.g., clutter characteristics estimated during the previous CPI [75], to generate transmit antenna weights for the current CPI pulse train.

Alternatively, knowledge-aided clutter modeling could be used to estimate the interference environment a priori, an area being heavily researched by the DARPA KASSPER program [45]. Techniques which augment the estimated covariance (computed from radar returns) with a knowledge-aided estimate have also been developed and called both “pre-whitening” [13] and “colored loading” [58]. In any case, having an estimate of the interference prior to transmission allows STIP to utilize transmit DOF provided by *real* space-time illumination patterns followed by traditional STAP (utilizing receive DOF) on receive.

Although limited in scope, possibly the first (and perhaps the only) published exploration of time-varying transmit antenna patterns in an adaptive radar context is found in a spaced-based radar research of Schindler and Steyskal [88]. In this work, the authors propose the use of pulse-dependent transmit patterns and variable interpulse spacing to help achieve a DPCA condition in a sparse array with random sensor placement [88].

Ultimately, the contribution of STIP to overall adaptive radar performance comes in its ability to shape the clutter such that partially adaptive STAP processors achieve greater performance and/or require less training data *quantity* to achieve a specified level of performance.

1.4.2 Scene Adaptive Illumination Patterns. The ability to accurately detect and track moving ground targets in densely populated urban, or otherwise heterogeneous environments, from an airborne platform presents both an important and

challenging surveillance problem. This task, particularly in bad weather conditions, is typically assigned to a GMTI radar for which the MDV is a key performance parameter. In recent years, researchers have turned to Knowledge-Aided Space Time Adaptive Processing (KA-STAP) [6, 21, 41, 68, 73, 75, 89] and Fully Adaptive Radar (FAR) [48] paradigms to invoke the power of *a priori* knowledge in achieving more robust performance and lower MDV.

As mentioned earlier, mitigating heterogeneous clutter effects is the key to effectively lowering MDV. While there are many causes of clutter heterogeneity (see [63, 70]), AIP is demonstrated here by attacking the problem of Targets in the Training Data (TTD), which is an active area of research [7, 12, 63, 68, 72, 82, 85, 101]. Some Knowledge-aided approaches for battling TTD propose removing potentially corrupted TD samples based on *a priori* knowledge of road locations, platform position and orientation [7, 12, 68, 101]. In addition to NHD, other common techniques such as diagonal loading the estimated covariance matrix and using non-adaptive processors (e.g., DPCA) have also been suggested to combat TTD [72].

While these techniques have demonstrated substantial performance improvements, they are not without some drawbacks. Effective NHD is difficult in very dense target environments [12, 72], and even if the corrupted TD can be successfully identified, its removal reduces the available TD for estimating interference statistics. Like NHD, knowledge-aided removal of TD based on known road locations (thus *assumed* target presence) also has the net effect of reducing TD, sometimes unnecessarily. Diagonal loading is reported to be effective in some cases [72] but not all [12], and DPCA requires stringent hardware tolerances and zero crab angle to be effective [72].

This research proposes a new approach for minimizing the negative impacts of TTD. Using *a priori* road location information, modern AESA array technology, and geometries consistent with close-in sensing applications, the transmit antenna pattern is adaptively altered to illuminate the scene such that *illumination pattern nulls* are placed along road locations running through the training data. By not

illuminating the vehicular targets with transmit energy, the contaminating reflected target energy is effectively reduced, thereby converting target corrupted training data into a more homogeneous clutter condition. The use of AIP for this purpose is referred to throughout this document as Scene Adaptive Illumination Patterns (SAIP).

SAIP is independent and perfectly complementary to the existing NHD techniques previously mentioned. It is expected that the synergistic use of SAIP and existing NHD-like techniques will result in improved adaptive radar performance in target-rich environments and other heterogeneous environments also. The specific contribution of STIP to overall adaptive radar performance is its ability to “convert” (to some degree) heterogeneous clutter into a more homogeneous state, resulting in a net increase in clutter quality and quantity, the latter being realized upon the common application of NHD to heterogeneous clutter data.

1.4.3 Approach and Methodology. While the Multi-Channel Airborne Radar Measurements (MCARM) and KASSPER data sets have aptly provided a common reference for benchmarking interference suppression algorithms using *fixed* transmit patterns, they are inherently insufficient for comparing interference suppression performance of techniques utilizing AIP, to include STIP and SAIP as considered here. Why are they insufficient? For all AIP techniques, the reflected and received energy (from targets, interference, etc.) is intrinsically dependent on the illumination pattern.

Existing datasets (such as those from the MCARM and KASSPER programs) have already been illuminated, i.e., sampled, by a fixed illumination pattern. The radar illumination pattern *determines* the returned data, much like a camera flash in a pitch-dark room determines what is captured on film. While image processing techniques (analogous to radar receive filtering) can be applied and evaluated on the recorded image (analogous to radar data), one cannot evaluate new camera flashes (analogous to radar illumination patterns) without re-taking the same picture. Thus, a complete end-to-end target and interference (clutter) model incorporating the effects

of arbitrary illumination patterns is required for conducting AIP FAR research. One of the major contributions of this work is providing this modeling, simulation and analysis capability.

To investigate AIP techniques, radar system modeling must be extended back into the transmitter such that the transmit/illumination pattern variation can be incorporated on an interpulse basis. An illumination pattern that changes throughout the CPI will affect the magnitude and phase of signal-dependent reflections and models thereof, including both the clutter model and target return models. However, signal-independent returns and models thereof, e.g, jammer models, are unaffected by the application of AIP. The analytic development of required modifications and extended model capabilities have been accomplished and are included in Chapter II.

1.5 Contributions and Document Overview

This research characterizes performance improvements which are obtained by incorporating transmit diversity through illumination pattern adaptivity into the cadre of existing radar signal processing techniques. For demonstration purposes, STAP receiver processing is used to characterize the benefits of employing AIP. AIP is applied to address two of STAP's biggest challenges: 1) poor training data quality, and 2) limited training data quantity. These limitations are addressed either through using SAIP to mitigate dense target environments in which the training data is contaminated with a large number of targets, or by using STIP to reduce the required training data quantity in the classic side-looking linear array STAP scenario (both of which are applicable to GMTI applications). Figure 1.3 provides the organizational research structure which is divided into three basic areas: 1) Extensions to existing radar models that incorporate Adaptive Illumination Patterns-Transmit Interpulse Pattern Diversity (AIP-TIPD), 2) Development and application of Space Time Illumination Patterns (STIP), and 3) Development and application of knowledge aided Scene Adaptive Illumination Patterns (SAIP). Research contributions are summarized as follows:

Adaptive Illumination Patterns (AIP)

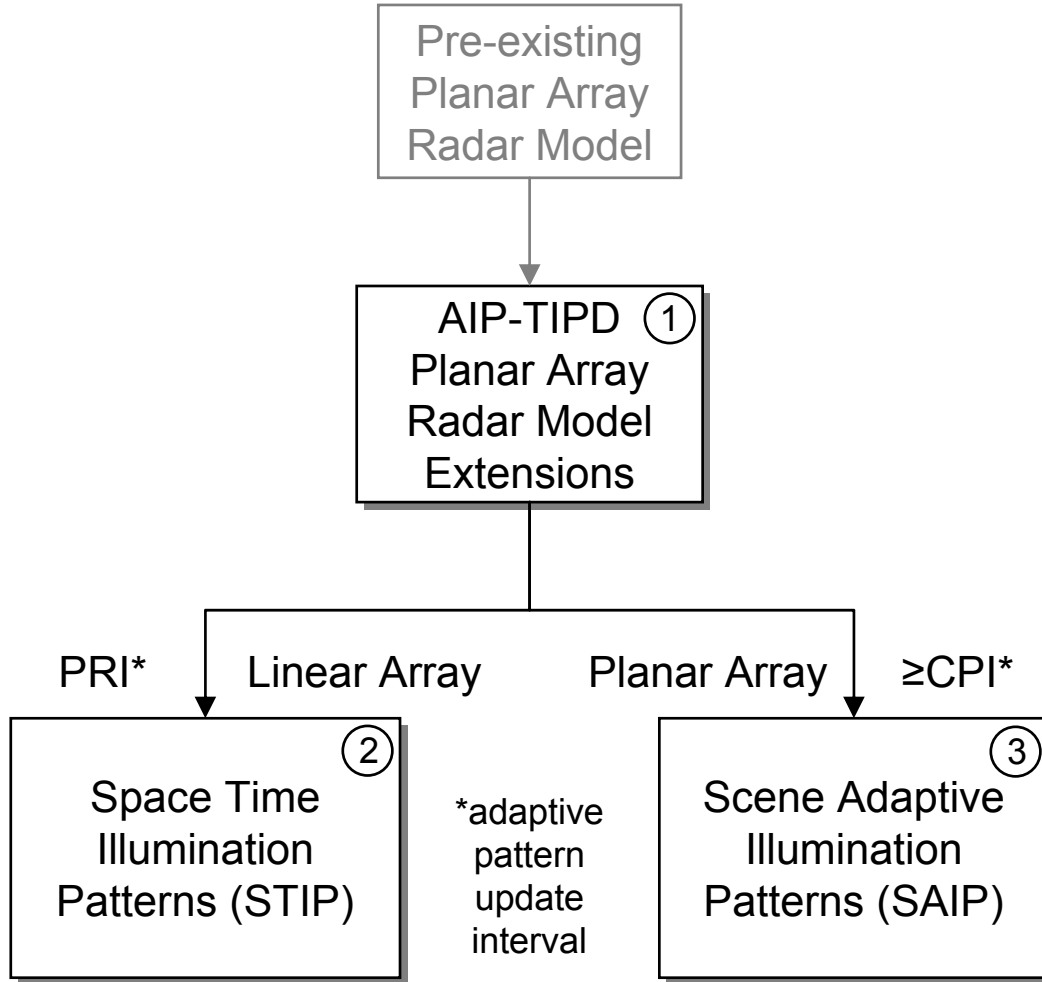


Figure 1.3: Organization of research structure and technical contribution areas, including 1) incorporation of Adaptive Illumination Pattern-Transmit Interpulse Pattern Diversity (AIP-TIPD) extensions into pre-existing radar models, 2) development and application of STIP to pre-shape (re-distribute) clutter power such that STAP processing performs better with less Training Data, and 3) development and application of knowledge aided SAIP to minimize heterogeneous clutter effects in target saturated environments.

1. Development of Adaptive Transmit Pattern Model: Extended previous radar model of [52,61,99] to incorporate effect of adaptive transmit pattern on target and clutter responses [24].
 - Incorporates arbitrary spatial transmit weights for a planar Array (3D STAP).
 - Incorporates arbitrary pulse-varying set of transmit weights using a planar Array.
 - Proved that the clairvoyant clutter covariance matrix incorporating TIPD is valid for *any* arbitrary statistical distribution *and/or* deterministic clutter reflectivity.
 - Incorporated analytic modeling of subarrays in the clutter covariance model which reduces computational load, memory requirements, and decreases modeling and simulation time.
 - Modified clutter snapshot model for range bin-by-range bin generation of clutter incorporating TIPD planar array (elevation dependent) illumination patterns.
2. Space Time Illumination Patterns (STIP): Introduced and developed the concept of STIP to accomplish space-time beamforming for simplified receiver processing [27]
 - Extended linear array radar model of [61,99] to incorporate Transmit Interpulse Pattern Diversity (TIPD) functionality.
 - Demonstrated performance matching that of an optimum filter using optimum TIPD weights with simplified Doppler receive filtering. Processing burden shifted from receiver to transmitter.
 - Developed understanding of the nature of joint space-time beamforming, detailing the differences between illumination and filtering.

3. Scene Adaptive Illumination Patterns (SAIP): Introduced and developed the concept of SAIP to improve STAP performance in dense target environments [25].

- Uses knowledge-aided technique to synthesize transmit patterns (adapt scene illumination) based on known road locations. Removal of mobile scatterer responses from road locations effectively “cleans up” training data.
- Demonstrated performance improvement for planar array using SAIP with STAP receiver processing for close-in sensing applications.

The remainder of this document is organized as follows:

In Chapter II, the clutter and target models of [52, 61, 99] are extended to incorporate the ability to model arbitrary, plus-dependent, antenna pattern effects on target and clutter returns for linear and planar arrays. A proof extending the validity of the covariance matrix to arbitrary deterministic and/or random clutter scattering models and an analytic development of sub-array modeling is included as well.

Chapter III provides a brief STAP overview with specific focus on the STAP processors used for this research. Since STAP is used here to demonstrate the potential of AIP, the STAP processors chosen here are those that are well-known and widely used as benchmarks, rather than the most recent state-of-the-art STAP algorithm available. The specific STAP processors chosen include the non-adaptive Signal Match (SM) filter, fully adaptive Matched Filter (MF), the fully adaptive Adaptive Matched Filter (AMF), and the partially adaptive Factored Space Time (FST) processor.

Chapter IV provides the first application of AIP considered, specifically, STIP. This chapter relates the differences between illumination and filtering, as performed by the real transmit and synthesized receive patterns, respectively. The utility of knowledge-aided TIPD is demonstrated to enable STAP-like performance with simple receive processing. The topic of transmit pattern synthesis is addressed and preliminary synthesis methods introduced. Output signal to interference-plus-noise ratio (SINR) results are provided using STAP based processing in conjunction with an optimal implementation of STIP on transmit, demonstrating the performance-enhancing

potential of STIP to improve STAP performance. Conventional fully adaptive MF and non-adaptive SM processor results are presented for comparison.

Chapter V provides the second application of AIP considered, specifically, the use of knowledge-aided SAIP to reduce contaminating returns from targets in the training data, which improves STAP performance. It also details some specific issues related to adaptive close-in sensing where elevation diversity occurs across the range gates of interest. SINR Loss results are provided using the Adaptive Matched Filter to demonstrate improved Minimum Discernable Velocity performance in the presence of dense target environments.

Chapter VI summarizes the research contributions and offers closing thoughts.

II. Adaptive Illumination Patterns for Planar Array Radar

To investigate Adaptive Illumination Pattern (AIP) techniques, radar system modeling must be extended back into the transmitter such that the transmit/illumination pattern effects are effectively incorporated into simulated received data. Whereas adaptive receiver processing schemes can be readily applied and tested using many of the existing radar data sets, research involving illumination pattern adaptivity is most efficiently evaluated via modeling and simulation. This is true given that the radar data received is directly impacted by the illumination patterns, which themselves may be (in some way) adapted to the interference and/or target characteristics. Thus, high-fidelity modeling of the entire transmit-receive process is required for investigating AIP techniques. That being the case, having a standard validated model is vital to performing cooperative and comparative AIP FAR research.

Conducting Scene-Adaptive Illumination Pattern (SAIP) research requires incorporating a spatially adaptive but temporally fixed (over at least one coherent processing interval) illumination pattern into existing radar models. However, to properly investigate the application of Space Time Illumination Patterns (STIP), pattern variation must be implemented on an interpulse (pulse-to-pulse) basis. An illumination pattern that changes throughout the CPI will induce both *magnitude* and *phase* fluctuations in the signal-dependent reflections and models thereof, including both the clutter model and target return models. Thus, it is necessary to include the illumination pattern amplitude and phase responses when re-deriving the end-to-end radar model. The new model developed herein is based on radar models originally developed in [61, 99] and subsequently extended to planar arrays by [52]. The planar array extension of [52] is used here to model a rectangular grid of antenna elements (P rows by N columns) using the same coordinate system and relative uniform spacings established in [52], illustrated in Fig. 2.1.

The planar array development presented herein extends and validates the linear array AIP modeling described in [27] which provided an initial proof-of-concept approach for implementing Transmit Interpulse Pattern Diversity (TIPD), the fun-

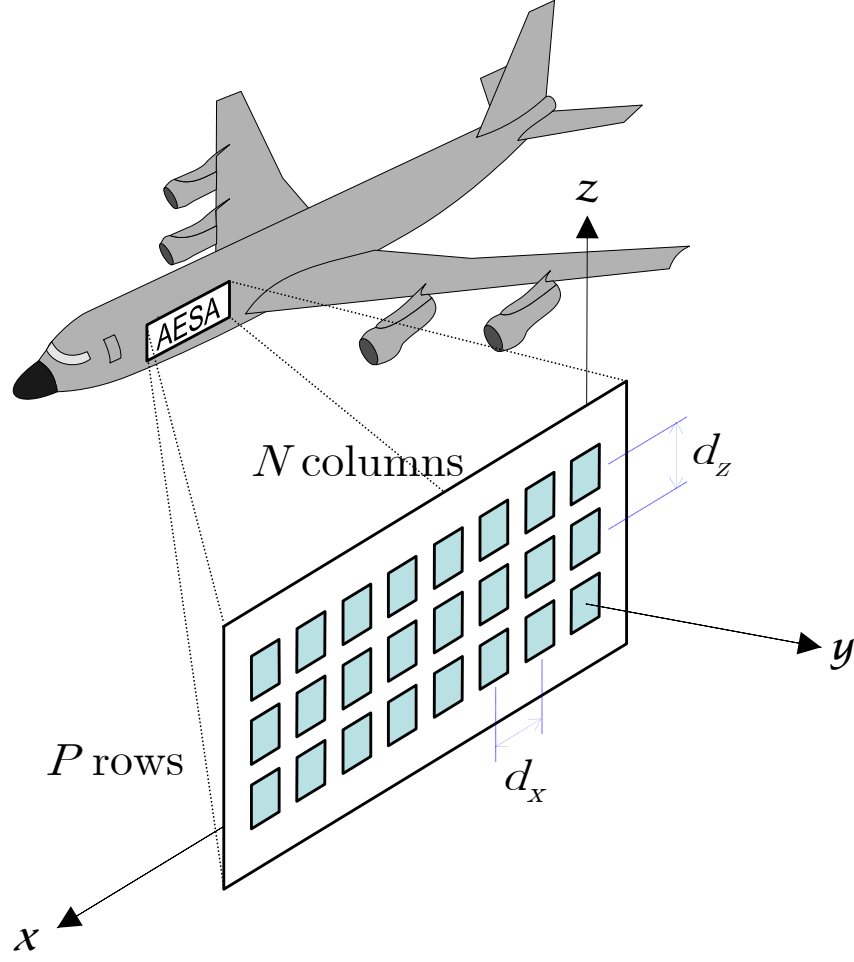


Figure 2.1: Phased array coordinate system and geometry

damental capability necessary to explore the impacts of STIP and SAIP. Note that the models developed herein are not dependent on the particular method used for generating the transmit/illumination patterns—a process which is anticipated to be as varied and critical to FAR performance as the weight estimation approaches are for STAP receive processing. For notational purposes and consistency, scalar quantities are shown as normal text (not bold), vectors are lowercase bold text, and matrices are uppercase bold text.

2.1 Target Response Model

Investigating the impact of Transmit Interpulse Pattern Diversity (TIPD) on radar performance requires revising the target response model derivation (based on Ward's development [99]) to incorporate time-varying transmit antenna pattern *magnitude* and *phase* factors. For clarity, the target is modeled as a point scatterer and the convention used in Ward's derivation is followed to ensure changes resulting from the incorporation of TIPD are readily apparent.

2.1.1 Radar Signal Model. Starting at the transmitter, consider a pulsed sinusoidal signal consisting of M total pulses given by

$$s(t) = a_s u(t) e^{j(\omega_0 t + \gamma)}, \quad (2.1)$$

where a_s is the peak (voltage) amplitude, ω_0 is the carrier frequency, γ is an arbitrary starting phase, and $u(t)$ is given by

$$u(t) = \sum_{m=0}^{M-1} u_p(t - mT_r). \quad (2.2)$$

Parameter T_r in (2.2) is the Pulse Repetition Interval (PRI) and $u_p(\cdot)$ is a constant envelope function defined as

$$u_p(t) = \frac{1}{\sqrt{T_p}} \text{Rect} \left[\frac{t - \frac{T_p}{2}}{T_p} \right], \quad (2.3)$$

where T_p is the pulse width and the Rect function is defined as

$$\text{Rect}[t] = \begin{cases} 1 & -\frac{1}{2} < t < \frac{1}{2} \\ 0 & \text{o.w.} \end{cases} \quad (2.4)$$

such that $u_p(t)$ has unit energy, i.e.,

$$\int_{-\infty}^{\infty} |u_p(t)|^2 dt = \int_0^{T_p} |u_p(t)|^2 dt = 1. \quad (2.5)$$

2.1.2 Transmit Antenna Model. Pulsed signal $s(t)$ is radiated through a phased array antenna, inducing (via the antenna transmit pattern) a spatial dependence on the composite signal's phase and amplitude. With the addition of TIPD, the transmit pattern is allowed to change on a pulse-to-pulse basis. The spatially dependent far field array response for the m^{th} pulse ($F_m(\theta, \phi)$) is given by [99]

$$F_m(\theta, \phi) = W_m(\theta, \phi) f(\theta, \phi), \quad (2.6)$$

where θ is the elevation angle, ϕ is the azimuth angle, $W_m(\theta, \phi)$ represents the complex array factor used to transmit the m^{th} pulse [27], and $f(\theta, \phi)$ represents the complex voltage pattern factor for each radiating element. As in previous developments [52, 99], this work assumes identical $f(\theta, \phi)$ pattern factors for all elements and matched polarization conditions between incident electric fields and array elements. Incorporating the antenna pattern effects of (2.6) on $s(t)$ of (2.1) is done by defining a time dependent antenna factor

$$F(\theta, \phi, t) = \mathcal{W}(\theta, \phi, t) e^{j\zeta(\theta, \phi, t)} f(\theta, \phi), \quad (2.7)$$

where the array factor magnitude $\mathcal{W}(\theta, \phi, t)$ and array factor phase $\zeta(\theta, \phi, t)$ are defined as

$$\begin{aligned} \mathcal{W}(\theta, \phi, t) &= \sum_{m=0}^{M-1} |W_m(\theta, \phi)| \cdot \text{Rect} \left[\frac{t - \left(mT_r + \frac{T_p}{2}\right)}{T_p} \right] \\ \zeta(\theta, \phi, t) &= \sum_{m=0}^{M-1} \angle [W_m(\theta, \phi)] \cdot \text{Rect} \left[\frac{t - \left(mT_r + \frac{T_p}{2}\right)}{T_p} \right]. \end{aligned} \quad (2.8)$$

In (2.8), the $\angle[\cdot]$ operator returns the angle of the complex argument and the $\text{Rect}[\cdot]$ function defined in (2.4) facilitates application of the m^{th} array pattern during the m^{th} pulse transmission.

2.1.3 Transmitted Signal. Combining the antenna pattern effects of (2.7) with (2.1), the *transmitted* signal s_{tx} can be expressed as

$$s_{\text{tx}}(\theta, \phi, t) = F(\theta, \phi, t)s(t) = a_s \mathcal{W}(\theta, \phi, t) |f(\theta, \phi)| u(t) e^{j[\omega_0 t + \zeta(\theta, \phi, t) + \angle[f(\theta, \phi)] + \gamma]}. \quad (2.9)$$

2.1.4 Reflected Signal. In keeping with previous derivations [52, 61, 99], the target is modeled as a far-field point scatterer having Radar Cross-Section (RCS) of σ_{tgt} and a Doppler frequency of ω_{tgt} . The target also induces a unique phase shift which is modeled here as a random variable ψ_{tgt} , uniformly distributed on $[0, 2\pi)$. Although random, it is common (in investigating adaptive radar processing techniques) to assume the target's phase response remains constant *throughout* the CPI (interval containing M consecutive pulses). The *reflected* signal from a target can thus be expressed as

$$s_{\text{ref}}(\theta, \phi, t) = A_{\text{ref}} \mathcal{W}(\theta, \phi, t - \Delta t) u(t - \Delta t) e^{j[\omega_0(t - \Delta t) + \zeta(\theta, \phi, t - \Delta t) + \omega_{\text{tgt}} t]} e^{j(\gamma + \psi_{\text{tgt}} + \angle[f(\theta, \phi)])}, \quad (2.10)$$

where Δt is the one way antenna-target propagation time given by

$$\Delta t = \frac{R_{\text{tgt}}}{c}, \quad (2.11)$$

where c is the speed of light and R_{tgt} is the target's range as relative to the reference array element ($n = 0, p = 0$). A_{ref} represents the temporally fixed (within the CPI) portion of the reflected voltage given by

$$A_{\text{ref}} = a_{\text{ref}}(a_s, |f(\theta, \phi)|, \sigma_{\text{tgt}}, R_{\text{tgt}}), \quad (2.12)$$

where a_{ref} in (2.12) is a function of transmit voltage a_s , element pattern magnitude $|f(\theta, \phi)|$, target RCS σ_{tgt} , and propagation distance R_{tgt} . As the reflected signal has not yet been received by an antenna, it cannot be expressed in volts but rather in voltage field intensity (V/m). For clarity, a_{ref} indicates the parameters affecting A_{ref} . The analytical relationship of each of these (and other) parameters on the final voltage expression is provided later.

Equation (2.10) can be simplified by observing that $\omega_0 \Delta t$, $\angle[f(\theta, \phi)]$ and γ in (2.10) are independent of n, p (receive element) and time throughout the CPI. As a result, they can be combined with the target's random phase response ψ_{tgt} without loss of generality, to make a composite random phase response given by

$$\psi = -\omega_0 \Delta t + \angle[f(\theta, \phi)] + \gamma + \psi_{\text{tgt}}. \quad (2.13)$$

Incorporating (2.13) into (2.10) yields a simplified *reflected* signal response of

$$s_{\text{ref}}(\theta, \phi, t) = A_{\text{ref}} \mathcal{W}(\theta, \phi, t - \Delta t) u(t - \Delta t) e^{j[(\omega_0 + \omega_{\text{tgt}})t + \zeta(\theta, \phi, t - \Delta t)]} e^{j\psi}. \quad (2.14)$$

2.1.5 Received Signal. The target return is next expressed relative to each array element to capture the signal wavefront phase progression. This is done by inserting a time delay τ_{np} on the reflected signal, $s_{\text{ref}}(\theta, \phi, t - \tau_{np})$, which represents the total propagation time (delay) from the target to the $(n^{\text{th}}, p^{\text{th}})$ element, expressed as

$$\tau_{np} = \Delta t + \tau'_{np}. \quad (2.15)$$

where Δt is defined in (2.11) and τ'_{np} represents the relative time-of-arrival difference between the $(n^{\text{th}}, p^{\text{th}})$ and reference $(n = 0, p = 0)$ array elements. After propagation back to the radar, the signal received by the $(n^{\text{th}}, p^{\text{th}})$ antenna element is given by

$$s_{np}(\theta, \phi, t) = \tilde{a} \mathcal{W}(\theta, \phi, t - 2\Delta t - \tau'_{np}) u(t - 2\Delta t - \tau'_{np}) e^{j[(\omega_0 + \omega_{\text{tgt}})(t - \Delta t - \tau'_{np}) + \zeta(\theta, \phi, t - 2\Delta t - \tau'_{np})]} e^{j(\psi + \angle[f(\theta, \phi)])}. \quad (2.16)$$

2.1.6 Received Voltage Model. Assuming far-field conditions and identical element patterns, \tilde{a} (which excludes the pulse-dependent array factor magnitude \mathcal{W}) is approximately constant for all (n, p) elements and m pulses over the CPI of interest. This term represents the received voltage amplitude measured by a single receive element assuming a *single* transmit element, accounting for all effects resulting from signal transmission, propagation, and reception. Taking into account free-space propagation under matched polarization conditions, and the fact that σ_{tgt} is a real-valued power ratio, Friis transmission principles [10] can be used to show

$$\tilde{a} = \frac{a_s |f(\theta, \phi)|^2 \sqrt{\sigma_{\text{tgt}}} \lambda_0}{\sqrt{(4\pi)^3} \sqrt{L_s} R_{\text{tgt}}^2}. \quad (2.17)$$

where λ_0 is the wavelength of the transmit frequency and $\sqrt{L_s}$ accounts for various hardware losses/inefficiencies in the process. The target RCS σ_{tgt} is commonly modeled as deterministic [52, 99]. If random pulse-to-pulse RCS changes are desired, such as a Swerling case 2 or 4 model [90], the target RCS would be removed from the pulse-independent factor of (2.17) and introduced as a distinct factor in (2.16).

The expression in (2.16) can be simplified as follows. The relative phase shift term τ'_{np} is commonly assumed to be negligible in the signal envelope function $u(t)$ because for most airborne scenarios $\tau'_{np} \ll T_p$ and thus τ'_{np} has an insignificant contribution to the starting/stopping time of the pulse envelope [99]. Furthermore, as can be seen explicitly in (2.8), the time argument in $\zeta(\theta, \phi, t)$ and $\mathcal{W}(\theta, \phi, t)$ of (2.16) also determines the envelope start/stop times as well. Thus, the τ'_{np} term is also negligible in the argument of ζ and \mathcal{W} . Finally, the phase term $-(\omega_0 + \omega_{\text{tgt}})\Delta t$ and the receive element's phase response $\angle[f(\theta, \phi)]$ are constant during the CPI and can be absorbed into the random phase term ψ , as done previously in (2.13). Incorporating these observations, (2.16) simplifies to

$$s_{np}(\theta, \phi, t) \approx \tilde{a} \mathcal{W}(\theta, \phi, t - 2\Delta t) u(t - 2\Delta t) e^{j[(\omega_0 + \omega_{\text{tgt}})t]} e^{-j[(\omega_0 + \omega_{\text{tgt}})\tau'_{np}]} e^{j\zeta(\theta, \phi, t - 2\Delta t)} e^{j\psi}. \quad (2.18)$$

2.1.7 Spatial Frequency Modeling. To establish a framework for defining spatial frequency, the relative inter-element phase delay $[(\omega_0 + \omega_{\text{tgt}})\tau'_{np}]$ of (2.18) is expressed as a function of element spacing and spatial incidence angles. As originally derived for linear arrays by [61,99] and subsequently extended to planar arrays by [52], the relative phase shift to the $(n^{\text{th}}, p^{\text{th}})$ array element relative to the $(n = 0, p = 0)$ reference element is given as

$$(\omega_0 + \omega_{\text{tgt}})\tau'_{np} = \frac{(\omega_0 + \omega_{\text{tgt}})}{c} (-nd_x \cos \theta \sin \phi - pd_z \sin \theta), \quad (2.19)$$

where d_x and d_z are the inter-element spacings shown in Fig. 2.1. As done in [52,99], let the array's horizontal ($\vartheta_x(\theta, \phi)$) and vertical ($\vartheta_z(\theta)$) spatial frequency terms be defined as

$$\vartheta_x(\theta, \phi) = \frac{d_x \cos \theta \sin \phi}{\lambda_0} \quad (2.20)$$

and

$$\vartheta_z(\theta) = \frac{d_z \sin \theta}{\lambda_0}, \quad (2.21)$$

respectively, where $\lambda_0 = 2\pi c/\omega_0$. A common assumption in airborne radars is the maximum unaliased target Doppler ω_{tgt} is orders of magnitude less than the transmit frequency ω_0 [99]. Thus, the impact of ω_{tgt} in (2.19) is negligible and can be omitted without loss of generality [99]. Using (2.20), (2.21), and the assumption stated above the inter-element relative phase shift in (2.19) is approximated as

$$(\omega_0 + \omega_{\text{tgt}})\tau'_{np} \approx -2\pi [n\vartheta_x(\theta, \phi) + p\vartheta_z(\theta)]. \quad (2.22)$$

2.1.8 Received Signal at Baseband. After down-conversion to baseband (i.e., removal of the carrier, $e^{j\omega_0}$), the spatial frequency representation of (2.22) is used to rewrite the *received* signal of (2.18) as follows, where the tilde on s_{np} notates the

approximations in (2.22)

$$\begin{aligned}\tilde{s}_{np}(\theta, \phi, t) &= \tilde{a}\mathcal{W}(\theta, \phi, t - 2\Delta t)u(t - 2\Delta t) \\ &e^{j\omega_{\text{tgt}}t}e^{j2\pi[n\vartheta_x(\theta, \phi) + p\vartheta_z(\theta)]}e^{j\zeta(\theta, \phi, t - 2\Delta t)}e^{j\psi}. \quad (2.23)\end{aligned}$$

2.2 Matched Filtering

The target response in (2.23) is now matched filtered on a pulse-by-pulse basis. To explicitly reveal the pulses embedded in (2.23), (2.2), (2.4), and (2.8) are substituted into (2.23), yielding

$$\begin{aligned}\tilde{s}_{np}(\theta, \phi, t) &= \tilde{a}e^{j\omega_{\text{tgt}}t}e^{j2\pi[n\vartheta_x(\theta, \phi) + p\vartheta_z(\theta)]}e^{j\psi} \\ &\sum_{m=0}^{M-1} \frac{1}{\sqrt{T_p}} \text{Rect} \left[\frac{t - 2\Delta t - mT_r - \frac{T_p}{2}}{T_p} \right] \\ &\sum_{i=0}^{M-1} |W_i(\theta, \phi)| \text{Rect} \left[\frac{t - 2\Delta t - iT_r - \frac{T_p}{2}}{T_p} \right] \\ &\times e^{j \left\{ \sum_{k=0}^{M-1} \angle[W_k(\theta, \phi)] \cdot \text{Rect} \left[\frac{t - 2\Delta t - kT_r - \frac{T_p}{2}}{T_p} \right] \right\}}. \quad (2.24)\end{aligned}$$

Note that all the envelopes are perfectly synchronized, such that for each m value in (2.24), there is only one value for i or k , namely $i = k = m$, which generates a non-zero envelope *inside* the m^{th} Rect function. Therefore, (2.24) collapses to

$$\begin{aligned}\tilde{s}_{np}(\theta, \phi, t) &= \tilde{a}e^{j\omega_{\text{tgt}}t}e^{j2\pi[n\vartheta_x(\theta, \phi) + p\vartheta_z(\theta)]}e^{j\psi} \\ &\sum_{m=0}^{M-1} u_p(t - 2\Delta t - mT_r) |W_m(\theta, \phi)| e^{j\angle[W_m(\theta, \phi)]}. \quad (2.25)\end{aligned}$$

The received pulse responses of (2.25) are match filtered via convolution with the desired impulse response $h(t)$, i.e.,

$$x_{np}(\theta, \phi, t) = \int_{-\infty}^{\infty} \tilde{s}_{np}(\theta, \phi, \tau) h(t - \tau) d\tau. \quad (2.26)$$

The matched filter impulse response for the pulse envelope function of (2.3) is given by

$$h(t) = u_p^*(-t), \quad (2.27)$$

where $*$ notates the complex conjugate operation. Substituting (2.25) and (2.27) into (2.26) yields

$$\begin{aligned} x_{np}(\theta, \phi, t) &= \tilde{a} e^{j2\pi[n\vartheta_x(\theta, \phi) + p\vartheta_z(\theta)]} e^{j\psi} \\ &\times \int_{-\infty}^{\infty} \sum_{m=0}^{M-1} |W_m(\theta, \phi)| e^{j\angle[W_m(\theta, \phi)]} u_p(\tau - 2\Delta t - mT_r) u_p^*(\tau - t) e^{j\omega_{\text{tgt}}\tau} d\tau. \end{aligned} \quad (2.28)$$

Since the array factor is not a function of time, (2.28) is written as

$$\begin{aligned} x_{np}(\theta, \phi, t) &= \tilde{a} e^{j2\pi[n\vartheta_x(\theta, \phi) + p\vartheta_z(\theta)]} e^{j\psi} \\ &\times \sum_{m=0}^{M-1} |W_m(\theta, \phi)| e^{j\angle[W_m(\theta, \phi)]} \int_{-\infty}^{\infty} u_p(\tau - 2\Delta t - mT_r) u_p^*(\tau - t) e^{j\omega_{\text{tgt}}\tau} d\tau. \end{aligned} \quad (2.29)$$

A change of variables is now introduced within the integral of (2.29). Letting $\beta = \tau - 2\Delta t - mT_r$, then $\tau = \beta + 2\Delta t + mT_r$, $d\beta/d\tau = 1$, and (2.29) becomes

$$\begin{aligned} x_{np}(\theta, \phi, t) &= \tilde{a} e^{j2\pi[n\vartheta_x(\theta, \phi) + p\vartheta_z(\theta)]} e^{j\psi} \sum_{m=0}^{M-1} |W_m(\theta, \phi)| e^{j\angle[W_m(\theta, \phi)]} \\ &\times \int_{-\infty}^{\infty} u_p(\beta) u_p^*(\beta + 2\Delta t + mT_r - t) e^{j\omega_{\text{tgt}}\beta} e^{j\omega_{\text{tgt}}(2\Delta t + mT_r)} d\beta. \end{aligned} \quad (2.30)$$

Note, this substitution resulted in a $2\omega_{\text{tgt}}\Delta t$ phase term in (2.30). Since this quantity is assumed constant for all m , n , and p , it can be moved outside the integral and absorbed into the random phase term ψ . Further, $2\Delta t$ and mT_r are independent of

β and can also be moved outside the integral, yielding

$$x_{np}(\theta, \phi, t) = \tilde{a} e^{j2\pi[n\vartheta_x(\theta, \phi) + p\vartheta_z(\theta)]} e^{j\psi} \sum_{m=0}^{M-1} |W_m(\theta, \phi)| e^{j\angle[W_m(\theta, \phi)]} e^{jm\omega_{\text{tgt}}T_r} \\ \times \int_{-\infty}^{\infty} u_p(\beta) u_p^*(\beta + 2\Delta t + mT_r - t) e^{j\omega_{\text{tgt}}\beta} d\beta. \quad (2.31)$$

Considering only the range gate containing the target, the arrival time of the m^{th} pulse response is known and given by $t = 2\Delta t + mT_r$. Evaluating (2.31) at this time (i.e., performing complex sampling the matched filter output at the PRF), the integral portion of (2.31) is approximated as [52]

$$\int_{-\infty}^{\infty} u_p(\beta) u_p^*(\beta) e^{j\omega_{\text{tgt}}\beta} d\beta = \int_0^{T_p} |u_p(\beta)|^2 e^{j\omega_{\text{tgt}}\beta} d\beta \approx 1, \quad (2.32)$$

where 1) it is commonly assumed $\omega_{\text{tgt}}T_p \ll 1$ such that $e^{j\omega_{\text{tgt}}\beta} \approx 1$ over the range of integration and 2) $u_p(t)$ was defined in (2.5) as having unit energy [99]. Thus, for a given range cell the sampled matched filter response for the m^{th} pulse, i.e., the matched filter response at $t = 2\Delta t + mT_r$, is represented as

$$x_{mnp}(\theta, \phi) = \tilde{a} |W_m(\theta, \phi)| e^{j2\pi[n\vartheta_x(\theta, \phi) + p\vartheta_z(\theta)]} e^{jm\bar{\omega}_{\text{tgt}}} e^{j\angle[W_m(\theta, \phi)]} e^{j\psi}, \quad (2.33)$$

where $\bar{\omega}_{\text{tgt}}$ is the *normalized Doppler* defined here as $\bar{\omega}_{\text{tgt}} = \omega_{\text{tgt}}T_r$. For completeness, an expression for the final composite random phase term ψ in (2.33) is provided. The composite ψ phase term includes all factors which did not vary as a function of m , n , or p throughout the development and is now explicitly given as:

$$\psi = \psi_{\text{tgt}} - 2(\omega_0 + \omega_{\text{tgt}})\Delta t + \gamma + 2\omega_{\text{tgt}}\Delta t + 2\angle[f(\theta, \phi)] \\ = \psi_{\text{tgt}} - 2\omega_0\Delta t + \gamma + 2\angle[f(\theta, \phi)]. \quad (2.34)$$

2.3 Amplitude Validation

By way of validating results to this point, the Signal-to-Noise Ratio (SNR) of the m^{th} received pulse (per element) is derived and compared with results in [52, 99]. The m^{th} pulse's match filtered amplitude response is derived using (2.17) and (2.33) and is given by

$$a_m = \tilde{a}|W_m(\theta, \phi)| = \frac{a_s|W_m(\theta, \phi)||f(\theta, \phi)|^2\sqrt{\sigma_{\text{tgt}}}\lambda_0}{\sqrt{(4\pi)^3}\sqrt{L_s}R_{\text{tgt}}^2}. \quad (2.35)$$

The received signal power in a_m is found by squaring (2.35) and is given by

$$S_m = \frac{a_s^2|W_m(\theta, \phi)f(\theta, \phi)|^2|f(\theta, \phi)|^2\lambda_0^2\sigma_{\text{tgt}}}{(4\pi)^3 L_s R_{\text{tgt}}^4}. \quad (2.36)$$

For a two-sided noise power spectral density of $N_o/2$ and radar system bandwidth of B , the effective radar system noise power at the matched filter input is given by $\sigma^2 = N_o B$. Using this noise power and signal power of (2.36), the SNR of the m^{th} received pulse (per element) ξ_m is given by

$$\xi_m = \frac{S_m}{\sigma^2} = \frac{P_t G_m(\theta, \phi) g(\theta, \phi) \lambda_0^2 \sigma_{\text{tgt}}}{(4\pi)^3 N_o B L_s R_{\text{tgt}}^4} \quad (2.37)$$

where

$$\begin{aligned} P_t &= a_s^2 \\ G_m(\theta, \phi) &= |W_m(\theta, \phi)f(\theta, \phi)|^2 \\ g(\theta, \phi) &= |f(\theta, \phi)|^2. \end{aligned} \quad (2.38)$$

The SNR expression in (2.37) is equivalent to the one given in [52, 99] yet accurately incorporates the effects of employing TIPD, i.e., the gain factor $G_m(\theta, \phi)$ is dependent on pulse number m and changes from pulse-to-pulse. Finally, using (2.17) and (2.38), define a final complex target amplitude term α_{tgt} as

$$\alpha_{\text{tgt}} = \tilde{a}e^{j\psi} = \frac{a_s g(\theta, \phi) \lambda_0 \sqrt{\sigma_{\text{tgt}}}}{\sqrt{(4\pi)^3} R_{\text{tgt}}^2} e^{j\psi}, \quad (2.39)$$

and use the complex notation for the array factor $W_m(\theta, \phi)$ to write the final matched filter response at the (n^{th}, p^{th}) array element from the m^{th} pulse as

$$x_{mnp}(\theta, \phi) = \alpha_{\text{tgt}} W_m(\theta, \phi) e^{j2\pi[n\vartheta_x(\theta, \phi) + p\vartheta_z(\theta)]} e^{j2\pi m\bar{\omega}_{\text{tgt}}}. \quad (2.40)$$

2.4 Data Formatting

At this point in the target model development, (2.40) differs slightly from previous planar array derivations [52] with differences including the pulse dependent array factor term $W_m(\theta, \phi)$ and the redefined received amplitude term α_{tgt} of (2.39). The data formatting process closely parallels the original work [52, 99], and collapses all element (n, p) and pulse (m) returns into a single vector. The only difference here involves redefining the temporal steering vector, denoted as $\mathbf{b}(\bar{\omega}_{\text{tgt}})$. In this context, a “steering vector” is a complex vector defining either the appropriate phase progression of either 1) a single received pulse across the array elements (either horizontal or vertical spatial steering vectors) or 2) a series of M pulses on a single element resulting from relative target motion (Doppler steering vector). For each received pulse, the horizontal steering vector $\mathbf{a}[\vartheta_x(\theta, \phi)]$, describing the phase progression across the N horizontal elements is given by [52, 99]

$$\mathbf{a}[\vartheta_x(\theta, \phi)] = [1 \quad e^{j2\pi\vartheta_x} \quad \dots \quad e^{j2\pi(N-1)\vartheta_x}]^T \quad (2.41)$$

where the array’s horizontal spatial frequency $\vartheta_x(\theta, \phi)$ was given by (2.20). Likewise, the vertical steering vector $\mathbf{e}[\vartheta_z(\theta)]$, describing the phase progression across the P vertical elements is given by [52]

$$\mathbf{e}[\vartheta_z(\theta)] = [1 \quad e^{j2\pi\vartheta_z} \quad \dots \quad e^{j2\pi(P-1)\vartheta_z}]^T. \quad (2.42)$$

where the array's vertical spatial frequency $\vartheta_z(\theta)$ was given by (2.21). For a series of M received pulses, the $M \times 1$ Doppler steering vector $\mathbf{b}(\bar{\omega}_{\text{tgt}})$ is defined as [52, 99]

$$\mathbf{b}(\bar{\omega}_{\text{tgt}}) = [1 \quad e^{j2\pi\bar{\omega}_{\text{tgt}}} \quad \dots \quad e^{j2\pi(M-1)\bar{\omega}_{\text{tgt}}}]^T. \quad (2.43)$$

2.4.1 Incorporating TIPD. To incorporate TIPD effects into the existing developmental structure, let $\mathbf{x}_{\text{vaf}}(\theta, \phi)$ be an $M \times 1$ complex vectorized array factor (vaf) containing the complex transmit array factor for each pulse in the CPI. Thus, $\mathbf{x}_{\text{vaf}}(\theta, \phi)$ is

$$\mathbf{x}_{\text{vaf}}(\theta, \phi) = \begin{bmatrix} W_1(\theta, \phi) \\ W_2(\theta, \phi) \\ \vdots \\ W_M(\theta, \phi) \end{bmatrix}. \quad (2.44)$$

The m^{th} array factor $W_m(\theta, \phi)$ can be expressed using the inner product of the phased array weights and a 2-D spatial steering vector comprised of elements from (2.41) and (2.42) [10]. For a given pulse m and target direction (θ, ϕ) , the complex array factor can be written as

$$W_m(\theta, \phi) = \{ \mathbf{e}[\vartheta_z(\theta)] \otimes \mathbf{a}[\vartheta_x(\theta, \phi)] \}^H \mathbf{w}_{\text{TX}m}, \quad (2.45)$$

where $\mathbf{w}_{\text{TX}m}$ represents an $N \times 1$ phased array transmit weight vector for the m^{th} pulse and \otimes represents the Kronecker product as defined in [42]. Using the vectorized array factor, conventional formatting can be preserved by redefining the Doppler (temporal) steering vector as follows

$$\tilde{\mathbf{b}}(\theta, \phi, \bar{\omega}_{\text{tgt}}) = \mathbf{x}_{\text{vaf}}(\theta, \phi) \odot \mathbf{b}(\bar{\omega}_{\text{tgt}}) \quad (2.46)$$

where \odot represents the Hadamard (element-wise) product.

2.5 TIPD Target Space Time Snapshot

Using the redefined Doppler steering vector $\tilde{\mathbf{b}}(\theta, \phi, \bar{\omega}_{\text{tgt}})$ of (2.46) and the original horizontal and vertical spatial steering vectors defined in (2.41) and (2.42), respectively, the *target space-time snapshot* $\boldsymbol{\chi}_t$ when TIPD is employed is given by

$$\boldsymbol{\chi}_t = \alpha_{\text{tgt}} \mathbf{e}[\vartheta_z(\theta)] \otimes \tilde{\mathbf{b}}(\theta, \phi, \bar{\omega}_{\text{tgt}}) \otimes \mathbf{a}[\vartheta_x(\theta, \phi)], \quad (2.47)$$

which is a single column vector containing radar target returns from all antenna elements and all pulses within a CPI. The space and/or time dependence of each steering vector is clearly shown in the form of $\boldsymbol{\chi}_t$ given by (2.47). Whereas in the original radar model the temporal steering vector $\mathbf{b}(\bar{\omega}_{\text{tgt}})$ was only a function of normalized target Doppler $\bar{\omega}_{\text{tgt}}$, the addition of TIPD induced an additional dependence on the ordered set of transmit antenna patterns $\mathbf{x}_{\text{vaf}}(\theta, \phi)$, creating a virtual, spatially dependent Doppler response. Thus, for a given target location (θ, ϕ) , the target's Doppler response can be controlled by modifying transmit antenna pattern characteristics. To be concise, the target space-time snapshot in (2.47) is written in an abbreviated form as

$$\boldsymbol{\chi}_t = \alpha_{\text{tgt}} \tilde{\mathbf{v}}_{\text{tgt}} \quad (2.48)$$

where $\tilde{\mathbf{v}}_{\text{tgt}}$ represents the TIPD target space-time steering vector, and the tilda is to remind the reader of the embedded array factor.

2.6 Modeling Antenna Subarrays

Dividing a phased array into multiple subarrays is done by coherently combining the outputs from specified subsets of the array's total number of physical elements. This process effectively forms a new composite array having an overall lower number of "elements" (subarrays) whose outputs are linear combinations of the physical antenna elements in a phased array. The practice of dividing an array into multiple subarrays is a well documented technique in STAP literature for reducing the spacial subspace

dimension, which is typically done to reduce the overall DOF and consequently the necessary training data quantity for STAP processing [63].

A commonly cited method for modeling subarrays in STAP radar models is documented in the sixth chapter of [63]). However, the method introduced there typically consists of DOF-reducing transforms designed for application to full (spatial) DOF pre-generated covariance matrices. For large array dimensions, this practice is undesirable since it requires the generation of a larger covariance matrix first, immediately followed by a rank-reducing transform.

The analytic modeling of subarrays in this research is done through simulating separate transmit and receive “element” patterns having different inter-element spacings. In this case, the transmit element pattern corresponds to a single, physical antenna element whereas the receive “element” pattern is redefined as resulting from a group of physical elements, or subarray. This new received element pattern is derived based on a combination of subarray weights and physical element patterns. As implemented, this technique has only been used to model non-overlapping subarrays (no subarray shares elements with other subarrays) and the array sizes and subarray groupings were constrained to provide uniformly sized subarrays with no array elements going unused. Finally, the inter-element spacing is lengthened to match the distance between the resultant subarray phase-centers.

This method of direct analytic subarray modeling avoids the necessity of first generating the full covariance matrix, prior to reducing it via a subarray transform. Further, a fully adaptive planar array illumination pattern can be simulated on transmit while the received radar data is simulated at the reduced spatial dimensionality of the subarrayed planar array. Using analytically modeled subarrays on receive also allows for the simulation of larger transmit arrays without substantially increasing computational load and memory requirements. The utility of these benefits is made clear by techniques employed in Chapter V.

To integrate the subarray process into the target model previously presented, the transmit and receive element patterns in the previous development are first separated. Note that only the transmit element pattern is used in the analytic development prior to (2.17), which marks the first appearance of the receive element pattern. Throughout the development, the transmit and receive element patterns are simply multiplied together. To separate them, redefine (2.17) as

$$\tilde{a} = \frac{a_s |f_{\text{tx}}(\theta, \phi)| |f_{\text{rx}}(\theta, \phi)| \sqrt{\sigma_{\text{tgt}}} \lambda_0}{\sqrt{(4\pi)^3 R_{\text{tgt}}^2}}. \quad (2.49)$$

where f_{tx} denotes the element voltage pattern on transmit and f_{rx} denotes the element voltage pattern on receive. The element patterns appear next in the amplitude validation section where the matched filter amplitude response given in (2.35) is redefined using (2.49) in place of (2.17), resulting in

$$a_m = \tilde{a} |W_m(\theta, \phi)| = \frac{a_s |W_m(\theta, \phi)| |f_{\text{tx}}(\theta, \phi)| |f_{\text{rx}}(\theta, \phi)| \sqrt{\sigma_{\text{tgt}}} \lambda_0}{\sqrt{(4\pi)^3 R_{\text{tgt}}^2}}. \quad (2.50)$$

Given (2.50), the received signal power previously given by (2.36) is redefined as

$$S_m = \frac{a_s^2 |W_m(\theta, \phi) f_{\text{tx}}(\theta, \phi)|^2 |f_{\text{rx}}(\theta, \phi)|^2 \lambda_0^2 \sigma_{\text{tgt}}}{(4\pi)^3 R_{\text{tgt}}^4}. \quad (2.51)$$

The impact of using subarrays can now be incorporated into a redefined per element, per pulse SNR expression. Using the previous SNR expression of (2.37), the new SNR expression is given by

$$\xi_m = \frac{S_m}{\sigma^2} = \frac{P_t G_m(\theta, \phi) g_{\text{rx}}(\theta, \phi) \lambda_0^2 \sigma_{\text{tgt}}}{(4\pi)^3 N_0 B N_{\text{sub}} P_{\text{sub}} L_s R_{\text{tgt}}^4} \quad (2.52)$$

where N_{sub} and P_{sub} represent the number of horizontal and vertical elements in the receive subarray (discussed next) and where

$$\begin{aligned} P_t &= a_s^2 \\ G_m(\theta, \phi) &= |W_m(\theta, \phi) f_{\text{tx}}(\theta, \phi)|^2 \\ g_{\text{rx}}(\theta, \phi) &= |f_{\text{rx}}(\theta, \phi)|^2. \end{aligned} \tag{2.53}$$

Note that the coherent signal gain due to summing multiple receive elements (which scales as a function of $[N_{\text{sub}} P_{\text{sub}}]^2$) is accounted for in the new element gain pattern magnitude $g_{\text{rx}}(\theta, \phi)$, and the non-coherent noise gain [67] due to the summation is incorporated through the new $N_{\text{sub}} P_{\text{sub}}$ terms in the denominator. Finally, the new complex target amplitude term incorporating subarray effects is based on (2.49) and (2.53) is given by

$$\alpha_{\text{tgt}} = \tilde{a} e^{j\psi} = \frac{a_s |f_{\text{tx}}(\theta, \phi)| |f_{\text{rx}}(\theta, \phi)| \lambda_0 \sqrt{\sigma_{\text{tgt}}}}{\sqrt{(4\pi)^3 R_{\text{tgt}}^2}} e^{j\psi}, \tag{2.54}$$

Note, when the transmit and receive element patterns are identical, substituting $f(\theta, \phi) = f_{\text{tx}}(\theta, \phi) = f_{\text{rx}}(\theta, \phi)$ in (2.49) through (2.54) results in the original expressions of (2.17), (2.35), (2.36), (2.38), and (2.39). With the transmit and receive “element” patterns now defined separately, the modeling of disjoint subarrays is accomplished by forming subarray groups and redefining the receive element count and spacing as

$$N' = \frac{N}{N_{\text{sub}}} \tag{2.55}$$

$$P' = \frac{P}{P_{\text{sub}}} \tag{2.56}$$

$$d'_x = d_x N_{\text{sub}} \tag{2.57}$$

$$d'_z = d_z P_{\text{sub}} \tag{2.58}$$

where N_{sub} is the number of element columns in one subarray, and P_{sub} is the number of element rows in one subarray. While N, P, d_x , and d_z are used for defining the transmit illumination pattern, i.e., the transmit array factor given in (2.45), N', P', d'_x , and d'_z are used to describe the array on receive. This new receive array geometry is incorporated throughout the development by exchanging the new “primed” terms in (2.55) with the original “non-primed” terms in (2.20), (2.21), (2.41), and (2.42). Finally, the new receive element pattern is given by

$$g_{\text{rx}}(\theta, \phi) = |W_{\text{sub}}(\theta, \phi) f_{\text{tx}}(\theta, \phi)|^2, \quad (2.59)$$

recalling that the same *physical* antenna elements are used for both transmit and receive. Since no subarraying is done on transmit, $f_{\text{tx}}(\theta, \phi)$ represents the physical element pattern and $W_{\text{sub}}(\theta, \phi)$ the array factor for the subarray, defined as

$$W_{\text{sub}}(\theta, \phi) = \mathbf{w}_{\text{sub}}^H \{ \mathbf{e}_{\text{sub}} [\vartheta_z(\theta)] \otimes \mathbf{a}_{\text{sub}} [\vartheta_x(\theta, \phi)] \}, \quad (2.60)$$

Note that (2.60) has the same form as (2.45) since each receive “element” (subarray) is effectively a mini phased array. In (2.60), $\mathbf{w}_{\text{sub}}^H$ represents the subarray weights, and \mathbf{e}_{sub} and \mathbf{a}_{sub} are the elevation and azimuth steering vectors for the subarray, given as

$$\mathbf{a}_{\text{sub}} [\vartheta_x(\theta, \phi)] = [1 \quad e^{j2\pi\vartheta_x} \quad \dots \quad e^{j2\pi(N_{\text{sub}}-1)\vartheta_x}]^T, \quad (2.61)$$

and

$$\mathbf{e}_{\text{sub}} [\vartheta_z(\theta)] = [1 \quad e^{j2\pi\vartheta_z} \quad \dots \quad e^{j2\pi(P_{\text{sub}}-1)\vartheta_z}]^T. \quad (2.62)$$

As is typical for subarrays, the subarray weights $\mathbf{w}_{\text{sub}}^H$ are calculated (using a simple beamforming constraint) to provide maximum gain in the transmit direction. It is noteworthy to mention that disjoint subarrays invariably cause grating lobe problems [62] and are seldom used in practice (one exception is elevation beamforming where an entire column of array elements is treated as one element and there are no grating lobes generated). The utility of subarray modeling is made apparent when

simulating Space Adaptive Illumination Patterns (SAIP) in close-in sensing environments, the details of which are provided in Chapter V.

2.7 Clutter Response Model

Using the target response model in the previous section, the original clutter model derivation of [52, 61, 99] is similarly modified to accommodate Transmit Interpulse Pattern Diversity (TIPD). The clutter model is based on the summation of point target returns, where each point target represents a slice or “patch” of terrain located in the target range gate. Like the target model, each clutter patch is modeled as a single point scatterer, temporally-stable throughout the CPI of interest (i.e., unchanging over M pulses). The point-scatterer representation arises from the vector sum of many independent equivalent elementary scatterers in the patch [23]. Since the individual clutter patches are modeled as point-target returns, the clutter model is extended by simply supplanting the original target/clutter patch (i.e., point-scatterer) model with the TIPD target model (2.47) developed in the previous section. The original planar array clutter model derivation is provided in [52], the details of which are not repeated here, except those portions which are necessary to explain the model’s parameters and noted TIPD modifications.

2.7.1 TIPD Clutter Space Time Snapshot. Maintaining notation consistent with [52], the new *clutter space-time snapshot*, incorporating the effects of TIPD, is given by [27]

$$\mathbf{x}_c = \sum_{i=0}^{N_r-1} \sum_{k=0}^{N_c-1} \tilde{\alpha}_{ik} \mathbf{e}[\vartheta_z(\theta_i)] \otimes \tilde{\mathbf{b}}(\theta_i, \phi_k, \bar{\omega}_{ik}) \otimes \mathbf{a}[\vartheta_x(\theta_i, \phi_k)], \quad (2.63)$$

where N_r indicates the total number of range rings being considered, N_c is the number of clutter “patches” segmenting each ring, $\tilde{\alpha}_{ik}$ represents the received voltage magnitude and phase from the i^{th} , k^{th} clutter patch, and the steering vectors \mathbf{e} , $\tilde{\mathbf{b}}$, and \mathbf{a} fully account for the received phase and array factor transmit gain (embedded in the

b term) of each returning pulse at each array element. The complex random return from each clutter patch (after matched filtering) is represented by [99]

$$\tilde{\alpha}_{ik} = a_{ik} e^{j\psi_{ik}}, \quad (2.64)$$

where ψ_{ik} represents the random phase response and a_{ik} is the random clutter patch voltage response. The steering vectors previously defined in (2.41) and (2.42) now point to the k^{th} clutter patch on the i^{th} range ring. Figure 2.2 provides a pictorial representation of the clutter model geometry for reference.

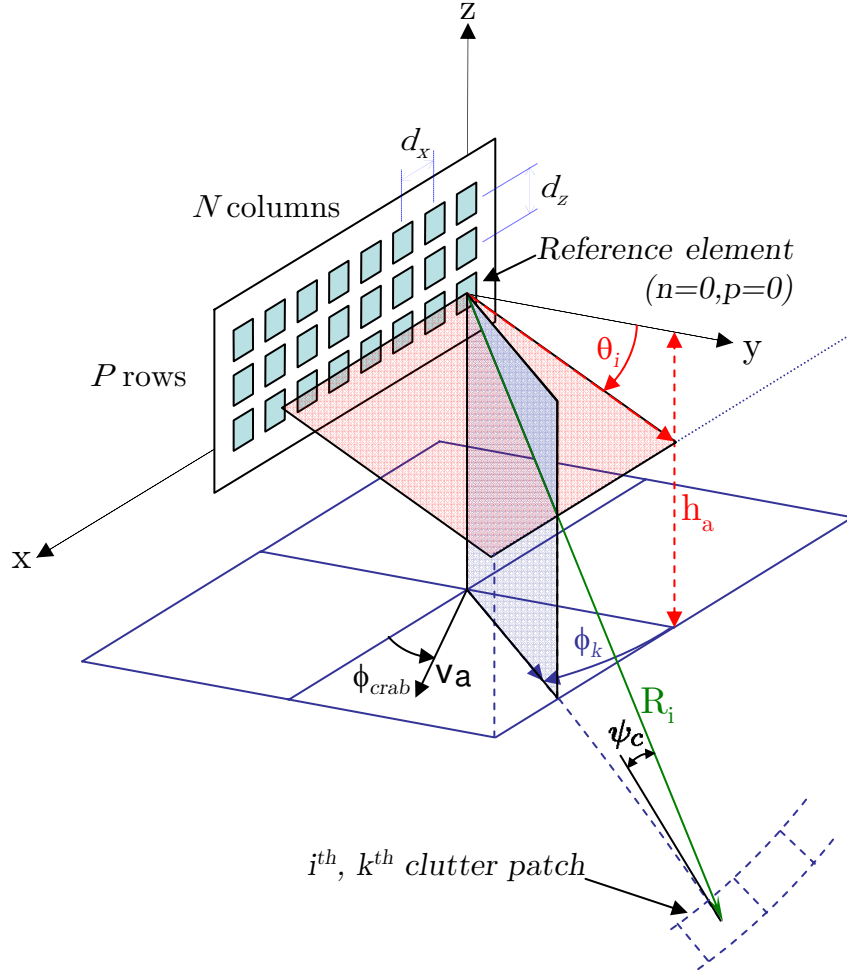


Figure 2.2: Airborne array geometry for the planar array clutter model.

The values for ϕ_k and θ_i are given by

$$\phi_k = \left\{ \frac{k2\pi}{N_c} : k = 0, 1, 2, \dots, N_c - 1 \right\} \quad (2.65)$$

and

$$\theta_i = -\sin^{-1} \left[\frac{R_i^2 + h_a(h_a + 2a_e)}{2R_i(a_e + h_a)} \right], \quad (2.66)$$

where h_a is the aircraft altitude Above Ground Level (AGL), and a_e is the effective radius of the earth, using the 4/3 radius model. R_i is the range to the i^{th} range ring given by

$$R_i = \{R_{\text{tgt}} + iR_u : i = 0, 1, \dots, N_r - 1\}. \quad (2.67)$$

The total number of real plus ambiguous range rings N_r is given by

$$N_r = \left\lfloor \frac{R_h}{R_u} \right\rfloor, \quad (2.68)$$

where $\lfloor x \rfloor$ denotes largest integer not exceeding x and R_h is the range to the horizon and R_u is the radar's unambiguous range. These ranges are given by

$$R_h = \sqrt{h_a^2 + 2h_a a_e} \quad (2.69)$$

$$R_u = \frac{cT_r}{2}, \quad (2.70)$$

where T_r is the pulse repetition interval. The Doppler steering vector $\tilde{\mathbf{b}}(\theta_i, \phi_k, \bar{\omega}_{ik})$ is as defined in (2.46), with the Doppler frequency of the k^{th} clutter patch on the i^{th} range ring defined as

$$\bar{\omega}_{ik} = \frac{2v_a \cos(\theta_i) \sin(\phi_k + \phi_{\text{crab}})}{\lambda_0 f_r} \quad (2.71)$$

where v_a represents the aircraft velocity and ϕ_{crab} represents the aircraft crab angle [16]. As a side note, setting the crab angle to +90 degrees allows this clutter model to simulate a forward-looking array [20]. Applying AIP to forward looking arrays is an area for further research.

2.7.2 *TIPD Clutter Covariance.* While the clutter snapshot of (2.63) is useful for monte-carlo analysis and training data simulation, the clairvoyant (true) clutter covariance matrix for a given range-gate is necessary for calculating performance bounds and SINR analysis. This clutter covariance is defined as

$$\mathbf{R}_c = \mathcal{E}\{\boldsymbol{\chi}_c \boldsymbol{\chi}_c^H\}. \quad (2.72)$$

and is thus dependent on the first and second order statistics of the random complex clutter patch returns $\tilde{\alpha}_{ik}$. It is common to assume the real and imaginary components of (2.64) to be jointly Gaussian and independent, though the next section will explore ways to relax this assumption. Regardless of the distribution chosen, the random voltage clutter response is historically [99] subject to two statistical constraints. First, it is assumed to be zero mean, i.e.,

$$\mathcal{E}\{\tilde{\alpha}_{ik}\} = 0, \quad (2.73)$$

which guarantees that (2.72) is a covariance matrix rather than a correlation matrix. Secondly, it is assumed that the clutter patches are uncorrelated, i.e.,

$$\mathcal{E}\{\tilde{\alpha}_{ik} \tilde{\alpha}_{mn}^*\} = \sigma^2 \xi_{ik} \delta_{i,m} \delta_{k,n}, \quad (2.74)$$

where ξ_{ik} is the single element (*transmit* and receive), single pulse clutter-to-noise power ratio (CNR) and $\delta_{i,m} \delta_{k,n}$ are two dirac delta functions which are zero unless $i = m$ and $k = n$, in which case they are both one. Without the array factor gain, ξ_{ik} represents the clutter-to-noise ratio assuming a single transmit and receive element. As a result of employing TIPD, the clutter-to-noise ratio (based on 2.37) is now defined as

$$\xi_{ik} = \frac{P_t g_{\text{tx}}(\theta_i, \phi_k) g_{\text{rx}}(\theta_i, \phi_k) \lambda_0^2 \sigma_{ik}}{(4\pi)^3 N_0 B N_{\text{sub}} P_{\text{sub}} L_s R_i^4}, \quad (2.75)$$

where P_t is transmit power, $g_{\text{tx}}(\theta_i, \phi_k)$ is the transmit element power pattern, $g_{\text{rx}}(\theta_i, \phi_k)$ is the receive element power pattern, λ_0 is the wavelength, σ_{ik} is the RCS of the k^{th}

clutter patch on the i^{th} range ring, N_0 is thermal noise power, B is system bandwidth, N_{sub} is the number of horizontal elements in a receive subarray, P_{sub} is the Number of vertical elements in a receive subarray, L_s is the system loss factor, and R_i is the range to the i^{th} range ring.

The uncorrelated clutter patch constraint (2.74) greatly simplifies the final expression for \mathbf{R}_c by eliminating cross-terms arising from (2.72). If (2.73) and (2.74) are satisfied, then (2.72) can be expressed as

$$\begin{aligned} \mathbf{R}_c = \mathcal{E}\{\boldsymbol{\chi}_c \boldsymbol{\chi}_c^H\} &= \sigma^2 \sum_{i=0}^{N_r-1} \sum_{k=0}^{N_c-1} \xi_{ik} \mathbf{e}[\vartheta_z(\theta_i)] \mathbf{e}^H[\vartheta_z(\theta_i)] \\ &\quad \otimes \tilde{\mathbf{b}}(\theta_i, \phi_k, \bar{\omega}_{ik}) \tilde{\mathbf{b}}^H(\theta_i, \phi_k, \bar{\omega}_{ik}) \otimes \mathbf{a}[\vartheta_x(\theta_i, \phi_k)] \mathbf{a}^H[\vartheta_x(\theta_i, \phi_k)] \end{aligned} \quad (2.76)$$

where CNR ξ_{ik} is defined in (2.75). Thus, the only changes required to the original clutter model [52, 61, 99] to reliably account for TIPD effects include 1) redefining the Doppler steering vector as $\tilde{\mathbf{b}}(\theta_i, \phi_k, \bar{\omega}_{ik})$ based on (2.46) and 2) using the modified CNR of (2.75) in clutter covariance analysis, which transfers the array pattern scaling from the latter to the former. It can be shown that for standard (non-varying) transmit pattern cases and complex Gaussian voltage modeling that (2.76) yields results equivalent to the original models [52, 99]. The following section examines the clutter return voltage model and proposes a new (w.r.t. [52, 61, 99]) generalization based on assumptions imposed on the clutter amplitude and phase distributions.

2.8 Simulation of Clutter Voltage Models

The challenge with statistically characterizing $\tilde{\alpha}_{ik}$ in (2.64) is embodied in specifying the joint probability density function of $N_c \times N_r$ (clutter patches times range rings) correlated complex random variables. In original model development of [99] and much of the subsequent STAP research, both the real and imaginary components of $\tilde{\alpha}_{ik}$ are modeled as independent, zero mean Gaussian random variables which are uncorrelated for all (i, k) (patches). Under these assumed conditions, the amplitude

a_{ik} of $\tilde{\alpha}_{ik}$ is Rayleigh distributed, the phase ψ_{ik} is uniform, both (2.73) and (2.74) are satisfied, and \mathbf{R}_c completely determines the clutter's joint probability density function as a multi-variate Gaussian distribution. However, challenging clutter environments are rarely modeled accurately by a multi-variate Gaussian voltage model, and STAP training data snapshots (taken from adjacent range cells) are rarely (if ever) homogeneous [93]. Entire volumes have been written on modeling airborne clutter statistics [14, 67, 98], with the widely varying clutter voltage models being highly dependent on the applicable clutter environment and surveillance geometry.

It is useful to consider the validity of the TIPD clutter model for other than standard Gaussian voltage models. The possible use of TIPD as a tool for knowledge-based STAP and adaptive transmit paradigms is predicated on exploiting *a priori* clutter information—especially non-Gaussian characteristics such as discrete interferers and targets in the training data. Some clutter models, such as those used in the KASSPER program [45], rely on Digital Terrain Elevation Data (DTED) and physics-based scattering models to calculate RCS on a patch-by-patch basis [12]. KA-STAP and adaptive transmit paradigms require the repeatable simulation of heterogeneous clutter, thus rendering purely homogeneous statistical clutter models nearly obsolete for adaptive transmit research. Therefore, it is desirable to establish the minimum constraints on the pdf of $\tilde{\alpha}_{ik}$, less restrictive than i.i.d. multi-variate Gaussian, for which the clutter model of (2.76) remains valid.

The generation of a valid covariance matrix \mathbf{R}_c as given by (2.76) requires that only the first and second-order statistics of $\tilde{\alpha}_{ik}$ meet conditions specified in (2.73) and (2.74). It is not necessary for \mathbf{R}_c to be a sufficient statistic for $\tilde{\alpha}_{ik}$ in order for \mathbf{R}_c to be a valid clairvoyant covariance matrix, as will often be the case for non-Gaussian clutter statistics. The next section explores the assumptions necessary for the conditions of (2.73) and (2.74) to be satisfied.

2.8.1 Incorporating Other Statistical and Deterministic Clutter Models. The extended STAP clutter model proposed here is not explicitly limited to a particular

voltage clutter response model. Many clutter voltage response models exist [23, 84]. The purpose here is to outline necessary conditions that the joint pdf of $\tilde{\alpha}_{ik}$ must meet to generate a valid clairvoyant clutter matrix as described by (2.76).

Certainly, any clutter voltage model which assumes statistical independence between clutter patch responses and a zero mean complex voltage satisfies the criteria, regardless of the distribution. However, adjacent clutter cells are not always statistically uncorrelated, resulting in the need to investigate radar performance in correlated clutter. In general, such an investigation requires abandoning the clutter covariance given by (2.76) because the cross-terms of the expectation operation in (2.72) no longer cancel. However, careful analysis of the complex clutter model suggests an alternate approach.

Amplitude characteristics of the clutter returns have been extensively studied [14, 67, 98, 99]. Such studies have found that clutter amplitude characteristics are dependent upon many factors and a plethora of statistical distribution models have emerged. Furthermore, such studies have commonly considered the phase response from a given clutter patch as being uniformly distributed regardless of environmental factors. As sensed by the radar, the composite phase response is derived from the superposition of many point-scatterers that are randomly distributed throughout the clutter patch [23]. While the amplitude response is dependent on the RCS, the phase response of an elemental scatterer is dependent on its distance from the radar. For example, at a transmit frequency of 1.24 GHz, a 180 degree phase shift is induced by only 12.0 cm of relative displacement along the antenna line-of-sight (LOS). Given the relatively short radar wavelength compared to the clutter patch size (often on the scale of 100 meters “deep”) and the independence of scatterer placement from cell-to-cell, the composite phase response is well approximated as uniform.

Taking the analysis one step further, there seems to be a natural statistical independence between the *composite* phase and amplitude random variables *emph-* within a clutter cell, regardless of their individual statistical distributions. The basis

for this natural independence is rooted in the assumption that the size of an elemental scatterer is statistically independent of its position. Even if a clutter cell is dominated by a single structure, such as building, estimating the phase response of a radar return centered at 1.24 GHz (24.0 cm wavelength) is equivalent to estimating it's line-of-sight distance within an ambiguous span of 24.0 cm. Although physically the composite phase and amplitude are inextricably linked, statistically there is little to no information upon which to build a joint distribution between the composite amplitude and phase response of a simulated clutter cell. In other words, the phase cannot be statistically predicted from the amplitude or vice-versa.

Given an assumed statistical independence between the composite clutter patch amplitude and phase response, the desired mean and power statistics necessary to validate the clairvoyant covariance matrix given by (2.76) can be achieved using an *arbitrary* statistical distribution for clutter patch amplitude a_{ik} , including those correlated across range cells, given the clutter patch *phase* is uniformly distributed and statistically independent from adjacent clutter patches and across clutter rings.

2.8.2 Validity Of Covariance Model For An Arbitrary Clutter Reflectivity Function. Proof:

Let $\tilde{\alpha}_x = a_x e^{j\psi_x}$ be the complex clutter patch response of the x^{th} clutter patch, chosen from the set \mathbb{P} of all clutter patches in a given range gate. Let each clutter patch have a unique *amplitude* probability density function (pdf) such that the pdf of the x^{th} clutter patch random amplitude a_x is given by $f_{a_x}(A_x)$ where A_x is the dummy variable for a_x . Let the clutter patch phase Random Variable (RV) ψ be uniformly distributed on $[0 \ 2\pi)$ and independent, identically distributed (i.i.d.) across \mathbb{P} . Thus, for any two clutter patches $x, y, \in \mathbb{P}$

$$f_{\psi_x}(\Psi_x) = f_{\psi_y}(\Psi_y) = \frac{1}{2\pi}, \quad 0 \leq \psi_x, \psi_y < 2\pi \quad (2.77)$$

$$f_{\psi_x, \psi_y}(\Psi_x, \Psi_y) = f_{\psi_x}(\Psi_x) f_{\psi_y}(\Psi_y) \quad (2.78)$$

Further, let the *amplitude* and the *phase* be statistically independent both within and across all patches in \mathbb{P} , i.e.,

$$f_{a_x, \psi_x}(\mathbf{A}_x, \Psi_x) = f_{a_x}(\mathbf{A}_x) f_{\psi_x}(\Psi_x) \quad (2.79)$$

$$f_{a_x, \psi_y}(\mathbf{A}_x, \Psi_y) = f_{a_x}(\mathbf{A}_x) f_{\psi_y}(\Psi_y) \quad (2.80)$$

Then for any clutter patch $x \in \mathbb{P}$

$$\begin{aligned} \mathcal{E}\{\tilde{\alpha}_x\} &= \mathcal{E}\{a_x e^{j\psi_x}\} \\ &= \mathcal{E}\{a_x\} \mathcal{E}\{e^{j\psi_x}\} \\ &= \mathcal{E}\{a_x\} [\mathcal{E}\{\sin(\psi_x)\} + j\mathcal{E}\{\cos(\psi_x)\}] \end{aligned} \quad (2.81)$$

Noting that

$$\begin{aligned} \mathcal{E}\{\sin(\psi_x)\} &= \int_{-\infty}^{\infty} \sin(\zeta) f_{\psi_x}(\zeta) d\zeta = \frac{1}{2\pi} \int_0^{2\pi} \sin(\zeta) d\zeta = 0 \\ \mathcal{E}\{\cos(\psi_x)\} &= \int_{-\infty}^{\infty} \cos(\zeta) f_{\psi_x}(\zeta) d\zeta = \frac{1}{2\pi} \int_0^{2\pi} \cos(\zeta) d\zeta = 0, \end{aligned} \quad (2.82)$$

then,

$$\begin{aligned} \mathcal{E}\{\tilde{\alpha}_x\} &= \mathcal{E}\{a_x\} [\mathcal{E}\{\sin(\psi_x)\} + j\mathcal{E}\{\cos(\psi_x)\}] \\ &= 0 \end{aligned} \quad (2.83)$$

which satisfies the first requirement of (2.73) for all i, k without requiring any conditions on the amplitude distribution. Next, consider the power statistic for the x^{th} clutter patch

$$\begin{aligned} \mathcal{E}\{\tilde{\alpha}_x \tilde{\alpha}_x^*\} &= \mathcal{E}\{a_x e^{j\psi_x} a_x e^{-j\psi_x}\} \\ &= \mathcal{E}\{a_x^2\} \\ &= \sigma^2 \xi_x \end{aligned} \quad (2.84)$$

where ξ_x is the desired clutter-to-noise power ratio for the x^{th} clutter patch. Similarly, the cross-correlation between any two clutter patches $x \neq y, x, y \in \mathbb{P}$ is

$$\begin{aligned}
\mathcal{E}\{\tilde{\alpha}_x \tilde{\alpha}_y^*\} &= \mathcal{E}\{a_x e^{j\psi_x} a_y e^{-j\psi_y}\} \\
&= \mathcal{E}\{a_x a_y\} \mathcal{E}\{e^{j\psi_x} e^{-j\psi_y}\} \\
&= \mathcal{E}\{a_x a_y\} \mathcal{E}\{e^{j\psi_x}\} \mathcal{E}\{e^{-j\psi_y}\} \\
&= \mathcal{E}\{a_x a_y\} \cdot 0 \\
&= 0 \quad \forall x \neq y
\end{aligned} \tag{2.85}$$

where the 4th line in (2.85) uses results from (2.81) through (2.83). Finally, results of (2.84) and (2.85) are combined using the two-dimensional Dirac delta function $\delta_{x,y}$ and written as

$$\mathcal{E}\{\tilde{\alpha}_x \tilde{\alpha}_y^*\} = \sigma^2 \xi_x \delta_{x,y} , \tag{2.86}$$

which satisfies the second requirement of (2.74) for all i, k without requiring any conditions on the amplitude distribution.

Q.E.D.

Given the assumptions used above remain valid, the proof shows that (2.76) generates a valid clairvoyant covariance matrix given any *arbitrary* joint pdf for clutter patch *amplitudes*. This includes distributions that may be correlated from patch-to-patch. The clutter model given by (2.76) can also account for deterministic-based modeling of the clutter patch amplitudes, an area previously studied in [95] and employed in the generation of the KASSPER data [45]. Considering perhaps the simplest deterministic amplitude case, i.e., a non-random amplitude response derived from (2.39) and given by

$$a_{ik} = \frac{a_s g(\theta_i, \phi_k) \lambda_0 \sqrt{\sigma_{ik}}}{\sqrt{4\pi^3 R_i^2}}. \tag{2.87}$$

This amplitude response, when combined with a uniformly distributed phase response for ψ_{ik} in (2.64), yields a complex $\tilde{\alpha}_{ik}$ having the desired statistics which satisfy (2.73) and (2.74) such that the clairvoyant covariance matrix given by (2.76) is valid.

2.9 Training Data Modeling

Equations (2.63) and (2.76) are used to calculate the clutter snapshot and covariance matrix for a single range gate. To explore adaptive receiver algorithms, the covariance matrix must be estimated. The dominate technique for estimating the covariance matrix and applying it to generate adaptive filters is known as Sampled Matrix Inversion (SMI) [86]. The SMI technique provides the maximum likelihood estimator for a Gaussian distributed clutter covariance matrix using clutter snapshots taken from adjacent range bins. The method assumes that these clutter snapshots, referred to as Training Data (TD), are statistically independent and identically distributed (i.i.d.)—i.e., they obey the same multi-variate Gaussian PDF. Thus, to calculate estimated covariance matrix each unambiguous range gate (or range “bin”) must be simulated to form the TD for STAP processing.

Most TD synthesis methods can be categorized into two fundamental types: those that generate i.i.d. TD and those that do not. Statistical i.i.d. TD is generated from the same, known covariance matrix describing the target range cell of interest (without the target present). This type of TD satisfies the cardinal assumption of the early STAP framework [86] and is often used for Monte-Carlo simulation of fully and partially adaptive STAP processors (note, optimum processors don’t require training data). Large quantities of TD can be quickly generated by “coloring” white data where the coloration is based on the known, clairvoyant covariance matrix of a given range cell. However, this process fails to simulate many of the real-world problems that greatly inhibit STAP performance, such as non-stationary clutter conditions, heterogeneous clutter, and amplitude fluctuations due to propagation loss and non-uniform illumination.

Additionally, the use of planar arrays create 3-D snapshots that are inherently non-stationary in elevation. Given the planar array’s inherent ability to discern the elevation angle of the energy received, data snapshots taken at varying elevation angles “record” or store that energy at different spatial locations in the 3D vector space. In

other words, the 3D planar array data is inherently non-stationary in the elevation dimension. While for most applications this is not an issue given the high Range-to-Height (R/H) ratios encountered and minimal elevation diversity, it becomes an issue for close-in sensing applications which are considered as part of this research.

The alternative to i.i.d. clutter modeling is to model each range gate independently, i.e., on a snapshot-by-snapshot basis. This method removes many limitations imposed by synthesizing i.i.d. TD and is the approach used throughout this research. This method is capable of accounting for non-homogeneous and non-stationary effects in the range (elevation) dimension. Modeling each range gate allows for site-specific modeling which is necessary for simulating knowledge-based radar data. Simulating targets in the training data is an example of knowledge-based radar TD and is covered in Chapter V.

2.10 Modeling Subarrays in the Clutter Model

The analytic modeling of subarrays is most beneficial when simulating the clutter. The same subarray modeling technique which was outlined in Section 2.6 for the target subarray model, can be readily applied to the clutter snapshot of (2.63) and covariance matrix of (2.76). The principal reason for using analytic subarray modeling is to reduce computational load and memory requirements when simulating scenarios utilizing elevation beamforming.

Elevation beamforming (each column of the phased array forms a single subarray) is probably the most common subarray approach used in STAP systems. For example, 8 rows of elements were combined into 2 rows through elevation beamforming in the commonly cited MCARM program [63]. Elevation subarrays can also be formed in planar arrays to increase radiated power levels and to reduce the elevation beamwidth, while still generating an equivalent linear array for 2-D (azimuth-Doppler) STAP processing.

For close-in sensing applications using a planar array, there is significant elevation diversity over the scene of interest and an adaptive subarray technique is implemented on receive. Specifically, elevation beamforming is accomplished individually for each snapshot of data such that the subarray elevation beam has maximum gain in the direction of the clutter elevation angle. This invokes the common hardware assumption for STAP processing in which the output from each array element is individually sampled. This elevation/range-dependent beamforming is implemented using the analytic subarray method introduced previously and results in substantial savings in computational time and required memory.

2.11 *Noise Model*

The planar array noise model used in this work is identical to that of the original model development [52], where the noise sampled on each element and pulse is assumed independent, resulting in a noise covariance matrix given by

$$\mathbf{R}_n = \sigma^2 \mathbf{I}_{MNP} \quad (2.88)$$

Summing the noise and clutter covariance matrices produces the signal-dependent clairvoyant covariance matrix, \mathbf{R} given by

$$\mathbf{R} = \mathbf{R}_c + \mathbf{R}_n \quad (2.89)$$

Since jammers are by definition signal independent interference, their signals are not affected by AIP and thus they are not considered within the scope of this research. As previously discussed, while AIP cannot mitigate jamming effects it may “free up” resources for STAP-like receiver processors to more effectively mitigate jammers by simplifying clutter suppression.

The use of AIP also has no effect on the noise model. The only necessary modification of the model used in this research is to support the subarray modeling

mentioned previous sections. The subarray process increases the noise power as the non-coherent independent noise samples are summed at the subarray output. The noise power increases as a linear function of the number of samples summed over [67], yielding a new noise covariance matrix which exhibits stronger power but has lower dimensionality. The resultant subarray covariance matrix is given by

$$\mathbf{R}'_n = \sigma^2 N_{\text{sub}} P_{\text{sub}} \mathbf{I}_{MN'P'} \quad (2.90)$$

where N_{sub} and P_{sub} are the subarray dimensions and N' and P' were previously defined as the new dimensions of the received array.

2.12 Summary

This chapter provides the analytic development for extending existing radar models to incorporate arbitrary pulse-dependent antenna patterns, a capability termed Transmit Interpulse Pattern Diversity (TIPD). This capability was incorporated into existing target, clutter, and noise models previously developed for conducting STAP research [52, 99]. The ability to analytically model disjoint (non-overlapping) receive subarrays was also developed and incorporated into the models. Incorporating subarrays allows the model to simulate planar transmit arrays and elevation beamformed linear arrays at the subarrayed dimensions, greatly reducing computational load and memory requirements of previous subarray modeling techniques. This section also proves validation of the provided clutter covariance model to accurately incorporate any statistical and/or deterministic clutter reflectivity models. The models developed herein unlock a previously unexplored capability which extends the knowledge base of fully adaptive radar research to include Adaptive Illumination Patterns (AIP). These patterns are used in subsequent documentation contained herein to investigate the impacts of Space Time Illumination Patterns (STIP) in Chapter IV and Scene Adaptive Illumination Patterns (SAIP) in Chapter V.

While the current Space-Time Adaptive Processing (STAP) paradigm assumes a constant transmit pattern during the Coherent Processing Interval (CPI), the ability to perform space-time beamforming on *transmit* has been demonstrated by allowing the antenna transmit pattern to vary on an interpulse (pulse-to-pulse) basis. This capability is referred to as Transmit Interpulse Pattern Diversity (TIPD). Unfortunately, the nature of STIP precludes benchmarking the performance of transmit pattern synthesis algorithms using existing benchmark radar data sets such as those from the Multi-Channel Airborne Radar Measurement (MCARM) and Knowledge-Aided Sensor Signal Processing Expert Reasoning (KASSPER) programs. Investigating and quantifying Fully Adaptive Radar (FAR) paradigms which incorporate STIP is therefore most efficiently accomplished using modeling and simulation of end-to-end radar performance.

This work provides a detailed analytic development and extension to existing target and clutter radar models, including a new capability to incorporate STIP. Logical assumptions are introduced that (when invoked) extend validity of the clutter covariance matrix development to include any arbitrary voltage amplitude model, statistical or deterministic. These models are offered as a tool for conducting FAR research incorporating STIP through transmit-to-receive radar system simulation.

III. Overview of STAP Processors

Space Time Adaptive Processing (STAP) is a term used to describe an entire area of research aimed at improving radar performance through developing and applying adaptive filters to sampled radar data. Although the main contributions of this research are in the realm of Adaptive Illumination Patterns (AIP), one of the chief beneficiaries of AIP technology is inevitably the radar's receive processor. In fact, any potential performance gains due to AIP implementation are inherently unrealized until the received data is processed. Therefore, the receiver processing method(s) which are employed in conjunction with AIP, to include STAP, influence the AIP design criteria. Such is the nature of Fully Adaptive Radar (FAR), where the transmitter and receiver are jointly designed to achieve maximum synergy. Therefore, an overview of common STAP techniques is necessary to understand both the design criteria for AIP as well as the reasons for noted performance improvements.

3.1 *STAP Framework*

Prior to addressing STAP filter synthesis, the general framework for applying filters to digitally sampled radar data is outlined. An adaptive (digital) filter consists of a $NMP \times 1$ vector of complex weights \mathbf{w} synthesized by some adaptive filtering method and constrained such that $\mathbf{w}^H \mathbf{w} > 0$ and the trivial zero solution is avoided. These weights operate on a $NMP \times 1$ sampled radar data snapshot \mathbf{x} containing a single complex radar data sample for each pulse (M total pulses) received by each element (from a $N \times P$ phased array) arranged in the same Kronecker product structure evident in (2.47) and (2.63). Each sample in space-time snapshot \mathbf{x} represents the peak output of the transmit signal's matched filter response for a specific element, pulse, and range gate.

The radar data snapshot is digitally filtered by \mathbf{w} via an inner product to produce a scalar observable. The observable is then incorporated into a "detection statistic" (usually by applying an adaptive scale factor), whose construction depends on the statistical estimator used to test for target presence. The resultant detection statistic

is compared to a decision/detection threshold γ (derived for a particular false alarm rate) to determine if a target is present (H_1 hypothesis) or not (H_0 hypothesis). For example, letting the detection statistic be the filter output, the binary hypothesis test can be written as

$$\mathbf{w}^H \boldsymbol{\chi} \underset{H_0}{\overset{H_1}{\gtrless}} \gamma, \quad (3.1)$$

where the binary hypotheses are defined as

$$H_1 : \boldsymbol{\chi} = \boldsymbol{\chi}_t + \boldsymbol{\chi}_n + \boldsymbol{\chi}_c \quad (3.2)$$

$$H_0 : \boldsymbol{\chi} = \boldsymbol{\chi}_n + \boldsymbol{\chi}_c, \quad (3.3)$$

and $\boldsymbol{\chi}_n$ represents white noise samples and $\boldsymbol{\chi}_t$ and $\boldsymbol{\chi}_c$ are as defined in (2.47) and (2.63), respectfully. The fundamental STAP filtering challenge involves synthesizing weight vector \mathbf{w} to optimize some specific criteria. For example, one simple criteria might be to minimize the interference plus white noise ($\min_{\mathbf{w}} \{\mathbf{w}^H [\boldsymbol{\chi}_c + \boldsymbol{\chi}_n]\}$) while maximizing the target gain ($\max_{\mathbf{w}} \{\mathbf{w}^H \boldsymbol{\chi}_t\}$). This represents one way to define the optimization criteria for \mathbf{w} and there are certainly others. However, this criterion is sufficient for instructional purposes to explain the basic STAP framework. Selected methods for synthesizing \mathbf{w} comprise the main topic of this chapter.

Since STAP is being introduced to *demonstrate* AIP potential, the STAP processors considered herein were chosen because they are well-known and widely used to benchmark performance. As such, they are not necessarily the most recent state-of-the-art STAP algorithms that are available. The specific STAP processors chosen here for demonstration include 1) the non-adaptive Signal Match (SM) filter, 2) the fully adaptive (optimum) Matched Filter (MF), 3) the fully adaptive Adaptive Matched Filter (AMF), and 4) the partially adaptive Factored Space Time (FST) processor.

3.2 *Non-Adaptive Signal Match (SM) Processor*

To appropriately bound the expected performance, both a completely non-adaptive processor (i.e., space-time filter) and a fully adaptive optimum processor

are used in evaluating received data. This section presents the non-adaptive “Signal Match” (SM) processor [62]. The SM processor is a multi-dimensional “maximum gain” beamformer [43]). Simply, it is a 3D steering vector that is steered (“matched”) to the expected target location in each dimension. For a N column by P row planar array radiating M pulses, the SM processor for a target located at elevation, azimuth, and normalized Doppler values of θ_{tgt} , ϕ_{tgt} , $\bar{\omega}_{\text{tgt}}$ is defined as

$$\mathbf{w}_{\text{sm}}(\theta_{\text{tgt}}, \phi_{\text{tgt}}, \bar{\omega}_{\text{tgt}}) = \mathbf{e}[\vartheta_z(\theta_{\text{tgt}})] \otimes \mathbf{b}(\bar{\omega}_{\text{tgt}}) \otimes \mathbf{a}[\vartheta_x(\theta_{\text{tgt}}, \phi_{\text{tgt}})], \quad (3.4)$$

where $\mathbf{e}[\vartheta_z(\theta_{\text{tgt}})]$, $\mathbf{b}(\bar{\omega}_{\text{tgt}})$, and $\mathbf{a}[\vartheta_x(\theta_{\text{tgt}}, \phi_{\text{tgt}})]$ are the elevation, Doppler, and azimuthal steering vectors defined in (2.42), (2.43), and (2.41). For the SM processor, as well as the remainder of those presented in this chapter, linear arrays are simply modeled by setting $P = 1$ in all applicable equations/models. Under the $P = 1$ condition $\mathbf{e} = 1$ and the planar results yield linear array models and weight vectors.

3.3 Fully Adaptive Processors

Fully adaptive processors are those which are adaptive over all NPM DOF, where N , P , and M are the number of element columns, rows, and pulses in a CPI. Conversely, partially adaptive processors reduce the adaptive DOF through the initial application of a non-adaptive transform to a lower dimensional vector space. This section examines two fully adaptive processors which are well known in the STAP community: 1) the optimal Matched Filter (MF) and 2) the Adaptive Matched Filter (AMF), which is a Constant False Alarm Rate (CFAR) modified rendition of the Sampled Matrix Inversion (SMI) technique developed in the early years of STAP [86].

3.3.1 Optimal Matched Filter (MF) Processor. The terminology used to describe STAP’s optimum processor is diverse and potentially confusing. As a performance bound, the optimum processor is perhaps the most often mentioned and defined STAP processor in literature. As result, it has become known by many aliases: 1) Klemm calls it the *optimum processor* in his STAP book [62], 2) Ward calls it the

optimum space-time filter in his often referenced report on STAP [99], and 3) Guerci uses the term *optimum beamformer* in his STAP book [43]. It has also been shown to be the Wiener Filter [38, 39, 59, 60, 100], since it optimizes the linear discrete-time STAP problem formulation that reduces to a Wiener-Hopf equation. Other authors have simply called it the *Matched Filter* (MF) [20, 26, 27, 52, 53] which is the terminology adopted herein. Regardless of the terminology used, all are consistent in defining the *optimal* space-time weight vector (to within a scale factor α) as

$$\mathbf{w} = \alpha \mathbf{R}^{-1} \mathbf{v}, \quad \alpha \neq 0, \quad (3.5)$$

where \mathbf{R} is the clairvoyant space-time covariance matrix under the H_0 hypothesis, and \mathbf{v} is a 3D space-time steering vector (a.k.a., SM “processor”) steered to the (potential) target location in azimuth, elevation, and Doppler.

The terminology adopted here (matched filter) is perhaps among the more confusing given its well-known use in conventional communications, filtering, and radar literature. In these conventional contexts, the matched filter is defined as the filter which maximizes the output peak signal power-to-average noise power ratio when the input noise spectral density is uniform [90] and the signals are typically only a function of time. Nonetheless, the MF is often redefined in the STAP context to represent the optimal space-time filter given by (3.5) and the name fits well with the nomenclature of the widely known “Adaptive Matched Filter” (AMF) discussed in the next section.

As previously mentioned, the STAP filtering solution can be optimized under different criteria, with the same filter of (3.5) emerging as optimal under several criteria [19, 62]. Given that the clutter statistics are zero-mean and jointly Gaussian, the solution given by (3.5) is optimal under the maximum likelihood criterion, as well as under the least mean-square-error criterion. Additionally, (3.5) maximizes the signal-to-noise power ratio and is the linearly constrained minimum noise variance (Wiener filter) solution as well. It is important to note that the optimality of the MF

processor is based on having clairvoyant knowledge of interference statistics, which by definition removes the MF from the list of “adaptive” algorithms.

3.3.2 Adaptive Matched Filter (AMF) Processor. While the MF provides an *optimal bound* for STAP filtering, it is *not* an adaptive algorithm in the sense that it doesn’t adapt to the environment. The Adaptive Matched Filter (AMF) [87] addresses this limitation. Samples of the interference environment consist of the $NMP \times 1$ space time radar data snapshots χ_k partitioned into $k = 1, 2, \dots, K$ unambiguous range bins. The clutter and noise in each snapshot is assumed independent from range bin to range bin. The mathematical formulation of the AMF assumes that this data, referred to as Training Data (TD), is statistically independent, identically distributed (i.i.d.), and conforms to a multi-variate Gaussian distribution. Given these assumptions, the maximum likelihood estimate of the covariance matrix computed from the training data is given by [86]

$$\hat{\mathbf{R}} = \frac{1}{K} \sum_{k=0}^{K-1} \chi_k \chi_k^H, \quad (3.6)$$

where $\hat{\mathbf{R}}$ is called the sample covariance matrix. Based on this estimate, Reed (in his 1974 seminal paper [86]) suggested synthesizing an adaptive processor given by

$$\hat{\mathbf{w}} = \hat{\mathbf{R}}^{-1} \mathbf{v}, \quad (3.7)$$

which clearly has the form of the optimum MF given in (3.5), but uses the sample covariance matrix $\hat{\mathbf{R}}$ in place of the clairvoyant covariance matrix \mathbf{R} . This technique was termed Sample Matrix Inversion (SMI), and it exhibited considerably better convergence properties than the other iterative weight estimation techniques in use at the time [81, 86]. The convergence of the covariance estimate (and thus the quality of the adaptive processor) is directly related to the quantity of the training data support vectors used to estimate $\hat{\mathbf{R}}$. The infamous Reed-Mallet-Brennan (RMB) rule predicts that for a system having NMP degrees of freedom, achieving a mean performance which is -3.0 dB below optimum requires $(2NMP - 3)$ i.i.d. data “samples” having

the statistics specified by the clairvoyant covariance matrix \mathbf{R} . For range sampling radars, these samples come from the (assumed target-less) clutter-plus-noise range cell data snapshots.

Strictly speaking, the processor given in (3.7) is not the AMF, although it is directly proportional to it. The SMI decision statistic proposed by Reed is [86]

$$|\hat{\mathbf{w}}_{\text{SMI}}^H \boldsymbol{\chi}|^2 = \left| \mathbf{v}^H \hat{\mathbf{R}}^{-1} \boldsymbol{\chi} \right|^2. \quad (3.8)$$

The final AMF decision statistic is a modified (scaled) version of (3.8) and given by [87]

$$|\hat{\mathbf{w}}_{\text{AMF}}^H \boldsymbol{\chi}|^2 = \left| \frac{\mathbf{v}^H \hat{\mathbf{R}}^{-1} \boldsymbol{\chi}}{\mathbf{v}^H \hat{\mathbf{R}}^{-1} \mathbf{v}} \right|^2. \quad (3.9)$$

This AMF statistic was published by Robey [87] in 1992, and it adds the CFAR property to the SMI statistic. For the Signal-to-Interference plus Noise Ratio (SINR) metrics used in this research, the absolute magnitude of the weight vector given by (3.9) or (3.8) cancels out and the *SINR performance* of the SMI and AMF statistics are equivalent.

As mentioned in Chapter I, the i.i.d. assumption is rarely, if ever, satisfied in practice. Under non-i.i.d. conditions, the TD is commonly referred to as being heterogeneous TD or non-homogenous clutter. While no set of real-world TD is truly homogeneous, neither is all TD *equally* heterogeneous, statistically speaking. The degree of TD heterogeneity is dependent on the radar's operating environment and varies widely, as does the type of phenomena which causes the heterogeneity. Some causes of heterogeneity can be addressed through adaptive illumination, and Chapter V demonstrates how AIP is used to create TD that is *more* homogeneous than that created by non-adaptive illumination patterns.

3.4 *Partially Adaptive Processors*

Due to the training data limitations previously mentioned, there has been much work done in the area of partially adaptive STAP processors [43, 62, 63, 99]. This work has taken place for mainly two very good reasons. First, to achieve suitable integration gain and aperture resolution, fully adaptive STAP has too much DOF to be implemented in practice. Partially adaptive processors have fewer adaptive DOF which translates to less required TD. Less TD quantity eases both the clutter heterogeneity problem (since TD tends to be more homogeneous over shorter range extents) and the problem of limited TD quantity. Second, high computational burdens associated with fully adaptive STAP are also eased through the use of partially adaptive methods, depending on the particular technique. This makes some algorithms fast enough to use them operationally in real-time.

As stated earlier, the use of STAP in this research is by way of demonstrating the impact of AIP as integrated into a FAR architecture. Given the quantity and diversity of partially adaptive STAP methods, it is beyond the scope of this research to examine even a representative cross-section of methods herein. This is especially true when considering that each partially adaptive method (or perhaps “class” of method) may require customized optimization criteria for AIP synthesis—one which could compensate for a particular method’s weaknesses, limitations, or non-adaptive dimensions. It is envisioned that the application of AIP to the field of partially adaptive STAP processors will result in additional performance gains for many partially adaptive processors. This research provides one such example using an early and relatively simple partially adaptive processor, namely, the Factored Space Time (FST) processor.

3.4.1 Factored Space Time (FST) Processor. As defined here, the Factored Space Time (FST) processor is similar to the common Factored Time Space (FTS) processor [40] from which its name is derived. The FTS processor is non-adaptive in Doppler (time) and provides spatial adaptivity. Conversely, the FST processor is

spatially non-adaptive and provides temporal adaptivity using an adaptive Doppler filter. While this configuration generally yields poor performance in conventional STAP processing, results in Chapter IV exhibit very noteworthy performance when used in conjunction with Space Time Illumination Patterns (STIP).

The FST processor is a member of the beam-space, pre-Doppler STAP family of partially adaptive processors [99]. This family of techniques first utilizes non-adaptive (digital) Fourier transforms to convert radar data from the element-space to the beam-space domain, expressing the radar data in terms of pulses and azimuth angle. The FST processor uses “factored” processing, i.e., the temporal and spatial processing is accomplished independently. First, the data is non-adaptively spatially beamformed to the location of the illumination pattern’s main beam, reducing the data to its temporal dimension (dictated by the number of pulses M). Then, an adaptive Doppler filter is used to filter the resultant data to generate a scalar filter output. FST processor performance is demonstrated in conjunction with STIP using a linear array in Chapter IV. The FST weights are computed using a similar procedure as used for FTS [40] and outlined in [62], and are given by

$$\mathbf{w}_{\text{fst}} = \mathbf{T} \left(\mathbf{T}^H \hat{\mathbf{R}} \mathbf{T} \right)^{-1} \mathbf{T}^H \mathbf{v}, \quad (3.10)$$

where the non-linear transform \mathbf{T} is given by

$$\mathbf{T} = \mathbf{I}_M \otimes \mathbf{a} [\vartheta_x(\theta_t, \phi_t)], \quad (3.11)$$

and dimensions $MN \times M$.

Chapter IV demonstrates how STIP can be employed in conjunction with this FST processor and the non-adaptive SM processor to achieve good STAP performance with a fraction of the the TD *quantity* required to achieve the same performance under standard illumination conditions.

3.5 STAP Performance Metrics

This section presents a brief overview of the STAP performance metrics used in this research. Two variations of the Signal-to-Interference plus Noise Ratio (SINR) are detailed, namely Output SINR and SINR Loss.

3.5.1 Output SINR. Output SINR is defined as the expected value of the signal power divided by the expected value of the noise-plus-interference power and is written as

$$\text{SINR}_{\text{out}} = \frac{\mathcal{E} \{ |\mathbf{w}^H \boldsymbol{\chi}_t|^2 \}}{\mathcal{E} \{ |\mathbf{w}^H (\boldsymbol{\chi}_c + \boldsymbol{\chi}_n)|^2 \}}. \quad (3.12)$$

For an arbitrary deterministic weight vector \mathbf{w} , non-fluctuating (non-random) target, and using the target, clutter, and noise models of Chapter II, the frequently derived [43, 62, 99] SINR result is given by

$$\text{SINR}_{\text{out}} = \frac{\sigma^2 \xi_{\text{tgt}} |\mathbf{w}^H \tilde{\mathbf{v}}_{\text{tgt}}|^2}{\mathbf{w}^H \mathbf{R} \mathbf{w}}, \quad (3.13)$$

where σ^2 is the per pulse, per element noise power and ξ_{tgt} is the per pulse, per element target signal-to-noise ratio. The maximum output SINR for the thermal noise limited (noise-only) case is given by

$$\max \{ \text{SINR}_{\text{out}} \} = \frac{\sigma^2 \xi_{\text{tgt}} \mathbf{w}^H \tilde{\mathbf{v}}_{\text{tgt}} \tilde{\mathbf{v}}_{\text{tgt}}^H \mathbf{w}}{\mathbf{w}^H (\sigma^2 \mathbf{I}) \mathbf{w}} = \frac{\sigma^2 \xi_{\text{tgt}} MNP \mathbf{w}^H \mathbf{I} \mathbf{w}}{\sigma^2 \mathbf{w}^H \mathbf{I} \mathbf{w}} = \xi_{\text{tgt}} MNP. \quad (3.14)$$

For notational simplicity and metric scaling convenience, ξ_{tgt} is typically assumed equal to 1, thus the maximum SINR_{out} under noise-only conditions is equal to the integration gain of MNP .

3.5.2 SINR Loss. The $\text{SINR}_{\text{Loss}}$ metric is often used for evaluating adaptive STAP processors and represents the SINR normalized by the maximum output SINR for optimum performance. Using the result from (3.14), $\text{SINR}_{\text{Loss}}$ is defined as

$$\text{SINR}_{\text{loss}} = \frac{\text{SINR}_{\text{out}}}{\max \{ \text{SINR}_{\text{out}} \}} = \frac{\sigma^2 |\mathbf{w}^H \tilde{\mathbf{v}}_{\text{tgt}}|^2}{MNP \mathbf{w}^H \mathbf{R} \mathbf{w}}. \quad (3.15)$$

3.6 Summary

This chapter provides background information on the STAP processors used in this research. The processors considered include 1) the non-adaptive Signal Match (SM), 2) the optimum Matched Filter (MF), 3) the full-rank Adaptive Matched Filter (AMF), and 4) the Factored Space Time (FST) processor. It is emphasized again that the role of the STAP processors in this research is to *demonstrate* the ability of Adaptive Illumination Patterns (AIP) to improve overall adaptive radar performance utilizing the Fully Adaptive Radar (FAR) paradigm. The processors discussed here were chosen because of their popularity as well-known benchmark STAP processors and in one case (i.e., FST) by nature of its low complexity and synergistic performance with AIP.

IV. Space Time Illumination Patterns (STIP)

This chapter defines and explores the use of Space-Time Illumination Patterns (STIP). The motivation and definition for STIP is first provided, followed by an examination of its phenomenological effects. Some approaches for pattern synthesis are addressed and the application of STIP to improve Space Time Adaptive Processing (STAP) performance is considered. STIP is a new concept which has only recently become feasible through the advent of emerging and next generation AESA technology. In very general terms, STIP brings to a transmitter what STAP brings to a receiver. However, there are some important differences between “space-time beamforming” as accomplished by STIP on transmit and space-time filtering as accomplished by STAP on receive.

The goal of this chapter is to first explore what STIP has to offer, and then to explore examples of how STIP and STAP may be collaboratively employed. The importance of a joint-design methodology when combining the two techniques (STIP and STAP) is highlighted. Initial application of STIP in this context suggests it is a viable technique for reducing the Training Data (TD) requirements and processor complexity of STAP on receive. For simplicity in understanding the new phenomenological effects induced by STIP, a linear array is considered throughout the chapter.

4.1 *Motivation for STIP*

The success of STAP at achieving interference suppression by *jointly* working across temporal and spatial domains motivates the investigation into the temporal variation afforded by transmit/illumination antenna patterns. STAP can be viewed as the synthesis and application of a time-varying (pulse dependent) set of spatial filters applied to received radar data. In this view, each spatial filter (defined by each subset of N weights in a $NM \times 1$ linear array weight vector) is equitable to the array factor portion of a phased array *receive* pattern, applied to sampled radar data.

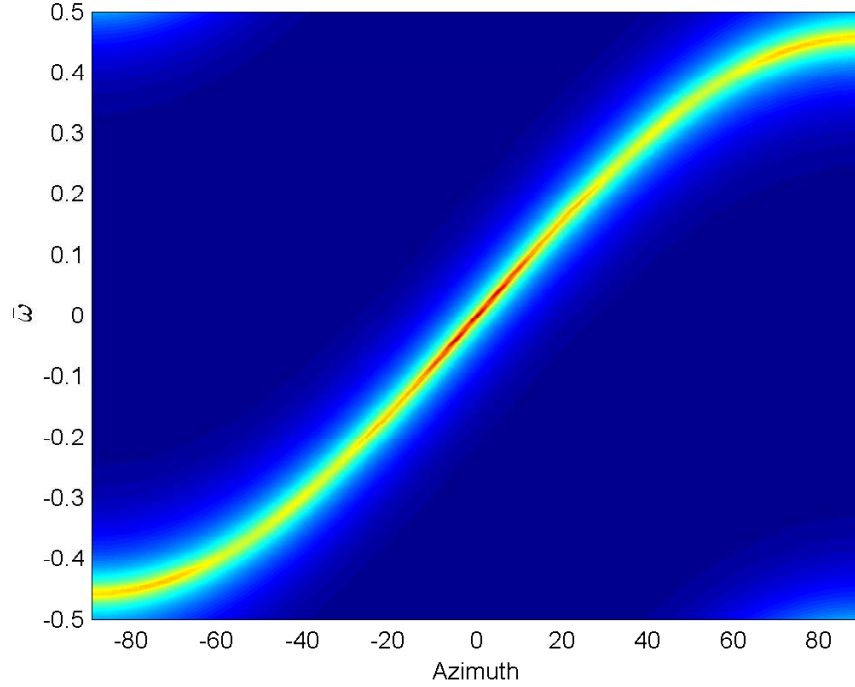


Figure 4.1: Minimum Variance (MV) spectrum of airborne clutter using a Standard Illumination Pattern (SIP). Plot shows clutter Doppler frequency varying as a function of azimuth.

4.1.1 A Deeper Look At Space-Time Processing. To further illustrate the time-varying, spatial filter view of STAP processing, consider a typical side-looking airborne radar (see Fig. 1.1) employing a linear $N = 8$ element phased array and transmitting $M = 4$ pulses. Furthermore, assume the aircraft velocity is such that the clutter Doppler frequency spans the unambiguous Doppler span of the system (i.e., $\beta \geq 1$ in Brennan’s clutter rank equation [99]). Small parameter values were chosen to simplify the results and analysis. This illustration employs a boresight (0° azimuth) mainbeam, a $\beta = 1$ condition, and zero crab angle. Using a standard illumination pattern (defined in more detail in Section 4.2.1), the minimum variance spectrum [62] of the resultant clutter is given in Fig. 4.1.

Figure 4.1 shows the “location” of the interference described by the interference covariance matrix \mathbf{R} as a function of azimuth and Doppler. A STAP filter improves performance by nulling this energy across the joint azimuth-Doppler space

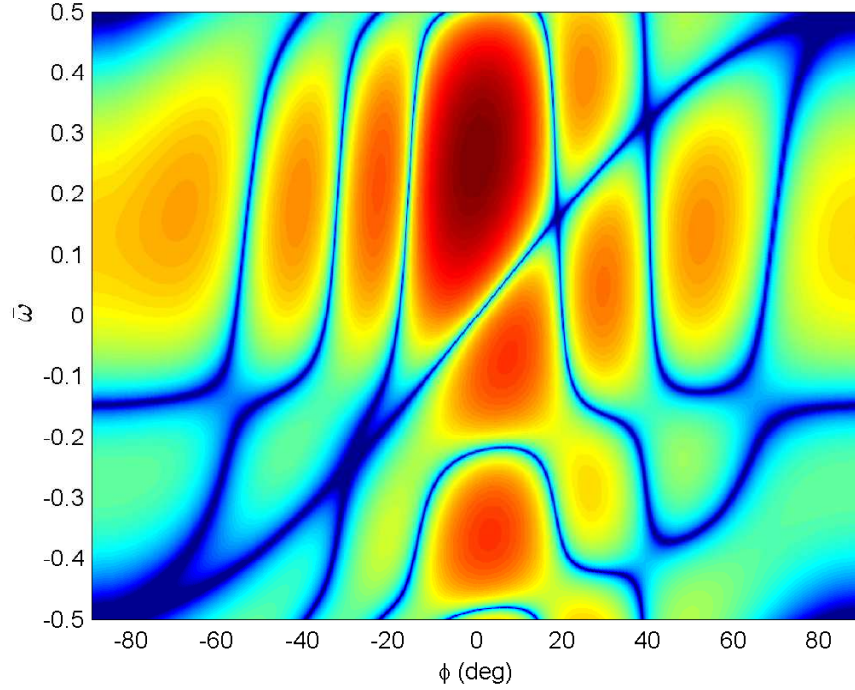


Figure 4.2: Azimuth-Doppler response of an optimum MF synthesized to null the interference shown in Fig. 4.1. In this case, the MF is “tuned” to a normalized Doppler frequency of 0.25.

while placing maximum gain in the (azimuth) direction of the mainbeam at a desired Doppler frequency. The net effect of a STAP filter can be visualized by examining its joint azimuth-Doppler (spatial-temporal) filter frequency response. The joint filter response of the optimum Matched Filter (MF) (see Chapt. II) “tuned” to a normalized Doppler frequency of 0.25 and synthesized in response to the interference environment depicted in Fig. 4.1 is shown in Fig. 4.2. Note that the s-shaped null appearing diagonally in Fig. 4.2 is precisely aligned with the clutter ridge shown in Fig. 4.1 and maximum mainbeam gain occurs at zero degrees azimuth and a normalized Doppler value of 0.25, as desired. The response shown in Fig. 4.2 is sometimes referred to as a STAP “antenna pattern” in the literature, as it illustrates a weight set’s (i.e., filter’s) “gain” (i.e., magnitude frequency response) as a function of azimuth (spatial frequency) and Doppler (temporal frequency). However, the result represented in

Fig. 4.2 does not represent a “physical” antenna pattern since a single antenna pattern (by definition) is only spatial in nature. Rather, Fig. 4.2 illustrates the results of a 2D Digital Fourier Transform (DFT) operating on the complex optimum MF weight set, where the weights are arranged such that the 2D DFT operates across the separable temporal and spatial domains represented in the STAP weight set. The partitioning of this joint weight set into separate spatial patterns is instructive for understanding the view of STAP weights described herein, and is considered next.

4.1.2 STAP Weights, AESA Weights, and Array Factors. Any complex “weight” has the ability to affect two basic signal parameters; it can 1) scale the amplitude and/or 2) shift the phase. This is true for any signal, whether it be a received sampled radar return (as in receiver processing) or an analog signal being transmitted or received through a phased array element of an AESA. The amplitude scaling and phase shifting operations can be visualized using a phaser representation where each phaser describes the weight’s magnitude and phase. Space-time weight sets are illustrated here using phaser notation, arranged according to the pulse and antenna element to which the weights are applied. An example of the phaser representation used here is shown in Fig. 4.3. Figure 4.3 provides a phaser diagram illustrating a complex weight applied to Element 1 (x axis) during transmission of Pulse 1 (y axis). The phaser depicts a phase value of 45° and maximum gain. The circle diameter denotes the maximum gain of the weight set. When representing a group of $M \times N$ weights, the circle radius is normalized to the largest amplitude gain contained in the weight set. Using this phaser notation, the optimum MF weights used to generate Fig. 4.2 are shown in Fig. 4.4, organized by the elements and pulses to which they apply. Using this representation, it is clear to see how a set of NM STAP weights can be viewed as M sets of $N \times 1$ spatial weights, where each $N \times 1$ weight set determines a spatial filter applied to a specific pulse. Furthermore, each spatial filter’s response is calculated using the same approach as is used for a 2D (azimuth/elevation) spatial array factor [10] of an N element linear array.

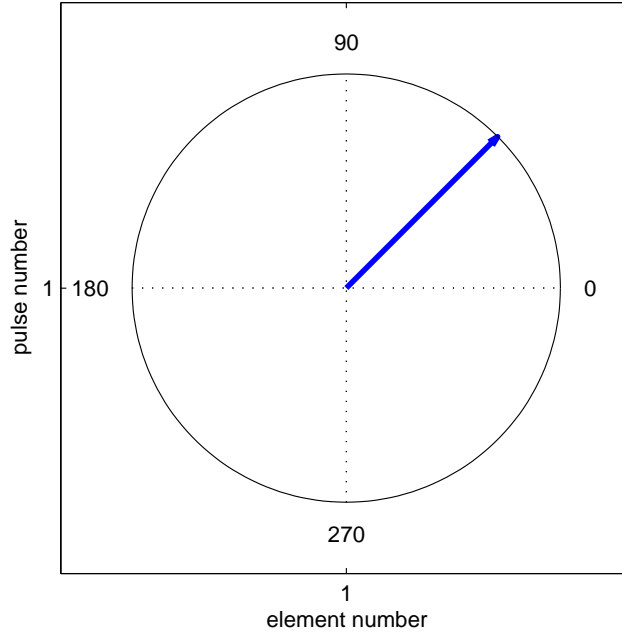


Figure 4.3: Phaser representation of a complex weight used on Element 1 during transmission of Pulse 1. This phaser depicts a phase value of 45° and maximum gain. The circle diameter denotes the maximum gain of the weight set.

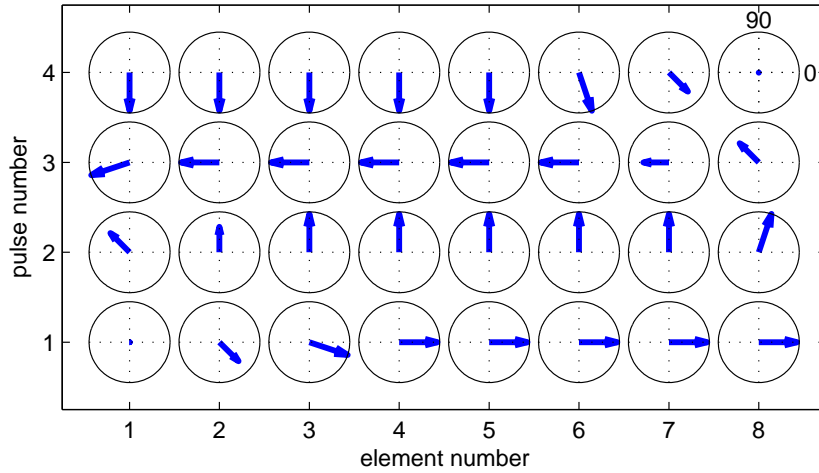


Figure 4.4: Phaser representation of optimal MF STAP weights synthesized in response to a sidelooking $\beta = 1$ clutter scenario (clutter PSD illustrated in Fig. 4.1)

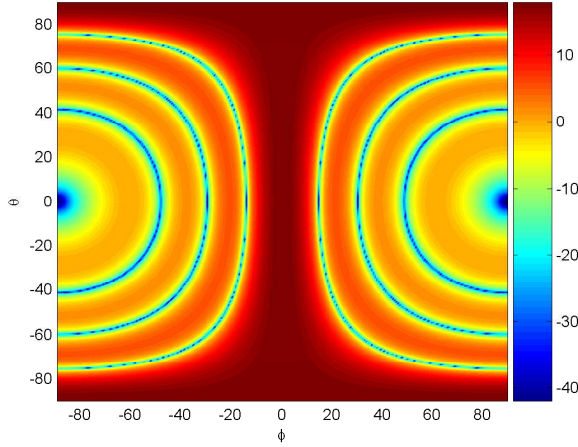


Figure 4.5: Linear array factor magnitude response as a function of azimuth (ϕ) and elevation (θ) given uniform weights. Gain is relative and expressed in dB.

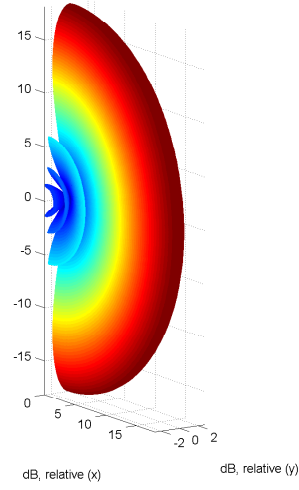


Figure 4.6: Linear array factor magnitude response plotted in spherical coordinates, relative dB scale.

Assuming half-wavelength ($\lambda/2$) element spacing, Fig. 4.5 illustrates the uniform weight (i.e., all weights equal one) array factor gain of an N element array as a function of azimuth and elevation. Figure 4.6 shows the same array factor expressed in cartesian coordinates (i.e., 3D space) to aid with pattern visualization.

Using Fig. 4.5 as a reference, consider the four spatial filters contained in the optimum STAP weight vector depicted in Fig. 4.4. The spatial filter (i.e., “virtual” array factor) effectively applied to each pulse is depicted in Fig. 4.7. These are referred to as “virtual” array factors since they “exist” only in the signal processing realm, rather than being physically observable/measurable in the “real-world.”

Upon careful inspection of Fig. 4.7, it is apparent that the array factors/spatial filters “applied to” Pulse 1 and Pulse 4 are very similar. In fact, for these optimum processor weights they are actually identical. Likewise, the gain patterns for Pulse 2 and Pulse 3 are also identical in this case. However, it can be clearly seen from Fig. 4.4 that the weights generating these specific patterns are NOT identical. This simple observation underscores the importance that the *phase* response of each array factor

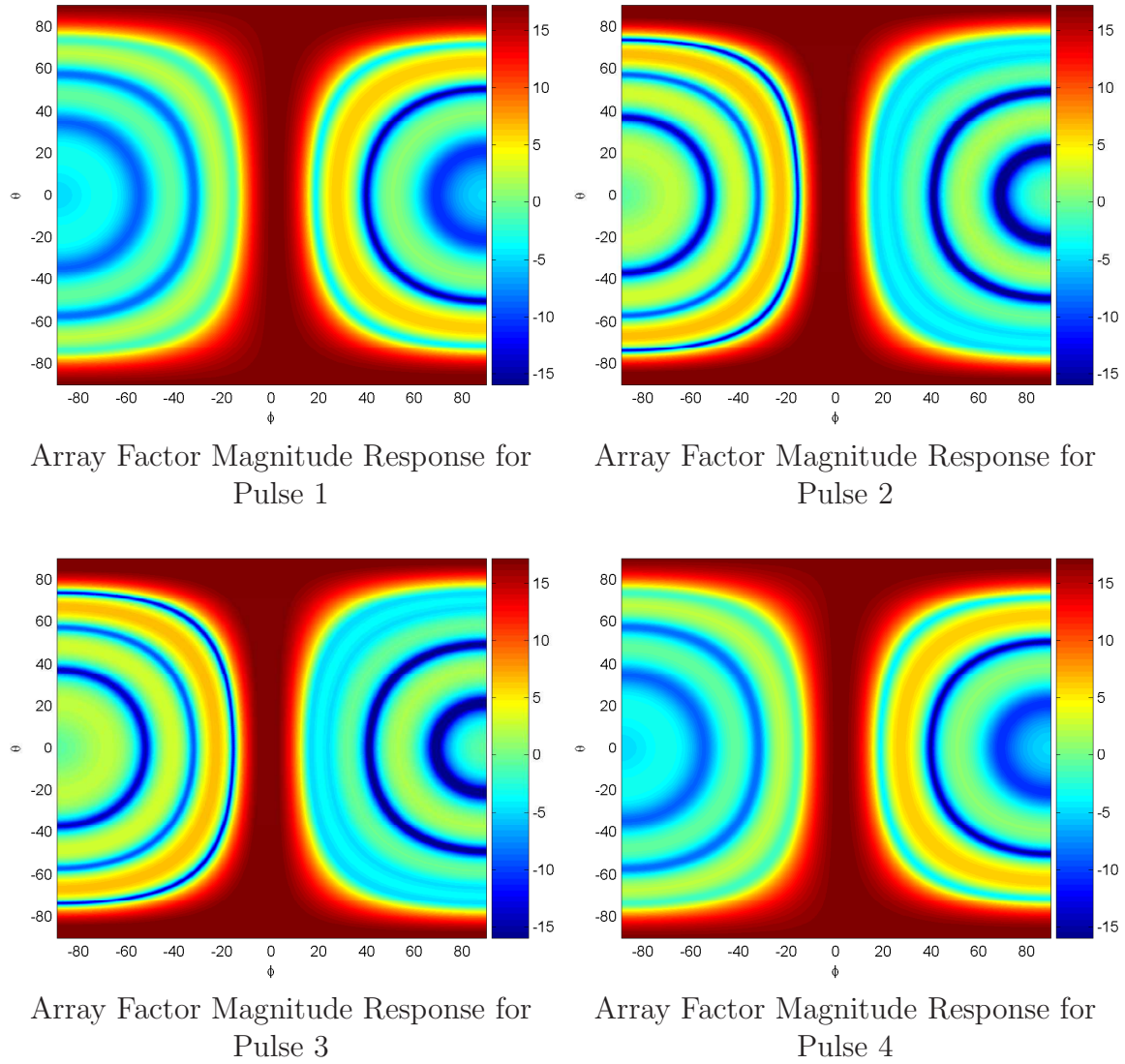


Figure 4.7: Each pulse’s spatial filter (virtual array factor) magnitude response derived from the optimum MF STAP weight vector depicted in Fig. 4.4. The linear array factors are plotted as a function of azimuth (ϕ) and elevation (θ).

must be examined as well. Thus, the phase response of each array factor is given in Fig. 4.8.

Visual inspection of the plots in Fig. 4.8 reveals the phase responses are indeed distinct and unique, unlike the magnitude patterns in Fig. 4.7. Although the “phase response” (i.e., phase *pattern*) of phased array antennas are often overlooked in antenna pattern discussions, a proper understanding of it is critically important to

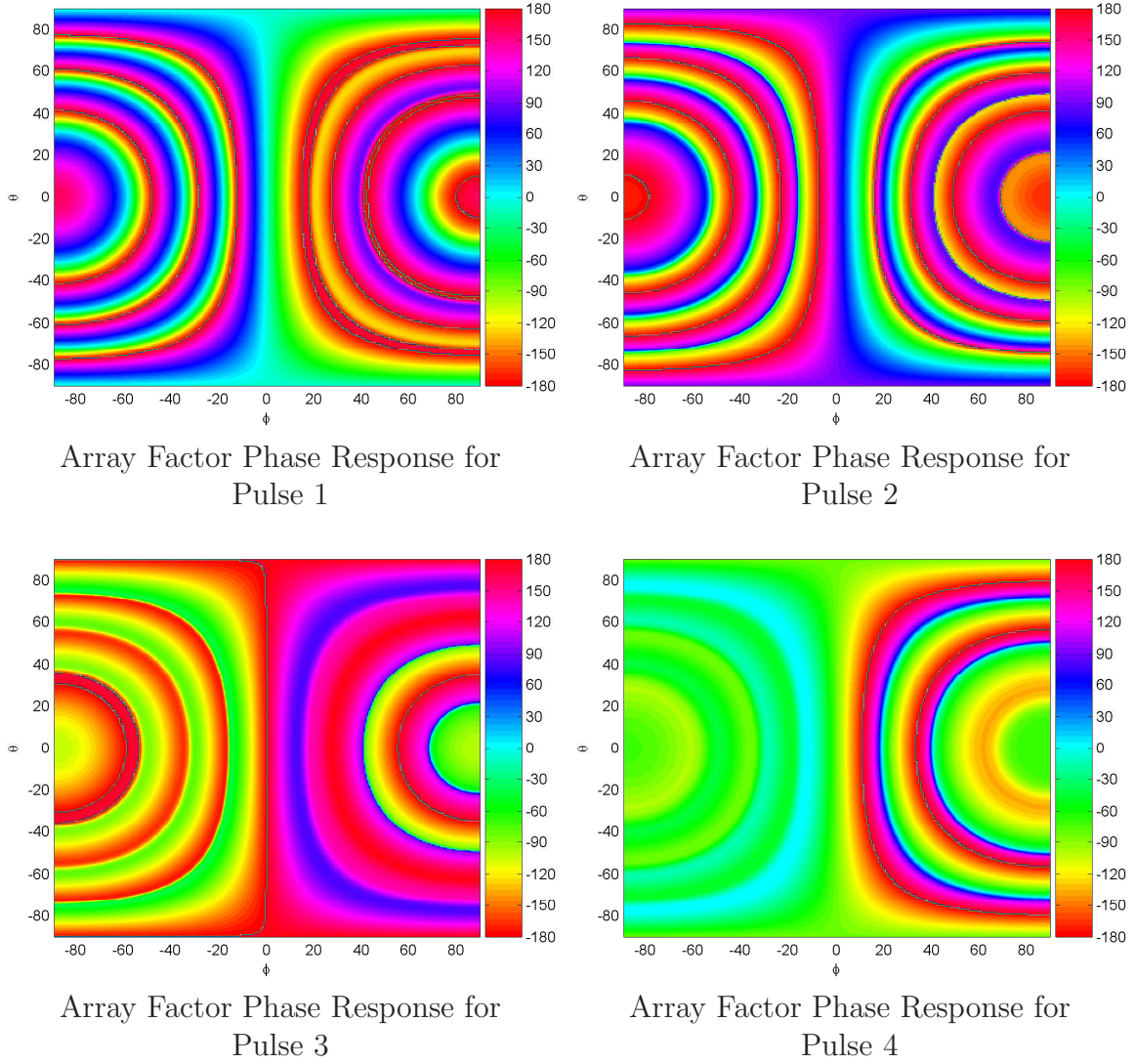


Figure 4.8: Each pulse's spatial filter (virtual array factor) phase response derived from the optimum MF STAP weight vector depicted in Fig. 4.4. The linear array factors are plotted as a function of azimuth (ϕ) and elevation (θ).

understanding STIP. Thus, some explanation of their meaning and characteristics is warranted.

The angle argument of the array factor for each pulse in Fig. 4.8 represents the *composite signal* phase resulting from the superposition of all the elemental signals. As indicated, this composite phase response varies as a function of azimuth and elevation angles. Phase is always defined relative to some fixed reference, and in this

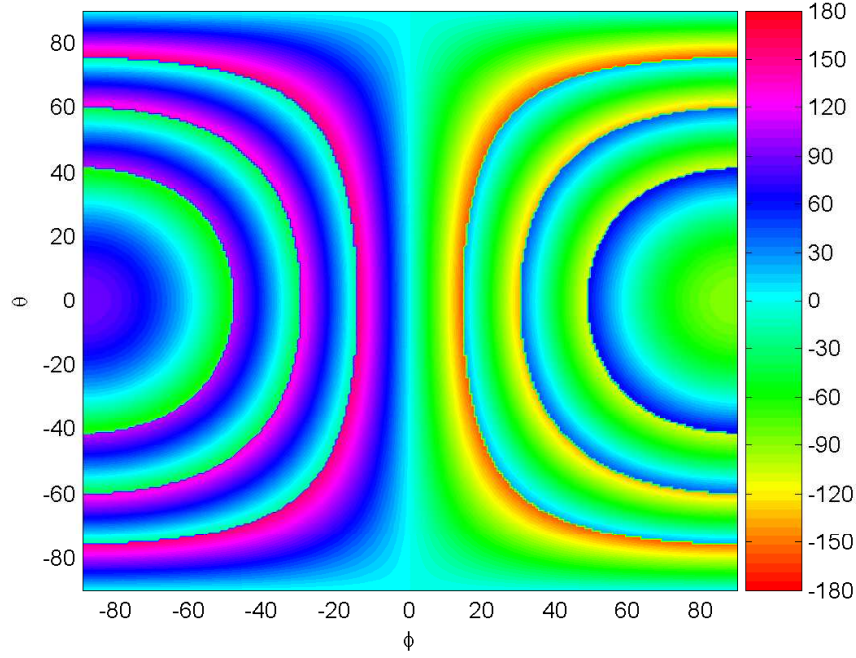


Figure 4.9: Linear array factor phase response as a function of azimuth (ϕ) and elevation (θ) given uniform weights. Phase is measured relative to the array reference element.

case the phase reference is the array reference element (illustrated in Fig. 2.1). The composite signal phase is thus measured (assuming far-field conditions) on an arc of fixed distance from the reference element located at the end of the array.

For comparative purposes, the phase response of a uniform array weight set (all weights equal one) is shown in Fig. 4.9. By comparison with its magnitude response which was introduced in Fig. 4.5, the uniform weight phase response appears to “jump” across the magnitude nulls. This well-known characteristic of the composite phase response (phase pattern) of a phased array antenna is also visible in Fig. 4.8.

While the pulse-to-pulse differences in the “virtual” array factors of Fig. 4.7 seem relatively minor, the pulse-to-pulse differences in the virtual array factor’s phase patterns of Fig. 4.8 are quite noticeable. The phase, and magnitude to a somewhat lesser extent, relationships between each of the array factors constitute the fundamental basis upon which adaptive, spatially dependent Doppler filtering is accomplished.

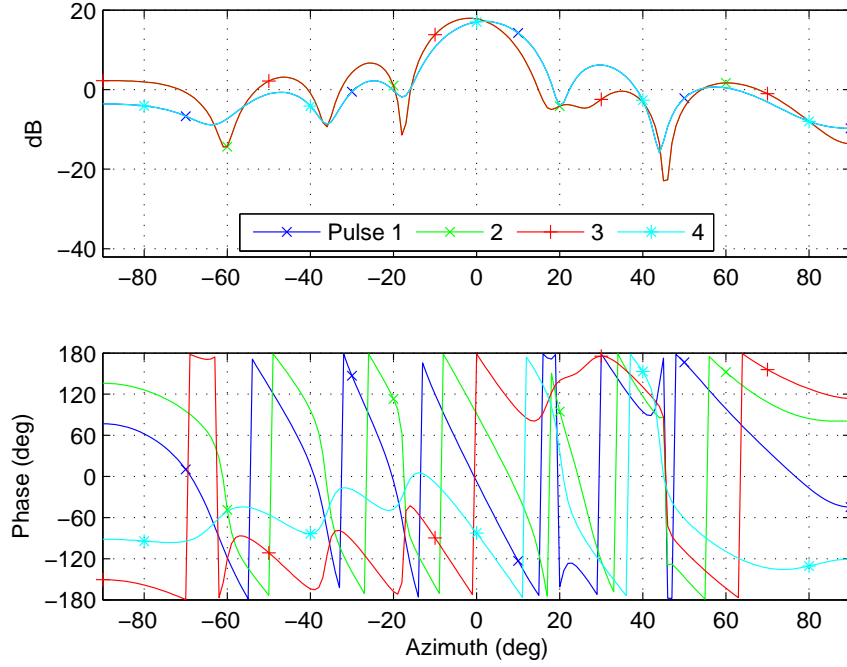


Figure 4.10: Azimuth antenna pattern cuts at -23.5° elevation of array factor magnitude and phase responses shown in Fig. 4.7 and Fig. 4.8, which were based on the optimum MF STAP weights depicted in Fig. 4.4.

From this point forward, the antenna magnitude and phase characteristics are represented at a single elevation angle which is sufficient for observing antenna magnitude and phase patterns applicable to the clutter and/or target in a particular range gate. For the optimum MF weight set explored here, an azimuth cut taken at -23.5° elevation is shown in Fig. 4.10.

By analyzing Fig. 4.10 it can be observed that there is phase “rotation” applied to a ground target in the mainbeam at an azimuth/elevation location of $(0, -23.5)$ degrees. The amount of rotation indicated is roughly a 90° phase shift per pulse. By comparison, the phase progression applied to a clutter return at an azimuth/elevation location of $(40, -23.5)$ degrees is much smaller (less than 60° total degrees). Studied carefully, this diagram once again exhibits the azimuth dependent adaptive Doppler processing characteristic of STAP.

Though it is not often mentioned in the literature, the transmit or illumination patterns of a phased array also have weight-dependent phase patterns, which can be physically measurable in the “real-world” (typically in an anechoic chamber). If the *transmit* weights change during the CPI, then the array phase patterns should be modeled as they will induce phase shifts on the reflected signals. Detecting the phase progression on successive pulses (within a CPI) is the basis for measuring and filtering Doppler. This establishes the need for modeling the array factor *phase* on transmit when it changes during a CPI (see Chapt. II).

4.1.3 Space-Time Filtering With Real Array Factors. Previous sections outlined a different perspective of STAP processing where STAP filtering is viewed as the synthesis and application of pulse dependent spatial filters applied to received radar data. Given this view, the ability to perform space-time filtering *via the AESA receive antenna* seems conceivable. Such a technique requires the $N \times M$ receive weight set to be known prior to receive processing. These weights are assumed to be available for the sake of this discussion—the weight synthesis problem is challenging, but independent of the implementation method described in this section. See Section 4.4.2 for one proposed weight synthesis method.

Applying “weights” to a radar signal can be done either digitally after signal is received, filtered, and sampled, and/or directly by scaling and shifting the analog signal using the AESA on receive. Each pulse received on each AESA element can be “weighted” by loading different array weights immediately after each transmitted pulse (see Chapter 37 of [94] for more information on AESA construction). While there would be some fundamental hardware limitations on AESA weight adaptability (limited dynamic range, phase quantization error, etc.), the final weighting of the radar data should be roughly the same. Once the weights are applied, the space-time “filtering” occurs by way of simply adding up all the samples.

While this process would be at best equivalent to STAP processing, (making it somewhat redundant), it suggests the possibility of instituting a similar space-time

weighting process *on transmit*. With this perspective in mind, and motivated by rapid advances in Active Electronic Scanned Arrays (AESAs), the use of pulse dependent *illumination* patterns is investigated using adaptive pulse-dependent *illumination weights*. Pattern sets which take advantage of the joint space-time adaptivity are termed Space-Time Illumination Patterns (STIP). A more precise definition of STIP is provided following the introduction of Standard Illumination Patterns (SIP) for comparative and elucidating purposes.

4.2 Defining STIP

Despite enormous advances in radar antenna technology over the years, only recently has AESA technology matured to the point where radar designers can now consider making intentional changes to *fundamental characteristics* of the radar’s antenna pattern. Such changes can be updated at rates approaching current low PRF limits and can be made accurately and reliably. New technologies will undoubtedly grow out of this new capability as AESA technology continues to advance. AESA antennas are sure to become (if they haven’t already) the standard antenna of choice for all future fighter aircraft and surveillance platforms.

The assertion of this research is that any adaptive transmit weight synthesis methods considered to date (with the one possible exception of [88]) have been constrained to at most $N + M$ DOF, which is the maximum available DOF using an adaptive but separable (or factored) transmit weight synthesis approach. A survey of STAP literature reveals that in a vast majority of cases the transmit weights are synthesized using only a single mainbeam (spatial) constraint and one temporal constraint (typically, $\bar{\omega}_{\text{tx}} = 0$). As best can be determined, the *joint* dimensionality of the transmit weights has not been previously explored. STIP was designed to exploit this previously untapped capability.

The STIP concept becomes more clear when considered alongside a robust definition of traditional illumination patterns. The next section defines “Standard” Illumination Patterns (SIP) which are used heavily in comparative analysis.

4.2.1 *Standard Illumination Patterns (SIP).* So called “Standard” Illumination Patterns (SIP) are defined here as array factors for linear phased arrays which are synthesized according to simple mainbeam constraints. A phased array antenna pattern is a product of both the array factor and the element pattern [10]. The element patterns are assumed isotropic unless otherwise noted and identical for all elements. Under this assumption (and only under this assumption), the terms array factor and array pattern may be used interchangeably. A classic example of a SIP weight set \mathbf{w}_s is one generated by a spatial steering vector “steered” to an azimuth and elevation of ϕ_{tx} and θ_{tx} , given by

$$\mathbf{w}_s = \mathbf{a}[\vartheta_x(\theta_{tx}, \phi_{tx})]. \quad (4.1)$$

With the exception of an amplitude taper to reduce sidelobe gain, the transmit weights given by (4.2) describe the linear array illumination pattern used for the vast majority of adaptive radar research (conformal arrays are obviously a special case not considered here). From a DOF perspective, these spatial transmit weights are specified using one of N available constraints. Amplitude tapers are not considered “constraints” since they do not reduce the available DOF [43]. These weights are typically fixed (non-varying) over the CPI of M pulses. Considering the weights used to transmit each pulse as separate weight sets, the entire set of MN Standard Transmit (STX) weights could be written as

$$\mathbf{w}_{\text{STX}}(\phi_{tx}, \theta_{tx}, \bar{\omega}_{tx}) = \mathbf{b}(\bar{\omega}_{tx}) \otimes \mathbf{a}[\vartheta_x(\theta_{tx}, \phi_{tx})]. \quad (4.2)$$

When written this way, those familiar with STAP processing may see (4.2) as a non-adaptive beamformer specified by one of NM available DOF. Using the phaser notation introduced earlier, a set of STX weights defined as $\mathbf{w}_{\text{STX}}(\phi_{tx} = 0, \theta_{tx} = 0, \bar{\omega}_{tx} = 0)$ using (4.2) is shown in Fig. 4.11. The magnitude and phase response for the SIP weights of Fig. 4.11 is provided in Fig. 4.12. The weights depicted in Fig. 4.11 correspond to the array factor magnitude depicted earlier in Fig. 4.5 and Fig. 4.6,

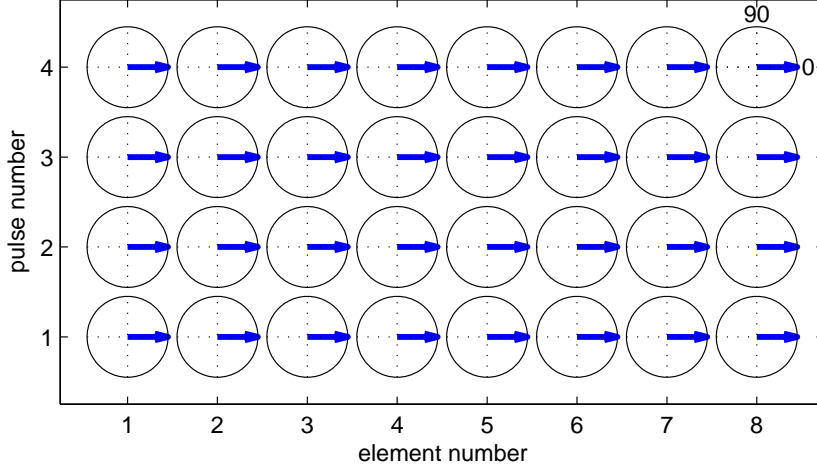


Figure 4.11: Phaser representation of a SIP weight set of an 8 element linear array spanning a CPI of 4 pulses tuned to 0° azimuth, 0 Hz Doppler.

and the array factor phase response given by Fig. 4.9, which are both summarized in Fig. 4.12. These SIP weights were also used in Section 4.1.1 to generate the clutter MV spectrum given in Fig. 4.1.

4.2.2 Space-Time Illumination Patterns (STIP). Chapter II presented radar model extensions that incorporate Transmit Interpulse Pattern Diversity (TIPD), which added the *capability* to model an arbitrary antenna transmit/illumination pattern for each transmitted pulse. To better understand and differentiate between SIP, TIPD, and STIP, consider the problem of updating/resteering the main beam location of an AESA mounted on a aircraft undergoing highly dynamic maneuvers. As the aircraft dramatically changes its position and attitude, the radar’s mainbeam may need to be “resteered” during the Coherent Processing Interval (CPI) to maintain mainbeam illumination of a particular target. To do so requires the illumination pattern weights be changed/updated during the CPI. Stimson validates the AESA’s need and ability to accomplish beam resteering, at a “nominal” rate of 2 kHz [94]. The

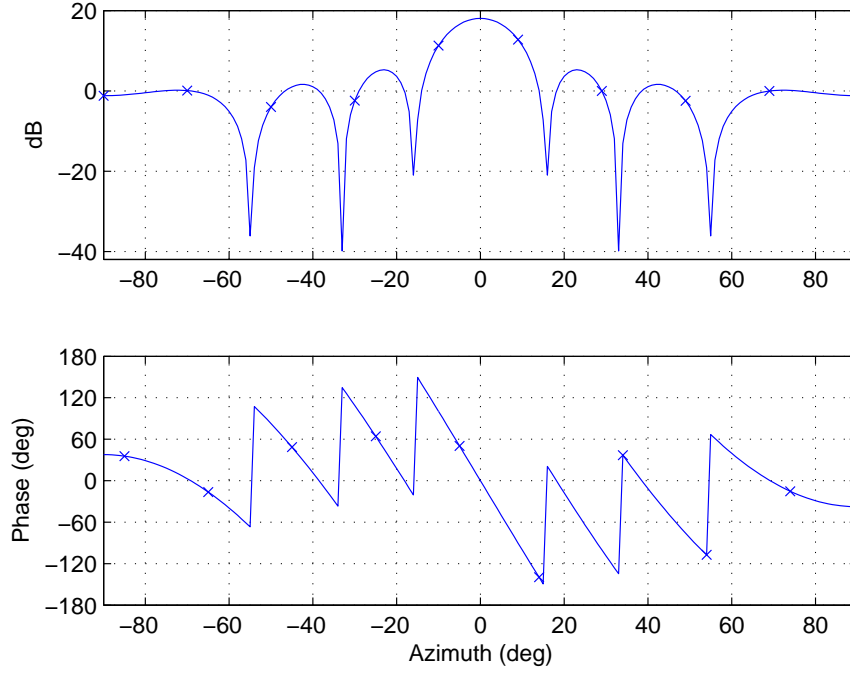


Figure 4.12: Illumination pattern magnitude and phase azimuth cuts at -23.5° elevation generated from the uniform weights depicted in Fig. 4.11.

ability to *model* these changing weights during a CPI is provided by TIPD extensions outlined in Chapter II. However, the process of updating the mainbeam pointing angle falls under the definition of SIP, not STIP, since the weight synthesis method consisted of updating a single spatial constraint (mainbeam location).

STIP constitutes a type of adaptive illumination that *utilizes* transmit interpulse pattern diversity to radiate a tailored transmit/illumination pattern on each pulse, but there is more to STIP than simple pulse diversity. Just as STAP filters can be constructed to filter (or “null”) energy across the joint azimuth-Doppler space, STIP patterns make use of NM DOF to cast “illumination nulls” in the azimuth-Doppler domain. However, STIP does not reduce or *remove* the clutter as STAP *filtering* does—it only dictates what “locations” in the joint space-time domain are not *illuminated*. As a result, the *location* of the clutter power in the azimuth-Doppler

domain is effectively *redistributed*. Alternately stated, the clutter Power Spectral Density (PSD) can be *reshaped* by using STIP during the transmit cycle.

Transmit patterns illuminate the scene (targets, ground, etc.) and dictate how pulse energy is spatially distributed. With a standard illumination pattern, a linear array of N elements can be used to create $N - 1$ “real” spatial nulls in azimuth. Specifying an illumination null at a particular azimuth angle creates a transmit/illumination pattern having a physical pattern null which nulls returns regardless of their Doppler frequency.

By using STIP, an illumination null can be specified at a single point in the joint azimuth-Doppler space such that the pulse-to-pulse series of antenna patterns creates a Doppler-dependent spatial null. In essence, the azimuth location is no longer nulled completely on each pulse, but the illumination patterns are constructed such that returns from the nulled azimuth angle cancel when their Doppler frequency is equal to the desired null value.

Transmitting energy creates clutter and the illumination pattern determines the shape of the clutter’s Power Spectral Density (PSD) (distribution of clutter power). While amplitude tapers are effective at reducing sidelobe gain, they also reduce the peak gain while widening the mainbeam. The use of STIP greatly expands the realm of clutter spectral shaping into a previously unexploited domain—the joint space-time domain. It is demonstrated later in this chapter that by prudently shaping the clutter energy improved performance is realized using simplified receiver processing.

4.3 STIP vs. STAP: Understanding Differences

While STAP provides good motivation for STIP, it is important to make a distinction between space-time beamforming, or scene *illumination* which is dictated by real patterns on transmit (AIP), and space-time processing, or *filtering* which results from “virtual” patterns formed by the receiver processing (STAP).

While STAP results in adaptive Doppler filtering, AIP does not accomplish any sort of Doppler “filtering” on transmit. Doppler filtering only occurs when responses from successive pulses are summed—an operation native to receive processing. On receive, conventional STAP processing is effectively a form of “space-time filtering” in that spatial and temporal nulls are synthesized to filter out interference (received energy) through selective amplitude/phase weighting and summation (coherent integration). Therefore, STAP nulls remove interfering energy which is actually present while STIP spatial nulls are placed to reduce interfering energy from being *received* altogether.

Another difference between STIP and STAP has to do with the more permanent influence and range independence of the illumination pattern. One transmit pattern illuminates all range gates simultaneously once per pulse, whereas on receive, each range gate can be individually processed by a customized STAP filter multiple times. Assuming each of the antenna element outputs are sampled individually (as in a standard STAP framework), an “infinite” number of virtual phased array receive patterns can be “synthesized” by simply re-weighting the received data prior to recombining it. This is how STAP processes a single snapshot of data at multiple Doppler frequency bins. Once a tailored illumination pattern is used, the scene has been sampled and the received data is fixed. Implementing another illumination pattern cannot be done “on” or “to” the same data and changes require retransmission to create a new data set for processing.

Another fundamental difference between synthesizing STIP and STAP illumination/processing weights is how the channel effects are accounted for. With STAP processing, the receive data inherently contains the channel effects, e.g., the Doppler shift of the clutter as a result of platform motion. However, STIP pattern synthesis methods must account for the channel effects (e.g., the clutter Doppler shift due to platform velocity) such that the desired result is attained. This concept is further examined in Section 4.4.1.

Ultimately, the final FAR system may rely on the synergistic effects of both techniques. For example, STIP may be used to tailor the scene illumination such that signal dependent interference (clutter) is reduced, minimized, reshaped, etc., with subsequent STAP processing providing the defense against residual signal independent interference. The extent to which STIP and STAP synergism may be exploited is of great interest and remains a topic for future research.

The process of adaptive illumination/pattern synthesis is anticipated to be as varied and critical to FAR performance as the weight estimation approaches are for STAP receive processing. The weight synthesis techniques explored here are detailed in Section 4.4.

4.4 *Illumination Pattern Synthesis*

A standard illumination pattern is typically derived from a single constraint, i.e., the look direction in azimuth/elevation. Taken collectively, a series of M illumination patterns comprising a CPI is also derived from a single constraint in space and frequency where the frequency constraint is zero Hertz. In reality, there are NM degrees of freedom in the transmit cycle, just as there are NM degrees of freedom in the receive (STAP) processing. The goal of STIP is to explore whether the $NM-1$ degrees of transmit DOF, which are currently not used, can be exploited to improve overall performance.

Using a method analogous to STAP weight generation, STIP pattern synthesis could be done by building a covariance matrix \mathbf{Q} which specifies a locus of L locations in azimuth-Doppler space that are *not* to be illuminated. In other words, \mathbf{Q} contains the desired locations of the “illumination nulls” and is defined as

$$\mathbf{Q} = \sum_{i=0}^L \alpha_i \mathbf{b}(\bar{\omega}_i) \mathbf{b}^H(\bar{\omega}_i) \otimes \mathbf{a}[\vartheta_x(\theta_i, \phi_i)] \mathbf{a}^H[\vartheta_x(\theta_i, \phi_i)] + \beta \mathbf{I}_{NM} \quad (4.3)$$

where the α_i and β parameters would be selected to establish relative constraint weighting and ensure invertibility. Using (4.3), the STIP weights (labeled here as

Adaptive Transmit (ATX) weights) could be synthesized using the optimum beam-former equation [43]

$$\mathbf{w}_{\text{ATX}} = \mathbf{Q}^{-1} \mathbf{w}_{\text{STX}}(\phi_{\text{tx}}, \theta_{\text{tx}}, \bar{\omega}_{\text{tx}}), \quad (4.4)$$

where \mathbf{w}_{STX} establishes the mainbeam constraint and desired Doppler frequency to search for targets (see section 4.2.1).

The synthesis process as just outlined should be intuitively comforting to those working in STAP. It seems as though one must simply define/determine the “locations” where interference is to be avoided and subsequently synthesize an illumination pattern (filter) that prevents those locations from being illuminated.

In the synthesis procedure outlined in (4.4), the “illumination nulls” of a specific STIP weight set are synthesized assuming a specific Doppler filter is to be employed by the receiver (specifically, the value of $\bar{\omega}_{\text{TX}}$ in (4.4). If the *receive* Doppler filter changes, the STIP weights will no longer cast the same illumination nulls since they were *designed* for a different Doppler filter. Alternately stated, the space *time* illumination characteristics change as a function of the *temporal* (Doppler) receiver processing. These types of transmit-receive interdependencies are a product of the adaptive transmit/FAR architecture and underscore the importance of jointly designing the transmit and receive weights to work together.

The following subsections introduce three methods for synthesizing illumination weights, including 1) use of optimum STAP (MF) weights, 2) use of estimated STAP weights based on the previous CPI, and 3) a knowledge-aided approach using radar clutter models to estimate interference spectrum for illumination weight synthesis.

4.4.1 Pattern Synthesis: Optimum STAP MF Weights. The first STIP weight synthesis method considered uses the optimum STAP MF weights as a source for illumination weights to generate transmit patterns. The process is described for a linear array and graphically depicted in Fig. 4.13 [27].

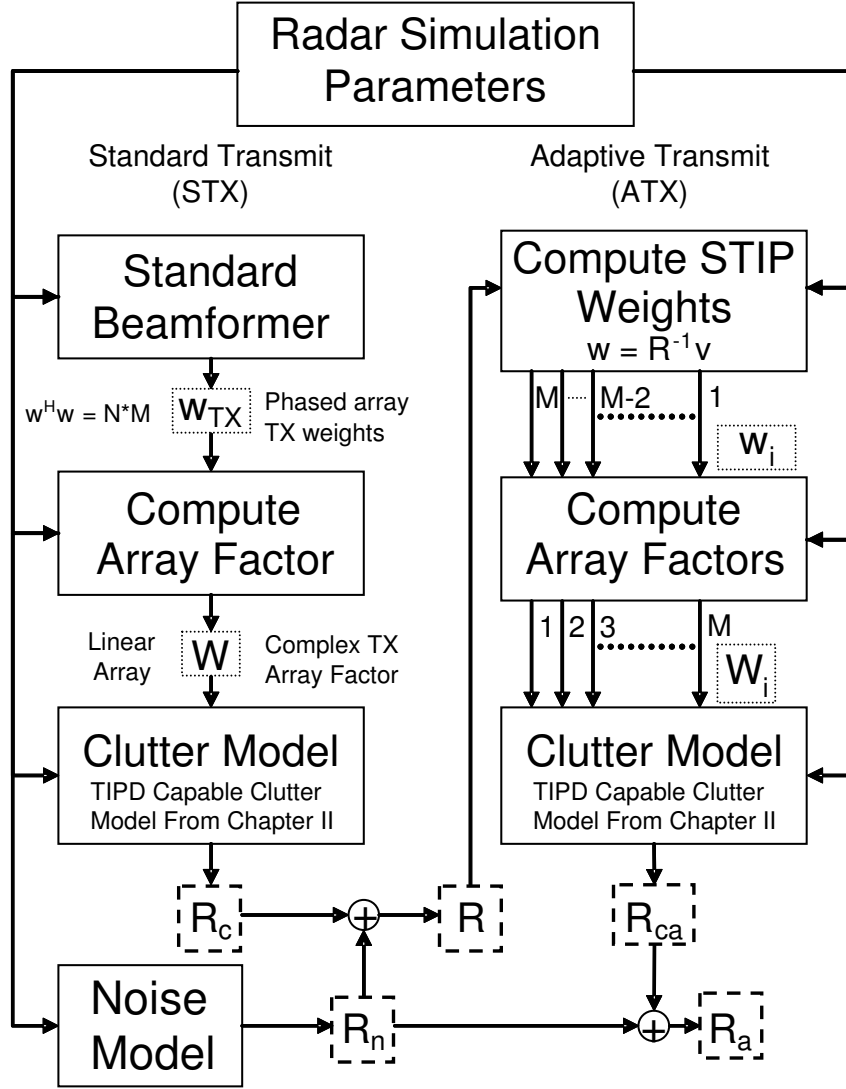


Figure 4.13: Block diagram detailing a STIP weight synthesis technique using optimal MF weights [27].

First, a standard illumination pattern is used to generate a known clutter covariance matrix \mathbf{R}_c as detailed along the left-hand side of Fig. 4.13. This process is referred to as *Standard Transmit*, or *STX*. The STX procedure uses a single constraint, non-adaptive transmit weight set. The “TX Antenna Model” block calculates the transmit array factor $W(\theta_i, \phi_k)$ for any normalized ($\mathbf{w}^H \mathbf{w} = N$) set of antenna weights. The clutter model is then used to generate a known, ideal clutter covariance

matrix \mathbf{R}_c which is added to noise covariance matrix \mathbf{R}_n to form the ideal clutter-plus-noise covariance matrix \mathbf{R} .

As depicted along the right-hand-side of Fig. 4.13, the *Adaptive Transmit* process, or *ATX*, generates complex element weights from the covariance matrix \mathbf{R} using the well-known optimum STAP MF. Given the construction of \mathbf{v} via the Kronecker product, the $MN \times 1$ dimensional weight vector \mathbf{w} can be parsed into M sets of $N \times 1$ spatial weight vectors and used as transmit array weights. Using this approach, the ATX method is inherently optimized for a given target Doppler frequency and azimuth location, specified by \mathbf{v} .

After STIP weight synthesis by the “Compute STIP Weights” block in Fig. 4.13, there is one additional step which is required to achieve desired results; the temporal order of the spatial weight set is reversed prior to computing the array factors. This is done by simply “time reversing” the weight sets without changing the transmit pulses. The result of this process is illustrated in Fig. 4.13 where the output of the “Compute STIP Weights” block shows reverse numbering from M down to 1. The necessity and phenomenology of this time reversal is illustrated by example in Section 4.5.

In the process outlined above the “clairvoyant transmit weights” are synthesized using clairvoyant knowledge of the interference environment. In practice, one might consider a modified technique whereby the estimated covariance from the previous CPI of data is used in place of the clairvoyant covariance, thereby generating the adaptive illumination weights for each pulse transmitted in the “next” CPI of M pulses. Such an idea is explored further in the following section.

4.4.2 Pattern Synthesis: Using Previous CPI Data. Some preliminary analysis appears in literature suggesting the use of previous CPI interference estimates to improve STAP performance [75]. In applications where the clutter scene is relatively stable from CPI to CPI, a usable estimate for the current interference environment can be readily obtained using data from the previous CPI. Such a technique could be used here to estimate the interference environment for generating illumination pat-

terns. This process could involve alternating between standard illumination and STIP transmission cycles such that the standard illumination cycle data is used to generate a conventional interference estimate (to which traditional STAP *could* applied) which is then be used to synthesize STIP weights using one of several techniques.

Using the STIP synthesis process presented in the previous section, all existing STAP weight vector synthesis techniques could be applied at this point to estimate STAP weights. Rather than provide a detailed report on the performance and qualities of the plethora of STAP techniques available (see [43, 62, 63, 99]), a few important properties relative to STAP weight generation are provided. First, preserving maximum mainbeam gain is essential. The mainbeam gain establishes the noise-only performance threshold and thus it is best if the mainbeam gain is maintained as high as possible.

Secondly, reducing sidelobe gain is also critical. This consideration is perhaps much more important in the generation of STIP weights than in STAP weights. Illumination patterns having higher sidelobe levels will *create* more interference power, whereas the impact of higher sidelobes in filtering received data is limited by the fixed energy received at the high sidelobe “location” in azimuth-elevation space as determined by the illumination pattern. Lastly, factored or partially adaptive STAP weight synthesis methods are not particularly useful in STIP weight generation given they don’t exploit the joint azimuth-Doppler potential that STIP is capable of exploiting. The importance of these considerations cannot be over-emphasized. *Non-adaptive* SIP patterns having low sidelobes and maximum mainbeam gain will often easily outperform *adaptive* STIP patterns characterized by high sidelobes and low mainbeam gain.

As mentioned earlier, when using estimated covariance techniques it would be important to choose/develop the estimation techniques for STIP and STAP jointly, such that maximum synergism can be achieved. Since the existing research [75] on the subject is based on industry standard datasets, the ability to properly simulate

clutter covariance “aging” would have to be developed for the radar models used here. These areas are thus not investigated here and are recommended for future research.

4.4.3 Pattern Synthesis: Knowledge-Aided Processing. Recent research in Knowledge-Aided Space-Time Adaptive Processing (KA-STAP) [6,13,21,31,41,68,73,75,89], adaptive pulse shaping [33–35,49,76–79], and Fully Adaptive Radar (FAR) [48] strongly suggests that the exploitation of relevant *a priori* knowledge in a Bayesian framework offers an undeniable advantage to adaptive radar processing schemes that can effectively incorporate such knowledge.

DARPA’s Knowledge-Aided Sensor Signal Processing and Expert Reasoning (KASSPER) program [47], now in its fifth year, has pushed the envelope in effectively incorporating existing knowledge into adaptive signal processing. The information presented in Section 4.4.2 on using prior CPI data to augment weight synthesis directly descends from the KASSPER program [47,75]. Given the analogous relationship established here between STAP and STIP weight generation, there is every reason to believe that knowledge-aided techniques that have been considered for STAP could be very effectively applied to STIP weight generation. In fact, these techniques are perhaps much more important for STIP weight generation than for STAP—since in practice STIP weight generation processes must rely on the best estimate of the environment to be sampled, before it is sampled.

There are many knowledge-aided, model-based, and expert reasoning based strategies developed for STAP that appear immediately applicable to STIP weight generation. The investigation of each technology, as well as the combination of multiple technologies, is viewed as a fertile area for future research and one critical to the long-term success of STIP technology. To highlight the potential of knowledge-aided techniques for STIP generation, a simple example utilizing model based weight synthesis is considered.

Under static clutter environmental conditions, the Doppler shift of all ground reflections as a function of azimuth-elevation angle is easily calculated by projecting

the speed and direction of the airborne surveillance platform onto any “patch” of ground. Given the accuracy of modern day navigation systems in determining aircraft attitude (to include crab angle) and ground velocity, the “location” of the clutter in the azimuth-elevation-Doppler space is generally knowable. Incorporate wind and the resulting Internal Clutter Motion (ICM) effect results in a “wider” clutter ridge, though its general location remains unchanged.

It is conceptually easy to visualize the synthesis of *spatial* antenna nulls which are directed at a particular azimuth-elevation location, even on transmit—it’s merely a function of steering one of the $N-1$ available array nulls to a given angle. Space time illumination patterns simply extend this capability to cast a null at a particular joint Doppler frequency *and* azimuth angle. Thus, since the clutter “location” in azimuth-Doppler space is geometrically determinable, it is *conceptually* feasible to construct model based STIP weights that cast space-time nulls at the clutter. Recall that these nulls are only “realized” given a particular *receive* Doppler filter. Fundamentally, physics suggests that such nulling is possible but implementation requires *detailed knowledge* of the antenna array, as well as *many* other aspects of the radar environment.

One major obstacle to realizing the full potential of either spatial nulling or space-time nulling *on transmit* is having an accurately calibrated transmit array, accounting for such errors as channel mismatch and antenna array misalignment [43]. Although this type of calibration data has been mandated for some next generation systems [46], calibration data is generally unavailable on most conventional radars. Most STAP techniques are able to “work around” or minimize the impact of these errors given they adapt to the data as received—natural compensation occurs given the techniques react to the received data which inherently contains these errors. Thus, given the data incorporates the mismatch effects the adaptive filters inherently account for them.

It is concluded that the area of knowledge-aided processing is a valuable enabling technology for STIP pattern synthesis. By augmenting STAP's historical reliance on measured radar data with external knowledge sources, knowledge-aided methods represent a key to practical STIP weight synthesis. The tremendous growth and successful contributions of knowledge-based/knowledge-aided processing directly support the future realization of practical STIP implementation.

4.5 *Fully Adaptive Radar: Joint STIP-STAP Operation*

This section explores results obtained by using joint STIP-STAP processing improve overall radar performance. Results from a system using standard (non-varying) illumination patterns are compared with one employing STIP. This comparison is carried out for a typical airborne Ground Moving Target Indication (GMTI) radar scenario. In this case, the optimum matched filter process, as outlined in Section 4.4.1, is used to synthesize STIP weights. Using this technique assumes the availability of *a priori* clairvoyant knowledge of the interference prior to transmission. Obviously, this “perfect” information is not available in practice but the technique is used here to highlight various phenomenological effects associated with incorporating STIP. Simulation parameters for the scenario considered are given in Table 4.1.

4.5.1 FAR: Baseline Results for Joint STIP-STAP Processing. Consider the $N = M = 10$ sidelooking airborne clutter scenario described by parameters in Table 4.1. Figure 4.14 shows the azimuth-Doppler response of the fixed, Standard Illumination Pattern (SIP) generated from uniform weights. Using the clutter model of Chapter II and parameters specified in Table 4.1, Fig. 4.15 shows the resultant clutter PSD which was generated with the SM spectrum estimator.

By visually comparing Fig. 4.14 and Fig. 4.15 responses, the clutter Doppler shift due to platform motion is readily apparent. The sidelobes of the radiated antenna pattern are shifted in Doppler just as if the entire row of spatial sidelobes were rotated counter-clockwise about the mainbeam. This azimuth dependent Doppler shift is a

Table 4.1: Simulation parameters for STIP illustration.

Variable	Value
M (pulses in CPI)	10
N (number of azimuth elements)	10
ϕ (Azimuth Transmit Direction)	0°
θ (Target/Clutter Elevation)	-4.1°
f_o (carrier frequency)	1240 MHz
f_r (pulse repetition frequency)	1984 Hz
τ (pulse width)	$0.8 \mu s$
P_t (transmit power)	115 kW
B (bandwidth)	800 kHz
F_n (receiver noise figure)	3 dB
N_c (number of clutter patches)	360
h_a (aircraft altitude)	2073 m
β (clutter ridge slope)	1
R (target range)	30 km
N_a (ambiguous range rings)	2
γ (clutter gamma)	-3 dB
Array Transmit Gain	$(NM)^2 = 20$ dB
Element Pattern	isometric
Element Gain	4 dB
Backlobe Attenuation	-90 dB
d_x (inter-element spacing, x -axis)	$c/(2f_0)$ m
Transmit Taper	Uniform (None)
L_s (system losses)	3 dB

function of sensor platform velocity, crab angle, and clutter azimuth angle, and is given by (2.71). The optimum MF STAP weights for detecting a target at 0.25 normalized Doppler is computed for the interference covariance illustrated in Fig.4.15. The resultant azimuth-Doppler response using these weights is given in Fig. 4.16. The plots in Fig.4.14 through Fig. 4.16 represent the standard illumination case and receive processing weights used in the STAP process. Attention is now turned toward providing a capability to detect a target at 0.25 normalized Doppler using joint STIP-STAP processing.

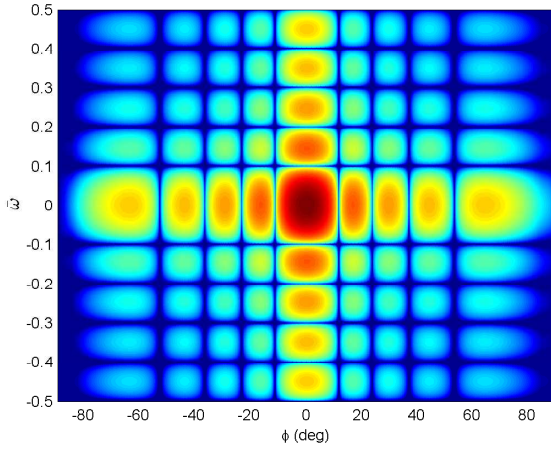


Figure 4.14: Azimuth-Doppler response of SIP transmit weights.

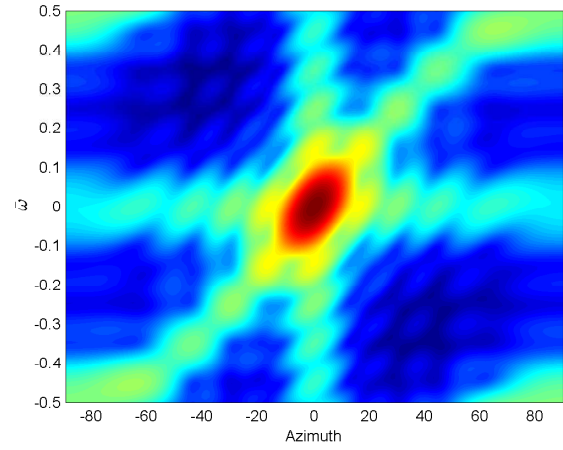


Figure 4.15: Clutter PSD for the scenario described in Table 4.1.

In discussing the synthesis of STIP weights, the pulse-dependent array factor view of STAP described in Section 4.1.1 is utilized to gain insight. Figures 4.17 and

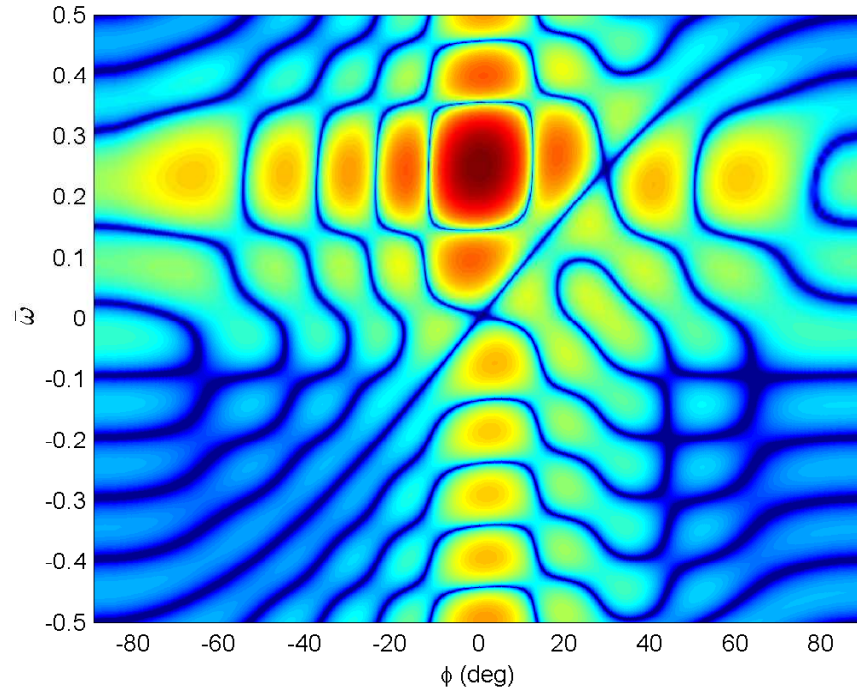


Figure 4.16: Azimuth-Doppler response of optimum MF weights to detect a target at 0.25 normalized Doppler ($\bar{\omega}$) for the clutter scenario depicted in Fig. 4.15.

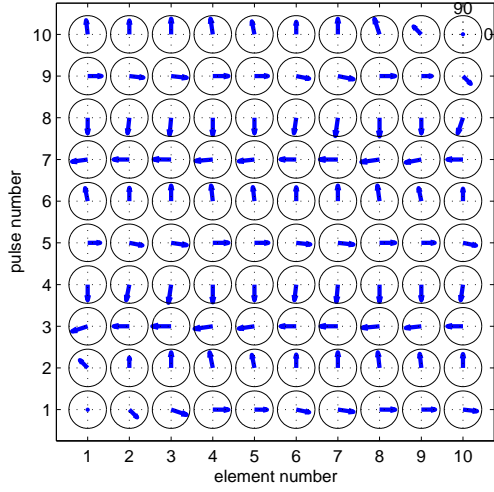


Figure 4.17: Phaser Diagram of optimum MF weights for $\bar{\omega} = 0.25$ given the clutter scenario depicted in Fig. 4.15.

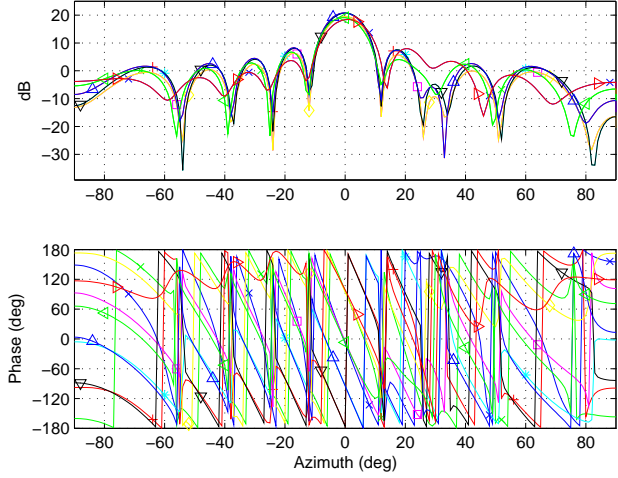


Figure 4.18: Array factor magnitude and phase responses for the optimum MF weights depicted in Fig 4.17.

4.18 provide the phaser diagram and array factor magnitude and phase response of the optimum MF transmit weights for this scenario. As outlined in Fig. 4.13, the optimum transmit weights are derived by first re-ordering (time reversing) the optimum STAP weights such that the spatial weights applied to the last received pulse are now applied to the first transmitted pulse and so on. This effectively flips the Doppler dimension of the azimuth-Doppler response in Fig. 4.16 about the zero Doppler axis. Next, for the sake of clarity in this illustration, a Doppler shift of 0.25 Doppler is applied to the weight set which removes the “global” azimuth independent Doppler progression of the weight set. This shifts the mainbeam response to a normalized Doppler of 0 Hz. The phaser diagram and array factor view of the resultant STIP weights is given in Figs. 4.19 and 4.20, respectively. By comparing Fig. 4.17 with Fig. 4.19, is interesting to note that only relatively small perturbations have been induced on the STIP weights relative to the uniform weights. The array factors calculated for these two weights also vary relatively slightly from one another, with a majority of the variation falling outside the main beam. Nonetheless, these seemingly small differences are directly responsible for the resultant azimuth-Doppler response

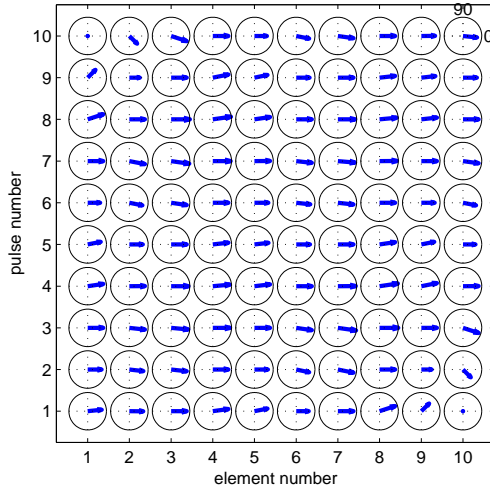


Figure 4.19: Phaser Diagram of STIP weights, derived from optimum MF weights by inverting pulse order and removing $\bar{\omega} = 0.25$ Doppler progression.

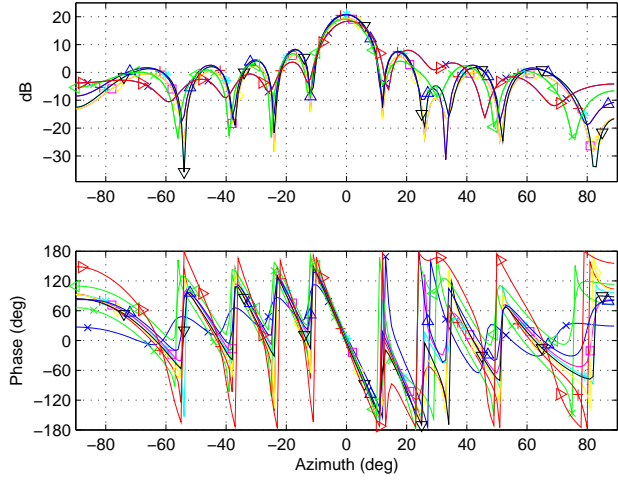


Figure 4.20: Spatial array factor magnitude and phase responses for the STIP weights depicted in Fig 4.19.

is shown in Fig. 4.21. As mentioned in Section 4.3, this figure represents the *notional* azimuth-Doppler “response” assuming a particular Doppler filter is used on receive. This distinction is necessary since Doppler filtering is inherently a receiver process and thus talking about the Doppler “response” of a set of transmit patterns is meaningless without assuming Doppler processing on receive.

It is interesting to note from Fig. 4.21 that the slope of the clutter null is inverted and the clutter null crosses zero azimuth at a 0.25 normalized Doppler—the exact location where the system has been “tuned” to detect a target. The clutter null inversion is a direct result of re-ordering the STAP weights on the pulses. Using the transmit weights depicted in Fig. 4.19, the TIPD clutter model of Chapter II is used to calculate the clutter and target responses. Figure 4.22 provides the corresponding clutter PSD. Figure 4.22 shows the same azimuth dependent Doppler shift in the clutter sidelobe energy noted previously in Fig. 4.15, although this time the inverted “S-shaped” clutter null visible in Fig. 4.21 is also shifted by the same phenomena. In effect, this causes the clutter null to be “straightened out,” such that it now casts

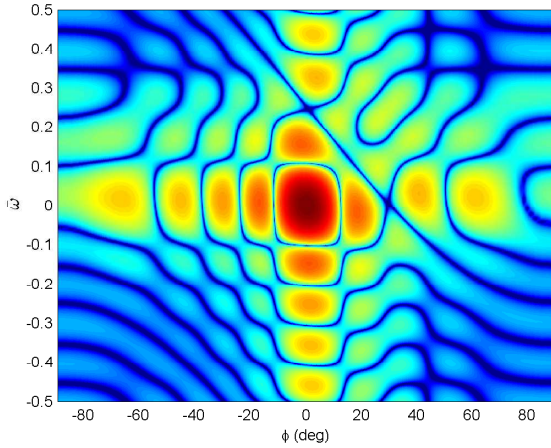


Figure 4.21: Azimuth-Doppler response of STIP transmit weights optimized for 0.25 normalized Doppler.

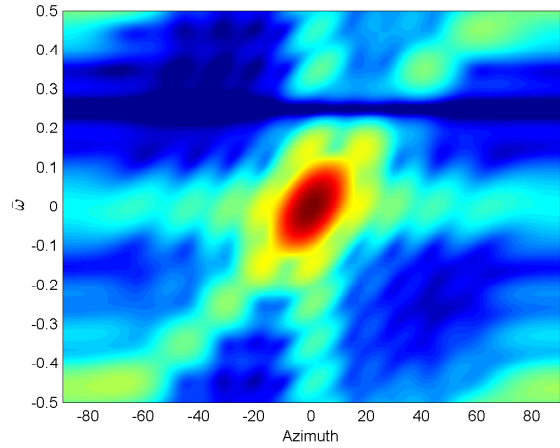


Figure 4.22: Clutter PSD resulting from STIP depicted in Fig. 4.19.

a clutter null at a single Doppler frequency (0.25 normalized Doppler) that is now persistent across all azimuth! This is a remarkable result, whereby the sidelobe-induced clutter interference has been removed/reduced at 0.25 normalized Doppler across all azimuth. In other words, the clutter spectrum which typically spans the joint azimuth-Doppler domain has been “factored” such that there is very little (if any) clutter energy present at 0.25 normalized Doppler, regardless of the azimuth angle. Thus, targets at a normalized Doppler value of 0.25 should be detectable *without* the need for *joint* processing on receive.

The optimum MF processor tuned to detect targets at 0.25 normalized Doppler is computed for the STIP generated clutter depicted in Fig. 4.22. The azimuth-Doppler response of this optimum STAP processor is given by Fig. 4.23. This “optimal” filter has nearly the same characteristics as a non-adaptive Doppler filter which indicates that very little (if any) *joint* space-time adaptivity is required to achieve noise-only performance under STIP illumination for a target at $\bar{\omega} = 0.25$. This example clearly shows how clutter shaping using STIP could result in very good receiver performance at a specified Doppler frequency using a simple non-adaptive Doppler filter on receive.

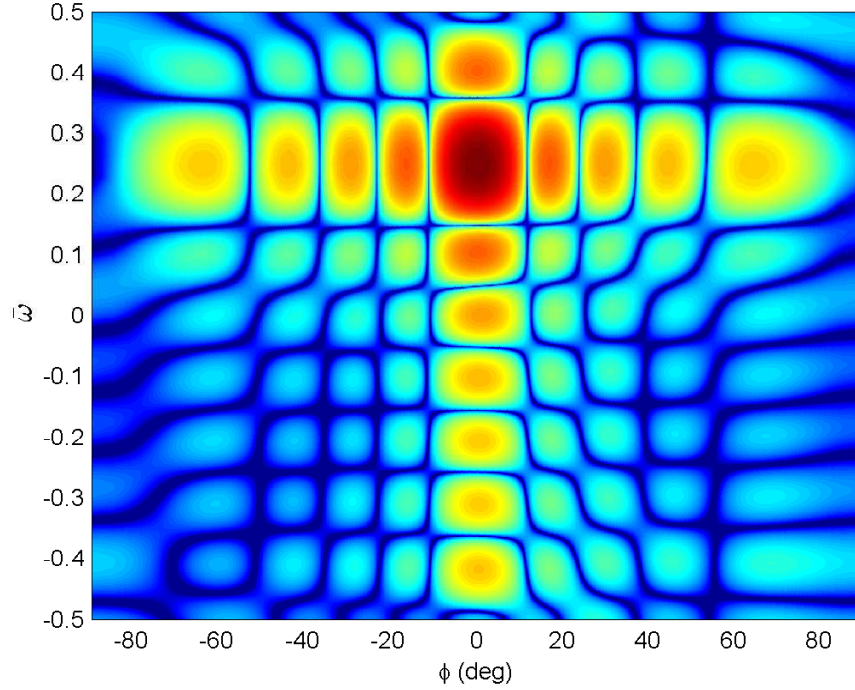


Figure 4.23: Azimuth-Doppler response for Optimum MF weights tuned to 0.25 normalized Doppler for clutter scenario depicted in Fig. 4.22.

4.5.2 Clutter Covariance Eigenvalue Analysis. Although the clutter has been “advantageously” shaped for a non-adaptive receive processor, the clutter rank *is* increased by using STIP techniques. The eigenvalue decompositions of the clutter matrixes depicted in Fig. 4.15 and Fig. 4.22 are given in Fig. 4.24

Brennan’s Rule [17, 99] predicts an interference rank of 19 which is clearly indicated in Fig. 4.24 for the standard SIP system. For the adaptive AIP system, the rank of the interference has increased to 26. This increase is not unexpected given that successive AIP pulses provide different illumination and thus violate one key assumption in the derivation of Brennan’s rule [99]. Bear in mind that conditions were enforced such that the SIP and AIP systems radiate identical average power over a CPI of M pulses and that the total interference power in the target range gate (covariance matrix trace) under SIP and AIP conditions was approximately -92.767 dBW and -92.751 dBW, respectfully (nearly identical). The interference rank differential

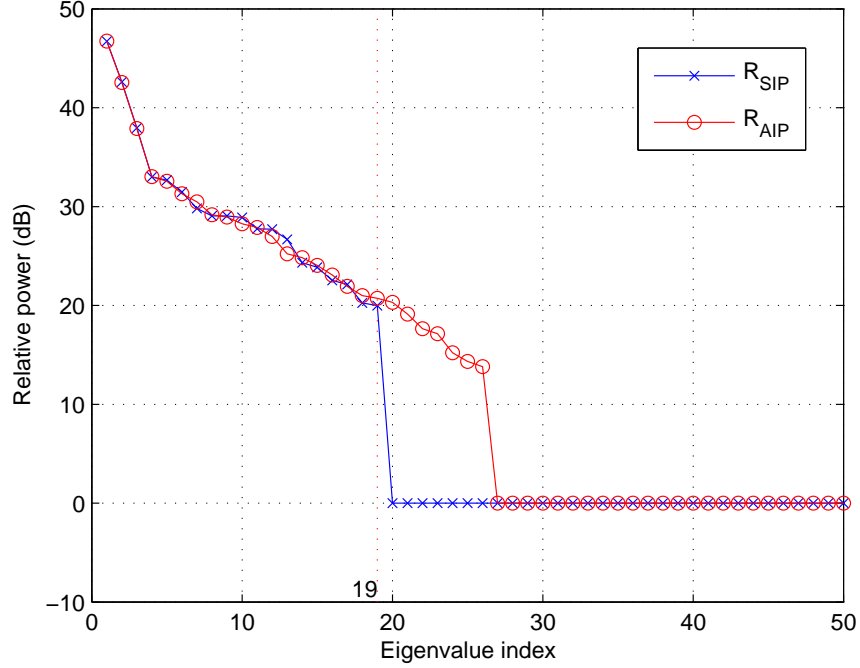


Figure 4.24: Sorted Eigenvalues of the interference covariance matrices resulting from SIP (\mathbf{R}_{SIP}) and adaptive STIP (\mathbf{R}_{AIP}).

between the two systems suggests that interfering power in the AIP system is spread over seven (26-19) additional dimensions. Detailed analysis revealed that although the power in the first 19 eigenvalues was very similar, the corresponding eigenvectors themselves were quite dissimilar. This finding was not surprising given the PSD's resulting from the SIP and AIP patterns are markedly different.

4.5.3 SINR Results. While the use of STIP increased the resultant clutter rank from 19 to 26, it reduced the *adaptive* DOF required to filter the clutter on receive from 19 to 0 for the particular “transmit” Doppler chosen. The non-adaptive performance which is suggested by Fig. 4.22 is verified using output SINR results provided in Fig. 4.25.

Two STAP processors are considered here under both standard (SIP) and adaptive (AIP) illumination conditions. The STAP processors considered are the optimal Matched Filter (MF) and the non-adaptive Signal Match (SM) as defined in Chapter III. Each point plotted in Fig. 4.25 represents the peak response of a Doppler

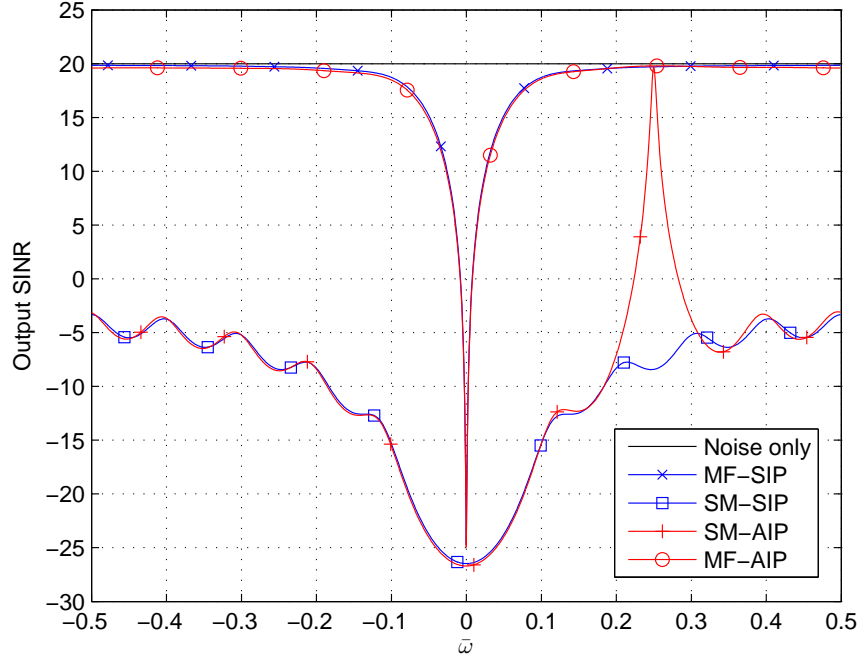


Figure 4.25: Output SINR results for the optimum Matched Filter (MF) and non-adaptive Signal Match (SM) processors under Standard Illumination (SIP) and Adaptive Illumination (AIP) conditions.

filter matched to the Doppler value shown. Note that at precisely the value of 0.25 normalized Doppler, the SM processor response under AIP conditions spikes up and approaches optimal MF performance. This response is directly attributable to the lack of clutter power in that Doppler filter, brought about through clutter shaping. Note also that the optimum MF performance under AIP conditions is nearly identical to the optimum MF performance under SIP conditions. This indicates adaptive illumination does not reduce the performance potential of STAP at frequencies other than that for which STIP weights were optimized. However, as discussed in the next section there is a practical issue which will impact STIP performance.

4.5.4 Transmit Power Assumptions. As reported earlier, the STIP transmit patterns are derived via the process outlined in Fig. 4.13. This process normalizes the adaptive weights to be the same as the non-adaptive weights, i.e., $\mathbf{w}^H \mathbf{w} = MN$,

which effectively sets the total radiated power of the AIP system to that of the SIP system over the CPI of M pulses. While this normalization process facilitates a “fair” comparison based on total radiated power, it results in individual AIP weight values that are greater than one, which is the maximum weight magnitude of the SIP weight set. For example, the optimal weight set depicted in Fig. 4.19 has a peak weight magnitude of 1.24 (note, this represents signal *amplitude* gain, not power gain).

In practice, this is akin to demanding a 53% increase in output power from a given T/R module in the AESA array. If one assumes the T/R modules are operated at their maximum transmit power level (typically true, so as not to artificially limit performance to less than the system’s capabilities) then this additional amplification is not available. Also, given the gain and phase relationships between all the synthesized weights must be maintained to achieve the desired result, a more practical comparison might be to normalize weight sets such that the maximum gain of any given weight is one. The sorted magnitude of the STIP weights depicted in Fig. 4.19 are plotted in Fig. 4.26 under both normalization conditions. This figure illustrates the distribution of element output transmit power necessary to achieve a constant total radiated power (over a CPI of M pulses), as well as the output power of the elements under a limited maximum element transmit power assumption. Assuming a maximum transmit gain of one, the STIP simulation was rerun and achieved results that were consistent with the previous results. The new results were scaled and reflect the known drop in radiated power. The resulting SINR results are displayed in Fig. 4.27. By limiting the maximum weight magnitude to unity, the inner product of the transmit weights (proportional to the radiated power over the CPI) dropped from 100% to 65% (20 to 18.1 dB) reflecting a 35% power decrease. As a result, the optimum MF Output SINR performance under STIP conditions given the same constraint dropped from 20 to 17.7 dB (41% power decrease). While at first glance these performance decreases seem substantial, they are actually smaller than the performance hit due to most antenna tapers (windows) commonly used in practice to reduce sidelobe gains. According to [57], relative to a rectangular/uniform window having a baseline coherent gain

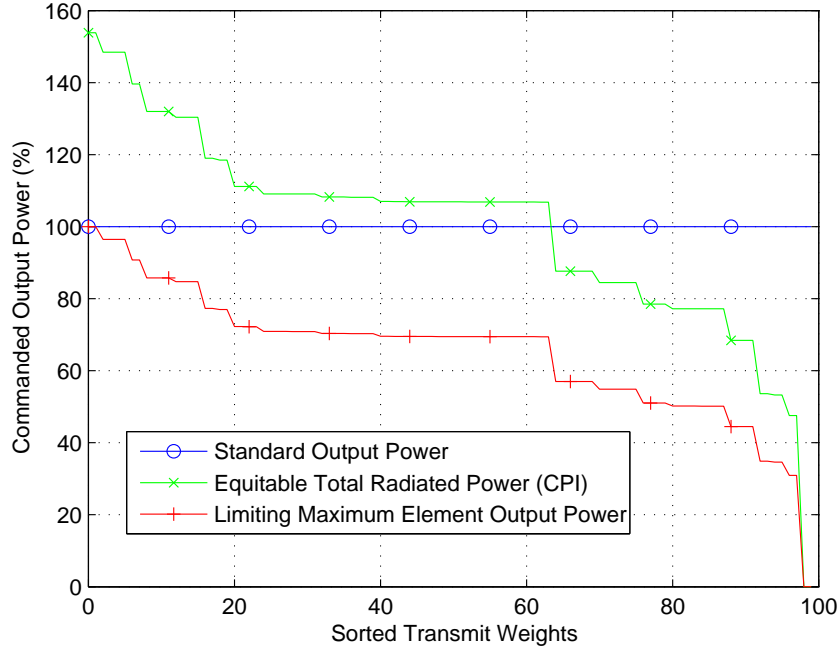


Figure 4.26: Sorted weight magnitudes under different normalization assumptions to facilitate SIP/AIP comparisons: 1) Equitable Total radiated power over CPI and 2) Equitable limited maximum element output power.

of one, a Hamming window drops the coherent gain to 0.54, a Blackman window drops the gain to 0.42, and a commonly used Blackman-Harris window drops the gain to 0.45. Thus, it is concluded that the losses incurred through the particular STIP weights analyzed here under a limited maximum element output power comparison are at least consistent with, if not somewhat better than, losses incurred through antenna sidelobe tapering. That being highlighted, the remainder of the results utilize STIP weights which are normalized to have equitable total transmit power over a CPI of M pulses.

4.5.5 Factored Space Time (FST) Processing Under STIP. As mentioned at the beginning of the chapter, the FAR concept works best when the transmit and receive processing are designed to work together. One example of the synergy is offered through the joint implementation of STIP (as described in the previous section)

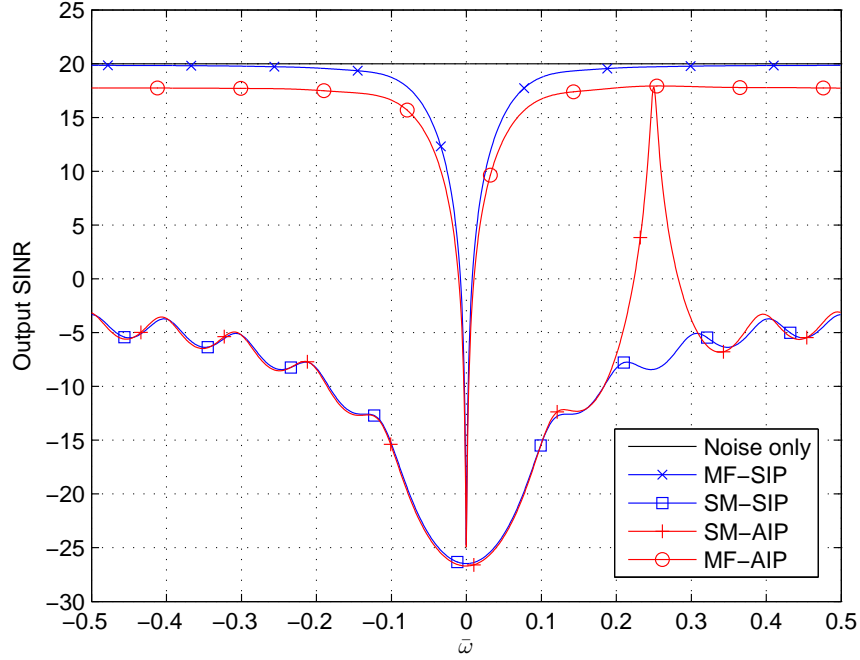


Figure 4.27: Output SINR results as presented in Fig. 4.25 except under a limited maximum element power assumption for comparing SIP and AIP results.

with the use of a simple partially-adaptive factored STAP processor described here as Factored Space Time (FST), and described in Chapter III. Figure 4.28 provides output SINR results for the FST processor using the same radar scenario simulated in the previous section.

The Factored Space Time (FST) processor first filters non-adaptively in azimuth (i.e., implements standard spatial receive beamforming in the transmit direction), and then adaptively in Doppler. Since FST is only adaptive in Doppler, it is unable to achieve noise-only performance in clutter dominated environments under SIP conditions, as illustrated by the FST-SIP curve in Fig. 4.28. However, as shown by the FST-AIP curve, STIP enables FST to achieve noise-only performance at a particular Doppler frequency (0.25 in this case).

There are several advantages for using partially adaptive processors, and FST is no exception. By being non-adaptive in the spatial dimension, the reduced adaptive

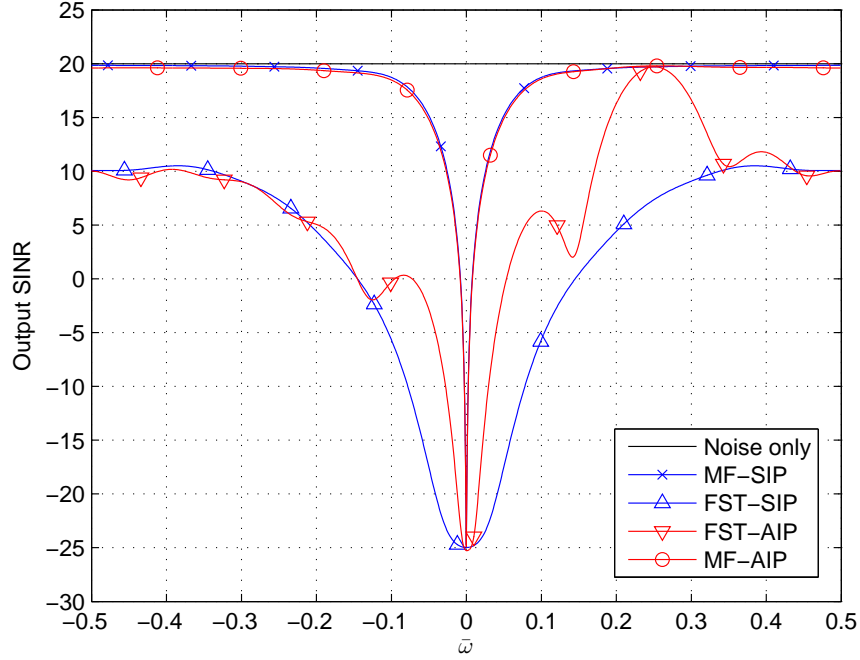


Figure 4.28: Output SINR results for the optimum Matched Filter (MF), non-adaptive Signal Match (SM), and partially adaptive Factored Space Time (FST) processors under Standard Illumination (SIP) and Adaptive Illumination (AIP) conditions.

DOF of the FST receive processor dictates a factor of N reduction in training data samples relative to a fully adaptive processor (via the RMB rule [86]), and even fewer training data samples if sub-CPI processing is used [62]. In general, lower training data requirements make STAP processing more implementable and robust in heterogeneous clutter environments. Subject to one STIP limitation as demonstrated here, i.e., the removal of clutter energy at a single Doppler frequency, the simplicity and robustness of FST processing make it attractive alternative for radar tracking when coupled with STIP on transmit.

Should Knowledge-Aided (KA) STIP weight synthesis techniques be developed and shown to be viable, the use of FST processing combined with KA-STIP offers the *potential* for achieving STAP processing capability without the expense of individual analog-to-digital converters on each array element. Given the historical success of non-data-adaptive Displaced Phase Center Antenna (DPCA) techniques, it seems

plausible to achieve an acceptable level of performance with antenna weights synthesized using onboard navigation data and the appropriate clutter models.

The FST processor does have one potential limitation. By employing a non-adaptive spatial filter up front, it makes itself very susceptible to spatially localized signal-independent interference, i.e., jamming. Without adaptive spatial nulling, the presence of broadband jammers would severely reduce the FST performance. However, the processor could employ an adaptive spatial transform rather than a non-adaptive one, crafted by sensing the signal independent interference separately from the signal dependent interference and adapting the spatial filter to null any (up to $N-1$) jammers in the scene. Signal independent interference samples are easily collected between CPIs, or in the short time period after pulse transmission but prior to the first ground return.

4.5.6 Multi-constraint weight vector synthesis. The STIP process explored thus far improves STAP performance at or near a single Doppler frequency. This is particularly well-suited for tracking applications where the location/speed of a target is known *a priori*. However, the synergistic advantages of using STIP and STAP (particularly FST processing) are not readily exploited for search modes, where the target's Doppler frequency is not exactly known. Furthermore, even for tracking applications it is desirable to have a wider Doppler span over which the target can drift between updates to increase tracking robustness. This section illustrates a modification to the proposed process that extends the usefulness of this particular STIP technique to improve performance over a larger range of Doppler frequencies.

The concept involves artificial replication of the interference environment at multiple Doppler frequencies. This is accomplished by Doppler shifting the interference covariance matrix \mathbf{R} and coherently adding the shifted version back to itself. Given a Doppler shifting vector defined as

$$\mathbf{v}_s = \mathbf{b}(\omega_{\text{shift}}) \otimes \mathbf{1}_{M \times 1} \quad (4.5)$$

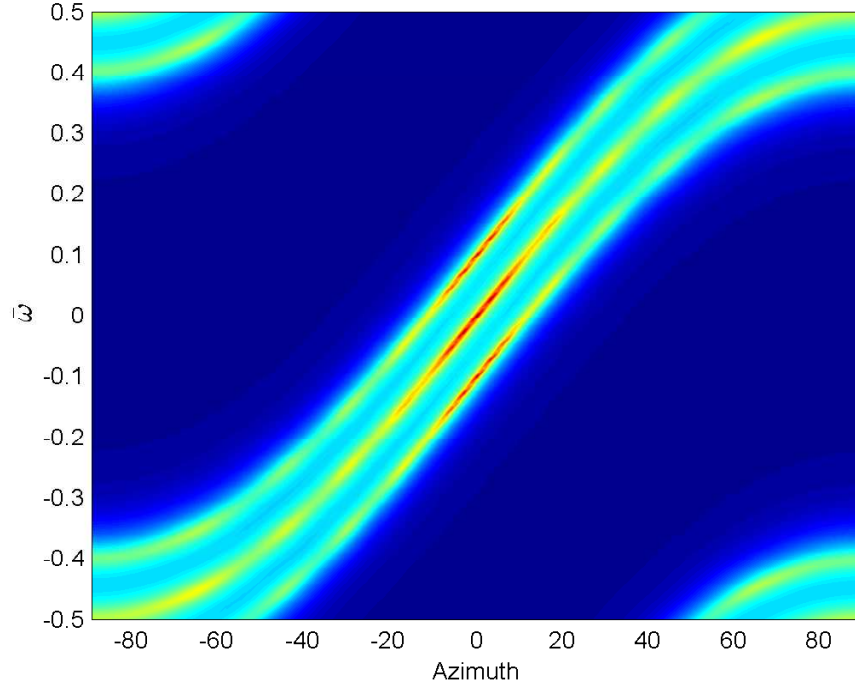


Figure 4.29: Artificially synthesized clutter interference Minimum Variance (MV) spectrum

where \mathbf{b} is a Doppler steering vector defined in (2.43), a new composite interference covariance matrix can be created by

$$\mathbf{R}_{\text{art}} = \mathbf{R} + \mathbf{v}_s \mathbf{v}_s^H \odot \mathbf{R} \quad (4.6)$$

where \odot represents a Hadamard (element wise) product. Using this technique, the “artificial” interference environment shown in Fig. 4.29 was created from the interference environment previously given in Fig. 4.1. As seen in Fig. 4.29, the clutter interference was replicated twice with each “copy” being first shifted $+/- 0.1$ in normalized Doppler. Using this new interference covariance matrix, the same process presented in Section 4.5.1 and outlined by the right-hand side of Fig. 4.13 was repeated with only a small change in the transmit Doppler value $\bar{\omega}_{\text{tx}}$ from 0.25 to 0.3.

Figure 4.30 illustrates the new STIP weights which contain a few more near-zero weight magnitudes compared to the baseline STIP weights displayed in Fig. 4.19. The

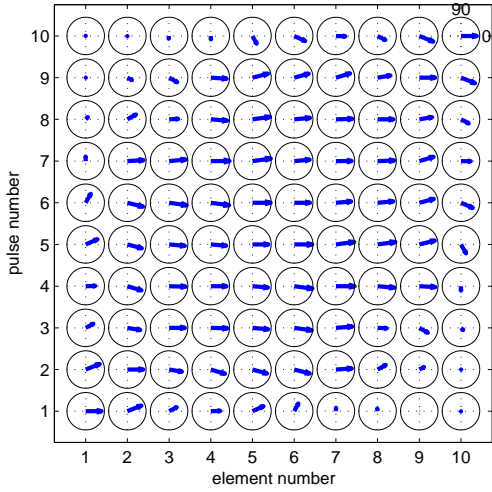


Figure 4.30: Phaser Diagram of STIP weights derived from the synthesized interference scenario depicted in Fig. 4.29.

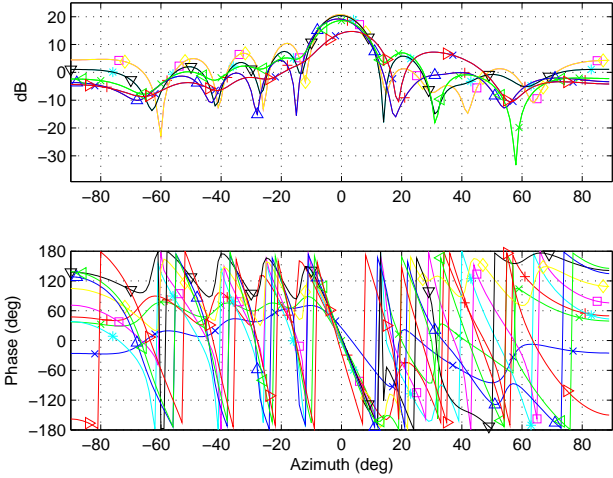


Figure 4.31: Spatial array factor magnitude and phase responses for the STIP weights depicted in Fig 4.30.

impact of more near-zero weights is the practical reduction in total output power over the CPI, as discussed in Section 4.5.4. The spatial array factors corresponding to the new STIP weights are displayed in Fig. 4.31. The loss of mainbeam radiated power is also visible here when compared to the previous array factors in Fig. 4.20.

The azimuth-Doppler response for the new weights is shown in Fig. 4.32 where the three nulls corresponding to one real and two synthesized clutter environments are clearly visible. As explained previously, the azimuth dependent Doppler shift due to aircraft velocity effectively “straightens” these nulls such that the resultant clutter spectrum, shown in Fig. 4.33, now exhibits three separate normalized Doppler frequencies (0.2, 0.3, & 0.4) which contain little or no clutter energy across all azimuth angles. This creates a larger region of Doppler over which the FST processor, in particular, achieves good SINR performance as shown in Fig. 4.34.

There is a cost associated with artificially modifying the clutter response. By specifying the higher-rank “artificial” interference scenario illustrated in Fig. 4.29, the resulting STIP weights have a wider range of amplitudes and include *more* near-zero weight values (see Fig. 4.30). Thus, there is a correspondingly lower overall

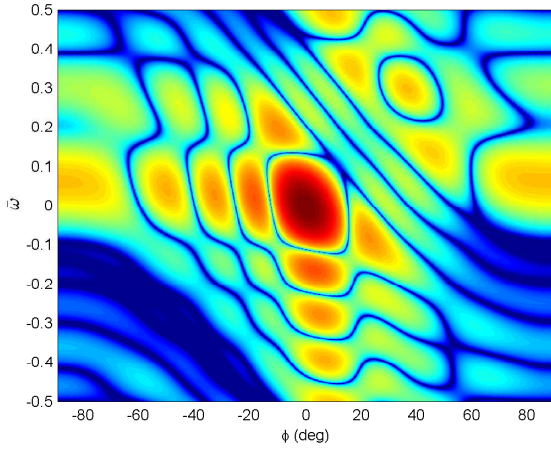


Figure 4.32: Azimuth-Doppler response of STIP weights depicted in Fig. 4.30 showing the introduction of two additional nulls.

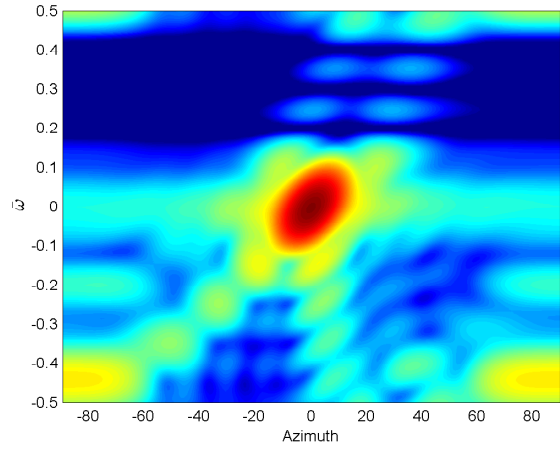


Figure 4.33: Clutter PSD resulting from STIP weights in Fig. 4.30 whose azimuth-Doppler response is given in Fig. 4.32.

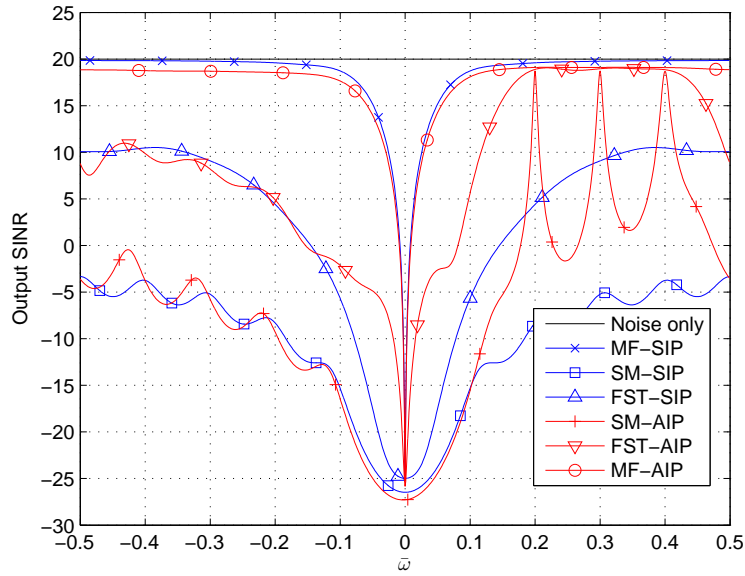


Figure 4.34: Output SINR results for an artificially synthesized interference spectrum, showing optimum MF, non-adaptive SM, and partially adaptive FST results under Standard (SIP) and Adaptive (AIP) illumination conditions.

output power under the limited maximum element output power assumption. The

output SINR performance under the limited maximum output power assumption is illustrated in Fig. 4.35.

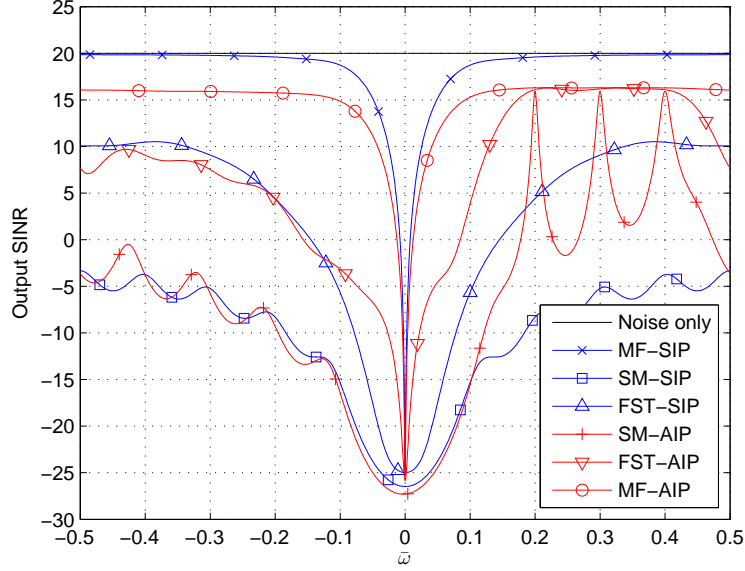


Figure 4.35: Output SINR results for the same scenario characterized in Fig. 4.34, but under a limited maximum element output power assumption

Results in Fig. 4.35 show that the optimum performance bound under AIP conditions is approximately 3.9 dB lower than the optimum performance bound under SIP conditions. As previously noted in Section 4.5.4, this loss is due to a decrease in the total illumination power provided by STIP weights compared to SIP weights under a limited maximum element output power assumption. These losses are the same type of losses incurred through the application of tapers or windows to phased array transmit patterns, which are commonly applied to reduce sidelobe gains. It can be seen from comparing the weight magnitudes in Figs. 4.19 and 4.30 that this type of loss increases under the artificially synthesized interference case, and additional testing verified that additional applications of the “shift and add” artificial interference synthesis technique further reduces output power under the maximum element power assumption. Thus, when synthesizing an artificial interference environment, there is a tradeoff between the maximum transmit power and the width of the Doppler region

over which clutter is suppressed by STIP on transmit. In this case, the performance of the partially adaptive FST and the non-adaptive SM receive processors under AIP illumination remains approximately 6 to 25 dB better than the performance of the same receive processors under SIP illumination conditions. However, the reader may recall that these gains remain inherently dependent on having clairvoyant knowledge of the interference spectrum prior to transmit. The performance of AIP is still ultimately dependent on the quality of the interference environment estimate, which remains an area of future research.

4.6 *Summary*

The power of STAP inherently lies in its ability to synthesize filters in the joint space-time domain, and can be viewed as the application of pulse dependent spatial array factors applied to sampled radar data. Using this view, Space Time Illumination Patterns (STIP) bring the power of STAP to the radar transmitter by exploiting previously untapped transmit DOF to create space-time illumination “nulls” on transmit.

Although Doppler filtering only occurs upon reception, STIP has demonstrated an ability to create joint space-time nulls that are effectively realized on receive using simple Doppler filtering. STIP pattern synthesis is expected to be as critical to performance as the covariance estimation process is to STAP. In the initial synthesis method proposed here, the STIP and STAP processes for synthesizing weights are closely related. The creation of effective STIP patterns relies on knowledge of the environment which presents an obvious challenge. However, the growing body of research in knowledge-aided and knowledge-based STAP techniques are providing results which are minimizing the challenge such that implementable STIP solutions may be possible in the near future.

A representative STIP application is introduced to permit comparison of systems using ‘standard’ illumination patterns (SIP) with systems employing adaptive STIP techniques. The STIP system considered used transmit patterns derived from optimum STAP weights. Such weights are generally not available in practice but were used here to highlight various phenomenological effects associated with incorporating STIP. Comparative analysis included a practical consideration whereby AIP and SIP results were compared assuming a limited maximum element output power constraint, rather than a total output power constraint over the CPI. Losses associated with AIP magnitude weight variation were found to be less than those experienced when common tapers and windowing functions are applied to reduce sidelobe gains.

Using the tailored transmit patterns, STIP effectively shaped the signal-dependent interference (clutter) such that a non-adaptive Doppler filter achieves noise-only performance. The differences between space-time beamforming of STIP and space-time filtering of STAP were explored, citing the potential synergy of jointly designing the techniques to achieve maximum synergy. Finally, one method for improving STIP enabled STAP performance across a wider band of Doppler frequencies was demonstrated. This method involved synthesizing an artificial interference spectrum to “widen” the Doppler region of noise-only performance by the non-adaptive and partially adaptive processors. However, there is a tradeoff between the width of the clutter-free Doppler frequency span and the amount of mainbeam gain provided by the adapted illumination patterns.

V. Scene Adaptive Illumination Patterns (SAIP)

This chapter details one application of Adaptive Illumination Patterns (AIP) whereby *a priori* knowledge of the radar scene is used to design an adaptive illumination pattern that improves adaptive receiver processing performance, such as Space Time Adaptive Processing (STAP). This application uses a planar array to generate an illumination pattern that has both horizontal and vertical adaptivity. The pattern is updated at intervals equal to or greater than the radar Coherent Processing Interval (CPI), resulting in constant amplitude and phase characteristics throughout the coherent processing. A close-in sensing geometry is a key part of the concept explained here, as it provides *elevation diversity* across the radar’s area of operation. The AIP implementation described herein uses Scene Adaptive Illumination Patterns (SAIP) to effectively mitigate a source of heterogeneous clutter, a well-known roadblock to effective STAP implementation in real-world applications.

5.1 Introduction

The ability to accurately detect and track moving ground targets in densely populated urban, or otherwise heterogeneous environments, from an airborne platform presents both an important and challenging surveillance problem. This task, particularly in bad weather conditions, is typically assigned to a Ground Moving Target Indication (GMTI) radar for which the Minimum Discernable Velocity (MDV) is a key performance parameter. In recent years, researchers have turned to Knowledge-Aided Space Time Adaptive Processing (KA-STAP) [6, 21, 41, 68, 73, 75, 89] and Fully Adaptive Radar (FAR) [48] paradigms to invoke the power of *a priori* knowledge in achieving more robust performance and lower MDV.

The use of knowledge-aided processing is often employed to combat problems associated with clutter heterogeneity. Space Time Adaptive Processing (STAP) is often first understood through a scholarly exploration of its solid mathematical framework from which “Reed’s rule” [86] was born. This important and commonly cited “rule-of-thumb” relates, as a linear function of the STAP processor’s Degrees-of-Freedom

(DOF), the amount of “training data” samples to average STAP performance, relative to an optimum performance bound. In GMTI STAP, the Training Data (TD) consists of returns from adjacent range rings. To achieve the average performance predicted by Reed’s rule for a given quantity of TD, the TD must be independent and identically distributed (i.i.d.) across range, a condition seldom present in practical applications.

The reality of heterogeneous clutter returns makes STAP-based GMTI inherently difficult. In an *academic* sense (i.e., assuming the existence of adequate training data), achieving a lower MDV requires “higher” temporal and spatial DOF, and consequently more training data (via Reed’s Rule [86]). Thus, practically speaking, low MDV requires TD to be i.i.d. over a large range extent. One need look no further than out an airplane window to realize meeting that condition is difficult, if not impossible, in most operating environments of interest. Thus, mitigating heterogeneous clutter effects is the key to effectively lowering MDV. While there are many causes of clutter heterogeneity (see [63, 70]), the use of AIP is invoked here to focus specifically on minimizing the impact of Targets in the Training Data (TTD), which is an active area of research [7, 12, 63, 68, 72, 82, 85, 101].

Perhaps the most common approach for dealing with TTD involves using a Non-Homogeneity Detector (NHD) to identify and remove heterogeneous TD samples, thereby improving covariance estimation (see Chapters 10 & 13 in [63] for summary of NHD methods). Some Knowledge-aided approaches for battling TTD propose removing potentially corrupted TD samples based on *a priori* knowledge of road locations, platform position and orientation [7, 12, 68, 101]. In addition to NHD, other common techniques such as diagonal loading the estimated covariance matrix and using non-adaptive processors (e.g., DPCA) have also been suggested to combat TTD [72].

While these techniques have demonstrated substantial performance improvements, they are not without some drawbacks. Effective NHD is difficult in very dense

target environments [12, 72], and even if the corrupted TD can be successfully identified, its removal reduces the available TD for estimating interference statistics. Like NHD, knowledge-aided removal of TD based on known road locations (thus *assumed* target presence) also has the net effect of reducing TD, sometimes unnecessarily. Diagonal loading is reported to be effective in some cases [72] but not all [12], and DPCA requires stringent hardware tolerances and zero crab angle to be effective [72].

This chapter proposes a new approach for minimizing the negative impacts of TTD. Using *a priori* road location information, modern AESA array technology, and geometries consistent with close-in sensing applications, the transmit antenna pattern is adaptively altered to illuminate the scene such that *transmit pattern nulls* coincide with road locations running through the training data. By not illuminating the vehicular targets with transmit energy, the contaminating reflected target energy is effectively reduced, thereby converting target corrupted training data into a more homogeneous, clutter-only condition. In a sense, this technique has the potential of “pruning” the radar returns of “heterogeneities” prior to their reception.

Note that the proposed technique is independent and perfectly complementary to the existing TTD minimization techniques previously mentioned. It is expected that the integrated use of Adaptive Illumination would only increase the effectiveness of existing NHD-like and knowledge-aided techniques, and the synergistic combination will result in improved performance in target-rich environments.

5.2 *Site-Specific Adaptive Illumination*

Nature dictates that radar systems can only detect that which is “illuminated” with radiated electromagnetic energy. The spatial allocation of radiated energy is determined by its transmit (illumination) pattern. Modern Active Electronically Steered Arrays (AESAs) have the inherent capability to adjust their illumination pattern in “real time”. The characteristic sidelobe structure of an AESA guarantees that those areas which lie in illumination pattern nulls are not as observable (subject to pattern null depth) by the radar despite the amount of receiver processing applied. While

tapering (windowing) an array pattern is a well developed technique for lowering the peak gain of antenna sidelobes, the *location* of transmit pattern nulls is generally not a design consideration—until now.

In some heterogenous environments, there are undoubtedly specific “objects” in the radar scene whose reflections directly contribute to the heterogeneous nature of the clutter returns. These would include so-called clutter discretely as well as moving objects which by nature of their additional Doppler shift degrade clutter homogeneity. The AIP concept introduced here involves using the spatial DOF of an AESA *on transmit* to adaptively cast illumination pattern nulls at those areas likely to contribute heterogeneous returns across range gates. Specifically, this work focuses on placing transmit nulls along road locations in the scene, potentially restoring a degree of homogeneity to road/target infested training data. This technique is referred to throughout as Scene Adaptive Illumination Patterns (SAIP).

To accomplish SAIP, the illumination patterns must be *effectively* adaptive in both azimuth and elevation. This requires a planar AESA transmit antenna. STAP is most often conducted using a linear array, or a planar array that is “converted” to a equivalent linear array by beamforming each column of elements in elevation. SAIP requires elevation adaptivity on transmit, but not on receive—thus, standard elevation beamforming and STAP processing is employable alongside SAIP without modification.

For elevation adaptivity of a planar array to be effective, surveillance must occur at low Range-to-Height (R/H) ratios where elevation diversity exists across the TD range extent. This represents a significant difference from typical STAP scenarios that are characterized by high R/H ratios. For example, the KASSPER challenge data set has a range extent of 15.0 km and an elevation diversity of only 1.4° . If the 15.0 km region started at 4.0 km rather than at 35.0 km, the elevation diversity across the TD would be 40 degrees. Such elevation diversity combined with sufficient vertical DOF allows adaptive transmit (spatial) nulls to be projected into the training data,

potentially attenuating heterogeneous reflections. This type of geometry is consistent with close-in sensing applications.

This type of adaptivity seems particularly well-suited for placing nulls along road locations given they resemble continuous “lines” of potential heterogeneity in azimuth-elevation space. However, depending on the road geometry and system parameters, a transmit null may not be the most appropriate anti-TTD tool. The “resolution” of a transmit null progressively degrades for objects at lower depression angles, and roads/targets confined to a small number of range gates may be more effectively removed via Knowledge-Aided removal of only a few range gates. However, this research clearly demonstrates the utility of SAIP when roads run across a significant number of range gates. As with any adaptive algorithm, the judicious selection of constraints is crucial to achieving the overall goal of improved system performance, and a good constraint selection strategy is necessary for SAIP to be effective.

5.3 Site Specific Target Modeling

A key assumption of this work is that the majority of moving targets in the training data is vehicular traffic traveling on known (*a priori*) road segments. To accurately simulate highway traffic, a site specific simulation similar to [12] is implemented. The scene chosen is geographically situated near Baltimore, MD., and the road locations were pulled from the Census Bureau’s 2004 Tiger/Line® database [1] using the Matlab® Mapping Toolbox. Two-way traffic was simulated on selected primary roads, distributed spatially according to a Poisson time-of-arrival model with an average spacing of 600 m. Simulated traffic was composed of 70% cars and 30% trucks, each having a Rayleigh distributed RCS with a mean value of 20 and 25 dBsm (taken from [90]) respectively. Target velocity was normally distributed with a mean of 65 mph and a variance of 10 mph.

It has been reported that the TTD having the most detrimental impact on MDV are those who’s spatial and Doppler frequencies are most similar to the slow-moving targets in the range cell under test [72]. These troublesome TTD “train” the adaptive

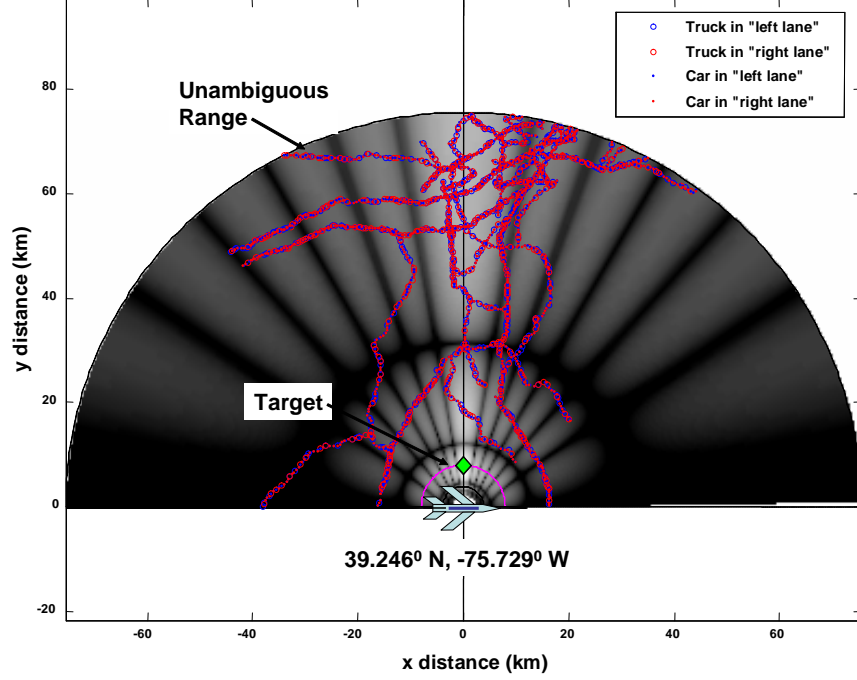


Figure 5.1: Local level projection of site-specific simulation showing road locations and target density laydown.

filter to null potential targets in the range cell of interest. The scenario examined here is based on an airborne radar located at 39.245° N latitude and 75.729° W longitude flying at a compass heading of 91° (due East) and depicted in Fig. 5.1. Simulated targets are superimposed on the array factor of the “standard” planar array illumination pattern projected onto the ground. This scenario was identified as a particularly challenging TTD situation since roads run through much of the training data at azimuth locations near the main beam. Such a scenario makes NHD especially difficult and would result in the removal of a large portion of training data. The notional radar’s parameters are listed in Table 5.1 and are loosely based on the MCARM program.

It is insightful to examine TTD locations in several domains to better understand the impacts of TTD on covariance estimation. Figure 5.2 shows the locations (relative amplitude weighting not illustrated) of the targets simulated and illustrated in Fig. 5.1 projected into the azimuth-Doppler domain. This figure helps to illustrate why TTD causes the estimated clutter “ridge” to appear wider than it really

is, which in turn causes the receive processor to form a wider-than-necessary clutter null, effectively (and unnecessarily) reducing the MDV.

For clarity, a few additional plots are provided which focus on the first 40 km of the radar range, over which the effects of SAIP can be clearly illustrated. Once again, these plots illustrate one realization of a random simulation for targets in the training data, where the target positions, velocities, and RCS values are randomized. Figure 5.3 offers a range-Doppler view of simulated targets, depicting TTD location (relative amplitude weighting not illustrated). Figure 5.4 shows a histogram of the number of targets per range cell seen in Fig. 5.3.

For each range bin containing a simulated target(s), a composite space-time snapshot of the target(s) is simulated and added to the modeled clutter space-time

Table 5.1: Radar simulation parameters.

Variable	Value
M (pulses in CPI)	25
N (element rows)	12
P (element columns)	14
ϕ (Azimuth Transmit Direction)	1°
θ (Elevation Transmit Direction)	-22.6°
ϕ_{crab} (Crab Angle)	0°
f_o (carrier frequency)	1240 MHz
f_r (pulse repetition frequency)	1984 Hz
τ (compressed pulse width)	$0.8 \mu s$
P_{ave} (average transmit power)	1.9 kW
B (bandwidth)	800 kHz
F_n (receiver noise figure)	3 dB
h_a (aircraft altitude)	3073 m
β (clutter ridge slope)	1
R_{tgt} (target range)	8 km
γ (clutter gamma)	-25 dB
g (Element Pattern)	Cosine
Element Gain	4 dB
d_x (inter-element spacing, x -axis)	$c/(2f_0)$ m
d_z (inter-element spacing, z -axis)	$c/(2f_0)$ m

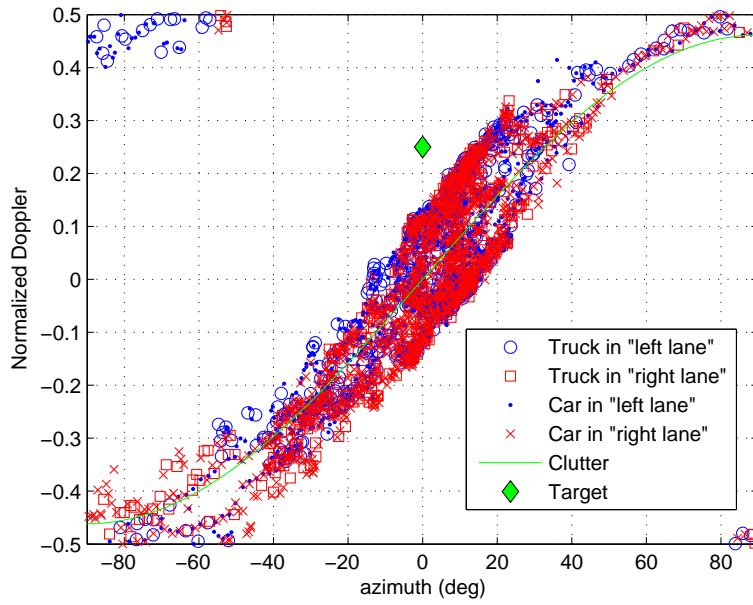


Figure 5.2: Simulated targets in Fig. 5.1 projected into the azimuth-Doppler domain.

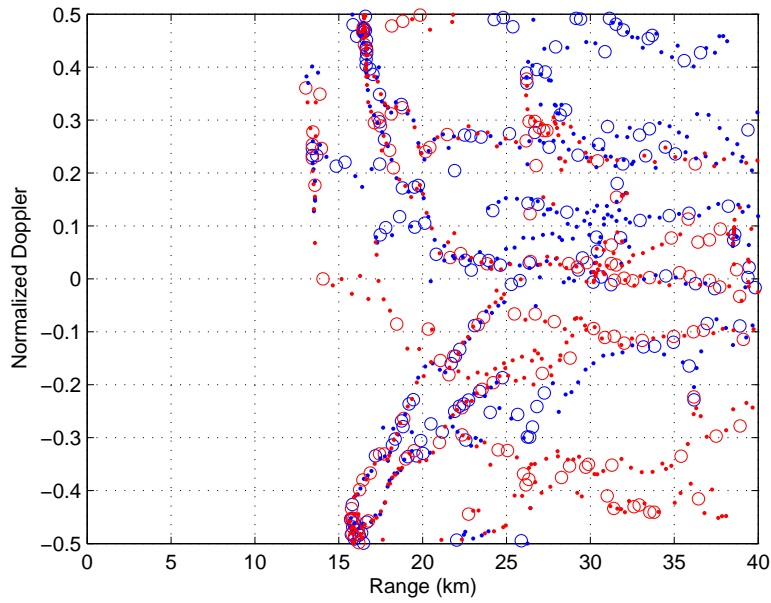


Figure 5.3: Targets from one realization of the TTD simulator (based on the road locations in Fig. 5.1) projected into the range/Doppler domain.

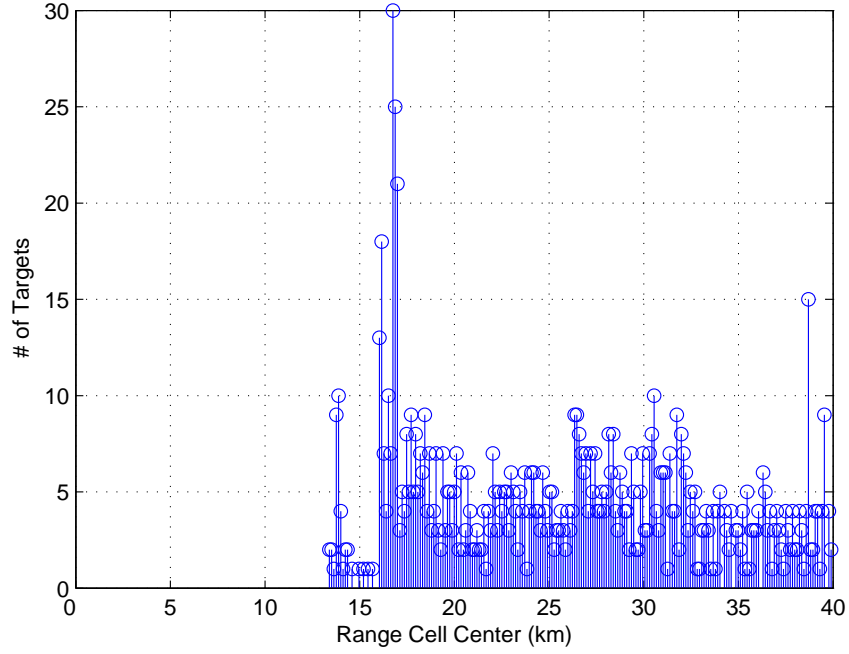


Figure 5.4: Histogram for number of simulated targets per range gate for target distribution shown in Fig. 5.3.

snapshot for the same range gate. It is important to note that the use of i.i.d. simulated clutter is not valid here, due to the impact of the antenna pattern across the training data. The effects of planar array antenna patterns combined with close-in sensing geometries are discussed next.

5.4 *STAP Considerations for Planar Array Close-in Sensing*

In combining a planar AESA with the high depression angles for geometries associated with close-in sensing applications, it is important to understand the effects of elevation sidelobes on the TD and STAP processing. As the mainbeam of a planar array is steered down to a high depression angle, the extent of the training data is no longer illuminated solely by the mainbeam but also by the elevation sidelobes. Since the gain of the first elevation sidelobe is at least 13 dB lower than the mainbeam, this causes amplitude heterogeneity of the training data located outside the mainbeam.

The effect is exasperated by high mainbeam depression angles, transmit pattern tapering, and additional elevation DOF, all of which have the effect of increasing amplitude heterogeneity across the full extent training data. However, this paper demonstrates that while using planar arrays with close-in sensing geometries causes non-uniform illumination, the TTD effects cause a relatively larger performance degradation. Tests conducted as part of this research revealed that the negative effects of clutter amplitude heterogeneity on covariance estimation are greatly ameliorated through the use of 3 dB of diagonal loading added to the estimated covariance matrix. Without diagonal loading, the AMF performance is substantially worse. Thus, with diagonal loading, careful management of system parameters, and the use of “smart” elevation beamforming on receive (more on this later), the gains from reducing TTD returns by using SAIP overcomes the small degradation caused by non-uniform illumination of the training data.

For reasons that are to be explored next, this work employs elevation subarraying prior to 2-D (azimuth-Doppler) STAP processing. The received planar array data is first beamformed in elevation and then Adaptive Matched Filtering (AMF) is applied to the resultant “equivalent” linear array data. However, the application of elevation beamforming to all the training data *at a fixed mainbeam elevation* further exasperates the amplitude heterogeneity problem—such a fixed beam would cause a 26.0 dB received clutter power loss just through the first sidelobe (a combined loss of 13.0 dB on transmit and 13.0 dB on receive). To minimize the power loss due to elevation diversity, a fixed elevation “beam” (matching the transmit direction) is not employed on receive. Assuming the standard STAP hardware model in which each antenna element is individually sampled, it is possible to iteratively apply elevation beamforming to each range gate independently. Making use of this flexibility, elevation beamforming is accomplished in the following way. Platform position and orientation is used to calculate the elevation angle of each range ring. After receiving (and time gating) the data, each $NMP \times 1$ 3-D (horizontal (x), vertical (z), and Doppler space) range

snapshot is elevation beamformed at the clutter’s respective elevation angle, giving maximum (elevation) beam gain to each resulting $NM \times 1$ 2-D range snapshot.

The resulting gain realized through this process is critical to applying STAP in a close-in sensing environment. Relative to using a fixed elevation beam pattern on transmit and receive, this technique effectively limits the elevation sidelobe losses to those of the illumination pattern. Though not implemented here, illumination pattern sidelobe losses may be further minimized by “spoiling” the transmit beam in elevation, or by adding additional elevation mainbeam constraints. For example, rather than having a single mainbeam, one could create multiple mainbeams in elevation, resulting in higher antenna pattern gain over the range/elevation extent of the training data. This is done by simply adding multiple elevation steering vectors together, where each elevation steering vector is “pointed” to a different elevation angle. However, adding more mainbeam constraints further limits the ability of the illumination pattern to cast a null at or near to the elevation constraint angle. Thus, these “extra” elevation beams must be chosen in light of the road segments to be nulled.

A reasonable question to ask is, “Why should elevation beamforming be done at all?” given the potential of 3-D STAP processing to further increase performance [52]. There are several very good reasons to do elevation beamforming in this context. First, in the GMTI application, there is no elevation diversity between the target and the clutter in a given range bin, thus elevation is not a useful discriminant for separating the target from the clutter. Second, subarraying in elevation reduces the clutter rank [26] and the total DOF of the system, which in turn lowers the quantity of training data required to achieve acceptable performance.

The third reason for subarraying the received data in elevation is because the combination of the close-in sensing geometry and the elevation adaptivity garnered by the planar array creates non-stationary clutter statistics that vary as a function of elevation. This non-stationarity is due to the changing “location” of the clutter energy in the 3-D horizontal (x), vertical (y), and Doppler space. Simply put, a 3-D

snapshot taken at an elevation angle of -30° has different clutter statistics (i.e., covariance matrix) than a 3-D snapshot taken at -10° elevation. However, elevation beamforming removes this non-stationary, restoring the range-independent relationship between the remaining two dimensions, Doppler and azimuth (for a side-looking array with zero crab angle).

Although there has been some research investigating the potential usefulness of planar arrays (or 3-D) STAP [50–56], the current body of STAP literature does not appear to address the training data issues associated with applying planar array STAP in a close-in sensing environment. As such, there are a few more operational considerations that are worth mentioning. First, one inherent limitation of planar array patterns lies in the limited elevation beamwidth and resulting range footprint of the main beam. This dictates that for a given CPI with a fixed pointing angle, a limited portion of the unambiguous range extent receives full illumination power, thus practically limiting the range extent over which one may search for targets (in a given CPI). The tradeoff is between the need to survey a larger portion of range gates in a single sweep and the need to null harmful TTD running across the azimuth angle of interest, but at a different elevation angle.

The implication is that multiple CPIs will be needed to survey an area that would be simultaneously illuminated with a linear array. However, the ability to improve MDV by notching out TTD may be worth the extended dwell time. By “scanning through” the range extent with multiple dwells, the TTD during one illumination cycle may be the target of interest during the next illumination cycle, and more reliable detection throughout the range extent should be possible by focusing on smaller range increments at any one time. This concept may be more graphically understood by revisiting Fig. 5.1 and noting 1) the size of the main beam and 2) the number of targets near 0° azimuth over the unambiguous range.

Finally, a few words about trends is insightful. While adding additional “columns” to the antenna array generally lowers MDV by limiting the clutter bandwidth, adding

more “rows” will not necessarily improve performance. Too many rows will contribute heavily to TD amplitude attenuation and heterogeneity, while too few rows may not provide sufficient illumination adaptivity to null multiple roads. Simulations also indicated a strong relationship between the radar range resolution (determined by the radar bandwidth) and the TTD impacts. In general, a coarse range resolution deemphasizes the impact of TTD, since the clutter area is much larger and thus tends to overpower or mask the target returns. Conversely, a high range resolution has the opposite effect and results in higher target-to-clutter ratios which adversely impact the covariance matrix estimates. Further, higher range resolution creates more training data, a larger percentage of which may be uncorrupted depending on target density. It is important to keep these considerations in mind when applying SAIP to mitigate TTD. A key factor for achieving good performance with SAIP is effective pattern synthesis, a topic to be covered next.

5.5 Adaptive Illumination Pattern Synthesis

The key to employing SAIP lies in synthesizing a transmit antenna pattern which projects nulls on selected roads in the scene. This is accomplished in a manner similar to building adaptive receive patterns to spatially null jammers. The first step is to build a “transmit” interference covariance matrix (\mathbf{R}_{tx}) from weighted spatial steering vectors directed at closely spaced points on each road segment to be nulled in the scene. These spatial steering vectors and resulting covariance matrix \mathbf{R}_{tx} can be calculated just prior to transmit using platform position/orientation data and a database of road locations. The construction of \mathbf{R}_{tx} is given by (5.1)

$$\mathbf{R}_{\text{tx}} = \sum_{i=0}^{N_s} \xi_i \mathbf{v}(\phi_i, \theta_i) \mathbf{v}(\phi_i, \theta_i)^H, \quad (5.1)$$

where $\mathbf{v}(\phi_i, \theta_i)$ is a spatial steering vector pointed at the i^{th} road “sample” defined as

$$\mathbf{v}(\phi_i, \theta_i) = \mathbf{e}(\theta_i) \otimes \mathbf{a}(\theta_i, \phi_i), \quad (5.2)$$

where $\mathbf{e}(\cdot)$ and $\mathbf{a}(\cdot)$ are defined in (2.42) and (2.41) respectively, and N_s is the total number of road samples (constraints), and ξ_i is the scalar weighting of each sample. The scalar weighting is based on the Signal-to-Noise Ratio (SNR) of a potential target having fixed RCS, and is given in (5.3)

$$\xi_i = \frac{P_t(NP)^2 g^2 \lambda M \sigma}{(4\pi)^3 P_n F_n L_s R_i^4}, \quad (5.3)$$

where P_t is the power per element, σ is the mean value of the largest modeled target (25 dBsm), λ is the wavelength, and the remainder of the terms are as defined in Table 5.1. This weighting function prevents over/under nulling by modeling interference proportional to potential target strength. The pulse integration gain is incorporated by M , and the array pattern is modeled as isotropic, having a gain of $(NP)^2 g^2$. The use of a *non*-isotropic pattern at this point in the weight synthesis process could result in potential interference sources not being considered, should that interference be located in a natural illumination null of the “standard” illumination pattern. Thus, an isotropic gain pattern is chosen such that all potential interference (i.e., targets on all roads) is equally considered when synthesizing adaptive patterns.

Choosing which road segments to include in the formation of \mathbf{R}_{tx} is critical to proper performance and remains an area for future optimization. For example, the analytical relationship between the locus of road samples (constraints) in az/el space and the resulting rank of the covariance matrix has not been related analytically. Such a derivation is difficult to synthesize, due to the widely varying shape of projected road segments, sampling density, and locations. There are, however, a few rules of thumb that are universally important. Constraints that are within (or even slightly outside) the null-to-null mainbeam width in either azimuth or elevation will reduce the mainbeam gain, which in turn reduces the target SNR as compared to the non-adaptive transmit pattern. Thus, road segments in the mainbeam must be excluded in the composition of \mathbf{R}_{tx} . Further, through analysis of the MCARM data, it was found that targets located outside the first couple azimuth sidelobes have little impact

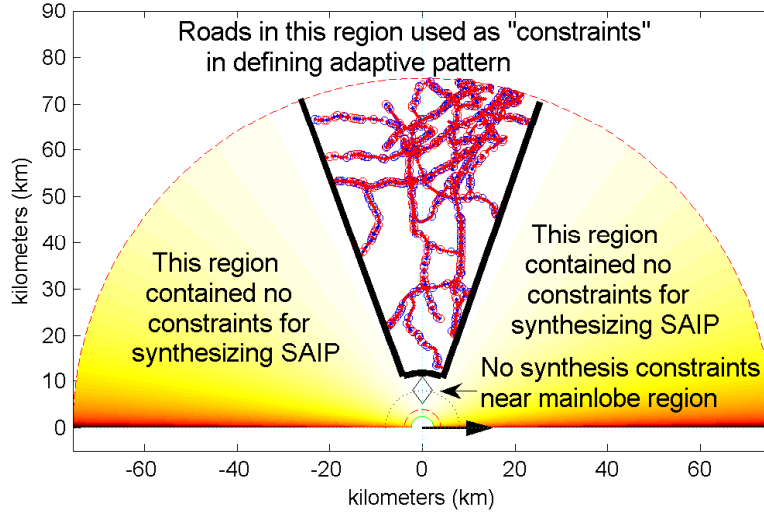


Figure 5.5: Selected road segments used as constraints for synthesizing adaptive illumination patterns. The “constraint zone,” outlined by a thick black line, is introduced to maximize the DOF usefulness and prevent self-nulling.

on performance [12]. As such, they should be excluded to avoid unnecessarily using up transmit DOF. Figure 5.5 provides a graphical representation of the “constraint zone” (potential interference locations to null) used when synthesizing the SAIP; the zone contains those road segments within the *azimuthal* region illuminated by the mainbeam and first (azimuth) sidelobes, but excludes those road segments within the elevation region containing the main beam itself. The elevation region of the mainbeam (which in this case comprises an illuminated region not more than 5 km in range) would define the area over which targets are searched for.

The constraint selection strategy must also consider a end-to-end approach for removing and/or suppressing TTD, including the use of all traditional methods developed for the received data. There are definitely some scenarios in which knowledge-aided TD excision [12] and NHD methodologies can more efficiently and effectively remove TTD effects from received data, e.g., those scenarios having roads which only traverse a few range cells at or near the main beam. In this situation, the use of adaptive illumination to null just a few range bins might lower the amplitude of adja-

cent range bins due to the finite width of the antenna pattern null. Conversely, when roads traverse many range bins at near perpendicular angles (to the range bin arc), the use of adaptive illumination only ‘notches’ out a small portion of each range bin arc, removing the non-homogeneous portion of that range bin and restoring blocks of TD to a more useful, homogeneous condition. A synergistic TTD removal strategy that takes advantage of SAIP on transmit and knowledge-aided excision and NHD methodologies on receive is likely to achieve much better results than either transmit or receive TTD mitigation methods can separately.

In the site-specific simulation examined here, the range cell under test is at a range of 8 km and an elevation angle of -22.6° . A portion of the non-adaptive transmit pattern projected onto the ground with an overlay of simulated targets is illustrated in Fig. 5.6. For proof-of-concept demonstration, the simulated target locations inside the “constraint zone” of Fig. 5.5 (randomly spaced at an average distance of 600 m apart) are used as the road samples for composing \mathbf{R}_{tx} . The resultant \mathbf{R}_{tx} is augmented with 0 dB of diagonal loading using $\sigma^2\mathbf{I}$ to set the noise floor and ensure invertibility. Finally, the SAIP weights are calculated using the optimum beamformer [43, 62]:

$$\mathbf{w}_{\text{tx}} = (\mathbf{R}_{\text{tx}} + \sigma^2\mathbf{I})^{-1}\mathbf{v}(\phi_{\text{tx}}, \theta_{\text{tx}}). \quad (5.4)$$

A portion of the resulting SAIP pattern based on the adaptive transmit weights \mathbf{w}_{tx} is illustrated in Fig. 5.7. In comparing the non-adaptive pattern in Fig. 5.6 with the adaptive pattern in Fig. 5.7, it is clear to see how targets are illuminated with much less energy by the adaptive SAIP pattern, particularly for the azimuth region containing the first sidelobes and mainbeam where the interference constraints of Fig. 5.5 are enforced.

5.6 *Simulation Results*

The effects of SAIP are first observed by examining the output of a classic non-homogeneity detector, namely the Generalized Inner Product (GIP). The GIP can

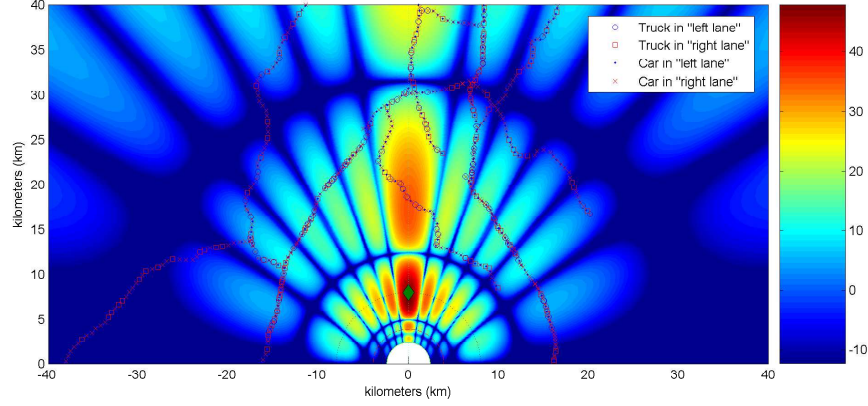


Figure 5.6: Projection of *Non-Adaptive, Standard Illumination Pattern* (SIP) onto the radar scene with target locations

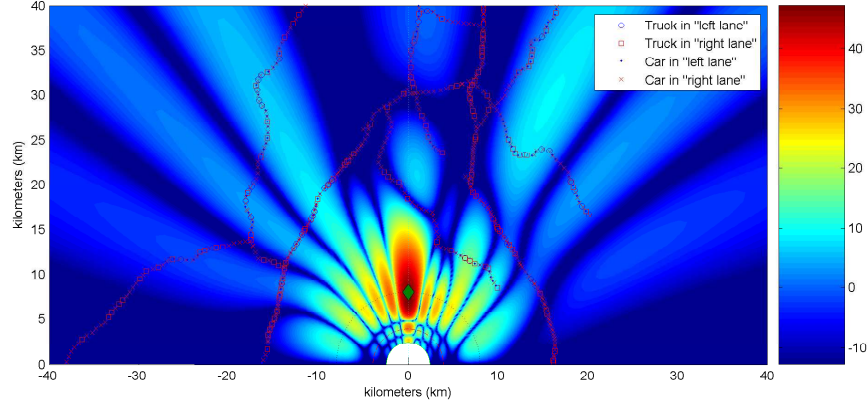


Figure 5.7: Projection of *Scene Adaptive Illumination Pattern* (SAIP) onto the radar scene with target locations

be calculated using either the known or estimated covariance, the latter of which is used here. For a snapshot of sampled radar data χ from a single range bin and an estimated covariance matrix $\hat{\mathbf{R}}$, the GIP is given by [82]:

$$\text{GIP} = \chi^H \hat{\mathbf{R}} \chi, \quad (5.5)$$

where $\hat{\mathbf{R}}$ is estimated from K range bin samples and defined in (3.6). In the case where the sampled radar data conforms to a zero-mean Complex Normal (CN) distribution,

i.e., $\mathbf{x} \sim CN(0, \mathbf{R})$ and \mathbf{R} is unknown, the mean of the GIP statistic is given by [83]

$$\mathcal{E}\{\text{GIP}\} = \frac{M}{1 - \frac{M}{K}}. \quad (5.6)$$

The GIP test results shown in Fig. 5.8 are from one specific TTD simulation but are representative of results obtained from other random target realizations. The GIP test is applied to the clutter returns/TD under three different illumination scenarios, including 1) a Standard Illumination Pattern (SIP) without TTD present, 2) the same SIP with TTD present, and 3) a Scene Adaptive Illumination Pattern (SAIP) with the same TTD present. The mean value of the GIP, i.e., $(\mathcal{E}\{\text{GIP}\})$ as given by (5.6) is also provided for reference.

Since the GIP test is an amplitude sensitive statistic, the effects of elevation nulls in the SIP illumination pattern (both with and without TTD present) are clearly visible at ranges of 3.5, 5, 12.4, and 31.25 km. This occurs because the training data amplitude is severely attenuated at null locations in the SIP. It is evident by the departure of the GIP statistic from its estimated mean value (dotted line in Fig. 5.8) that even the “clean” TD under SIP conditions is severely attenuated across range. The dominant factors that account for this attenuation are 1) the drastically changing grazing angle in this close-in sensing scenario (which heavily influences clutter reflectivity), 2) lower illumination pattern gain in the elevation sidelobes, and 3) range (R^4) attenuation effects. As seen in the SIP(TTD) results, the presence of contaminating TTD causes the GIP statistic to increase, and this phenomena is clearly visible in the SIP results starting at approximately 13 km and continuing through to 40 km. In contrast, the corresponding SAIP(TTD) GIP results clearly show a reduction of up to 20 dB in the spikes resulting from TTD presence. Note also that the characteristic dips due to elevation pattern nulls (visible in the SIP(TTD) results) are not evident in the SAIP(TTD) results. This is due to the non-uniform elevation sidelobe shape of the SAIP illumination pattern, most clearly illustrated in Fig. 5.7.

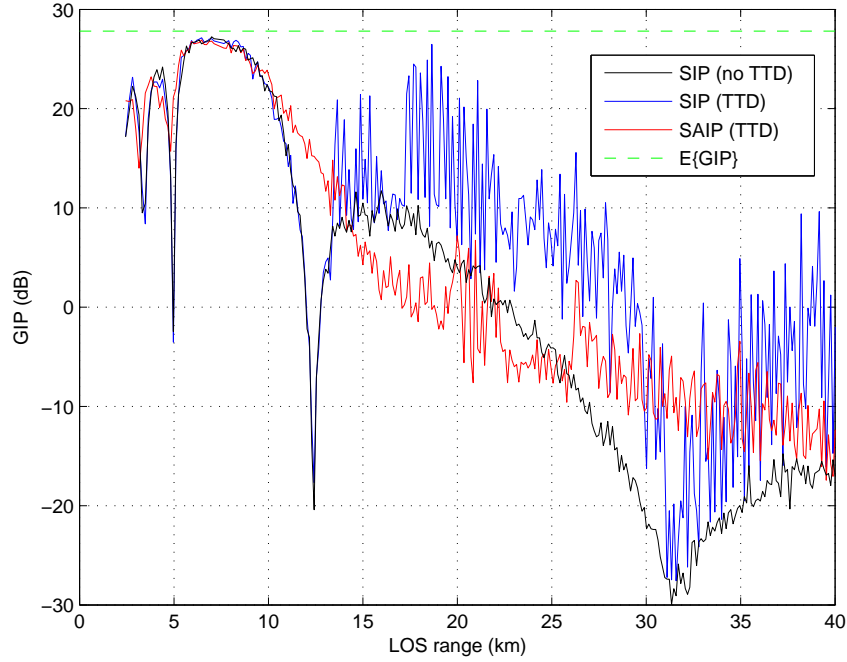


Figure 5.8: Generalized Inner Product (GIP) test applied to training data (TD) under three scene illumination conditions: 1) a Standard Illumination Pattern (SIP) without TTD present, 2) the same SIP with TTD present, and 3) a Scene Adaptive Illumination Pattern (SAIP) with TTD present.

A performance comparison for SINR Loss is made using the reportedly robust [93] Adaptive Matched Filter (AMF) [43] applied to the same scenario with different illumination patterns. For comparison purposes, the clairvoyant performance of the Matched Filter under standard illumination conditions is provided (MF-SI) and represents the maximum achievable performance. The average AMF performance under adaptive (SAIP) and standard illumination was computed from 30 runs. In each run, the target location, velocity, type, and RCS were randomly generated and AMF performance was evaluated using both non-adaptive and adaptive transmit patterns applied to identical target laydowns. In all cases, the estimated covariance matrix (used by the AMF) was based on all the training data and received 3 dB of diagonal loading. The SINR Improvement Factor (IF) is plotted in Fig. 5.9 for a 30 run average

of AMF results under standard illumination (AMF-SI) both with and without TTD present and adaptive illumination (AMF-AI) with TTD present.

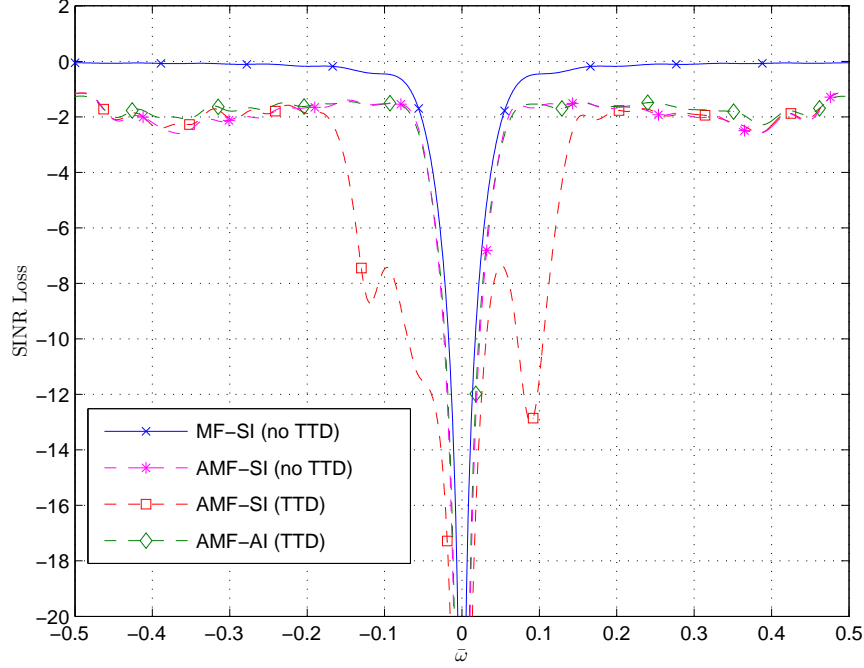


Figure 5.9: SINR Loss comparison for *Standard Illumination* (SI) and *Adaptive Illumination* (AI) Patterns: 1) Clairvoyant MF performance using SI [MF-SI] unaffected by TDD, 2) AMF performance using SI with no TTD present [AMF-SI (no TTD)], 3) AMF performance using SI with TTD present [AMF-SI (TTD)], and 4) AMF performance using AI with TTD present [AMF-AI (TTD)].

For STAP processing with 300 DOF and a total of 595 range cells (approx. 2:1 ratio for this scenario), Reed's rule predicts the average AMF performance to be approximately -3 dB less than MF performance. Outside the clutter null region, the AMF beats this prediction due to the diagonal loading of the estimated covariance matrix [22]. In this site-specific simulation, SAIP greatly improved the MDV, recovering 6 to 11 dB (relative to SAIP) of performance over about 10% of the unambiguous velocity on both sides of zero. The most affected velocities in the AMF-SI curve of Fig. 5.9 correspond to the LOS speeds of the targets receiving the most illumination. A normalized velocity of 0.1 exhibits the most loss, which corresponds to 54 MPH.

Had the roads been more perpendicular to the radar or had the targets been slower, the performance degradation would have been translated closer to zero.

5.7 Summary

This chapter demonstrates the utility of using Scene Adaptive Illumination Patterns (SAIP) to convert heterogeneous training data into more homogeneous training data, resulting in subsequent STAP performance improvement. The SAIP technique employs *a priori* knowledge of road locations coupled with platform location/orientation to synthesize adaptive *illumination nulls* which are projected onto road locations in the radar scene. Thus, target returns in the training data are effectively suppressed and the quality and quantity of available training data is restored for STAP processing. The impact of close-in sensing geometries was considered when using planar arrays with STAP processing, which highlighted the unfortunate attenuation of the training data by the elevation sidelobes. This problem was countered here using range cell specific elevation beamforming to reduce training data amplitude attenuation on receive. The use of SAIP patterns to improve overall performance fits well within the vision of achieving Fully Adaptive Radar (FAR) capability. Typically, the transmit array DOF are not utilized in today's radar. It is envisioned that methods for incorporating *a priori* knowledge to tailor transmit/illumination pattern characteristics will remain an active area of research for those wishing to take full advantage of transmit DOF to improve system performance.

VI. Conclusions

One of the fundamental challenges of airborne radar surveillance is minimizing the clutter’s degrading impact on target detection performance. The study and development of clutter mitigating techniques has spanned more than 33 years [18] and has resulted in many noteworthy advances [9, 29, 62, 63]. However, clutter mitigation remains a formidable obstacle to achieving the full performance potential of modern day radars [93].

The problems associated with effective mitigation of both signal-dependent interference (clutter) and signal-independent interference (jammers, hot clutter, etc.) is perhaps the central challenge to achieving robust Ground Moving Target Indication (GMTI) and/or Airborne Moving Target Indication (AMTI) capability. However, *half* of the interference generated is *created* by the radar itself—i.e., all of the signal-dependent interference is a result of radar transmission. The Doppler spread of ground returns, as received through the antenna pattern sidelobes, is perhaps the most problematic characteristic of airborne clutter.

Following current technology development trends of knowledge-aided processing, adaptive transmit, and Fully Adaptive Radar (FAR) architectures, this research focuses solely on the signal-dependent energy (interference) collected through antenna sidelobes which is *created* by the radar. While it is true that radar system designers have acknowledged the problem of sidelobe radiation for years, they have generally addressed the issue through the application of transmit tapers or windows that reduce sidelobe gain. The central question explored in this research, perhaps for the very first time, is: “How might a GMTI/AMTI radar which uses an *active* phased array take a proactive role in tailoring antenna sidelobe characteristics such that overall system performance is improved?”

6.1 Adaptive Illumination Patterns

The fundamental concept introduced by this research involves using Adaptive Illumination Patterns (AIP) which tailor scene illumination such that signal-induced

interference (i.e., clutter) is pre-structured to enhance receiver suppression capability. Since the resultant illumination patterns are intended to be adaptive on transmit, application of AIP is viewed as an extension of the FAR paradigm, where the common goal is to pursue increased radar performance through knowledge-aided transmit adaptivity. Specifically, the use of AIP is employed to improve STAP receive processing performance.

Although it is expected that no set of illumination patterns can be generated to improve upon optimum processor performance, i.e., performance obtained under clairvoyant covariance conditions, there are many real-world effects which may be better addressed using a synergistic combination of adaptive illumination patterns and STAP. In addition, implementing space-time adaptivity via real illumination antenna patterns may induce new phenomenological effects into received data which could be further exploited to improve overall performance in a FAR architecture.

This research is divided into two major thrusts which are distinguished based on the pattern update interval, as well as their purpose. The first thrust focused on illumination patterns which are *designed* to change on a pulse-by-pulse basis and characterizes the research related to Space Time Illumination Patterns (STIP). The second thrust focused on those patterns which are adaptive but temporally constant for at least one CPI. This characterizes the research related to Scene Adaptive Illumination Patterns (SAIP).

6.1.1 Space Time Illumination Patterns (STIP). The field of adaptive radar has countered the clutter problem by invoking the use of a phased array radar to sample the environment in both space and time. This space-time sampling is commonly followed by the application of adaptive, time-varying (i.e., pulse dependent) array *receive* processing of the radar data by techniques such as STAP. As developed here, STIP techniques take advantage of previously unutilized transmit DOF to exploit the same space-time adaptivity via custom designed pulse-dependent illumination patterns. Thus, STIP adds the phased array antenna pattern to the FAR toolbox,

yielding a tremendous capability for addressing the problem of signal-dependent interference during the transmit cycle.

As shown in this research, STIP has demonstrated the ability to nearly eliminate the clutter at particular, user selectable Doppler frequencies as well as over a range of Doppler frequencies. This permits non-adaptive receiver processing algorithms to achieve near noise-only performance in Doppler regions previously dominated by clutter. STIP is well-suited for potentially aiding or simplifying a tracking application where a target Doppler estimate is maintained. STIP also demonstrated the capability to improve partially-adaptive Factored Space Time (FST) processor performance to near noise-only (optimal) performance in selected Doppler regions. The reduced DOF of the partially-adaptive FST processing is usually accompanied by a reduction in required training data (via the RMB rule [86]). In general, lower training data requirements makes STAP processing more implementable and robust in heterogeneous clutter environments. For the weight synthesis methods used here, there is a tradeoff between the width of the clutter-free Doppler frequency span and the amount of mainbeam gain provided by the adapted illumination patterns.

Should Knowledge-Aided (KA) STIP weight synthesis techniques be developed and shown to be viable, the use of FST processing combined with KA-STIP offers the *potential* for achieving STAP processing capability without the expense of individual analog-to-digital converters on each array element. Given the historical success of non-data-adaptive Displaced Phase Center Antenna (DPCA) techniques, it seems plausible to achieve an acceptable level of performance with antenna weights synthesized using onboard navigation data and the appropriate clutter models.

6.1.2 Scene Adaptive Illumination Patterns (SAIP). Nature dictates that radar systems can only detect that which is “illuminated” by radiated electromagnetic energy. The spatial allocation of radiated energy is determined by the radar transmit (illumination) pattern. Modern Active Electronically Scanned Arrays (AESAs) have the inherent capability to adjust their illumination pattern in near “real-time”.

The characteristic sidelobe structure of an AESA guarantees those areas which lie in illumination pattern nulls are not as observable (subject to pattern null depth) by the radar despite the amount of receiver processing applied. While tapering (windowing) an array pattern is a well developed technique for lowering the peak gain of antenna sidelobes, the *location* of transmit pattern nulls is generally not a design consideration—until now.

In some heterogenous environments, there are undoubtedly specific “objects” in the radar scene who’s reflections directly contribute to the heterogeneous nature of the clutter returns. These would include so-called clutter discretely, as well as moving objects which by their nature induce additional Doppler shift that degrades clutter homogeneity. The AIP concept introduced here involves using the spatial DOF of an AESA *on transmit* to adaptively cast illumination pattern nulls in those regions most likely to contribute heterogeneous returns across range gates. Specifically, this work focuses on placing transmit nulls along road locations in the scene, potentially restoring a degree of homogeneity to road/target infested training data. This technique is referred to throughout as Scene Adaptive Illumination Patterns (SAIP).

This research proposed a new approach for minimizing the negative impacts of having targets in the training data. Using *a priori* road location information, modern AESA array technology, and geometries consistent with close-in sensing applications, the transmit antenna pattern is adaptively altered to illuminate the scene such that *illumination pattern nulls* are placed along road locations running through the training data. By not illuminating the vehicular targets with transmit energy, the contaminating reflected target energy is effectively reduced. This effectively converts target corrupted training data to be more representative of what is received under homogeneous clutter conditions. The use of AIP for this purpose is referred to throughout this document as Scene Adaptive Illumination Patterns (SAIP).

SAIP is independent and perfectly complementary to the existing Non-Homogeneity Detection (NHD) techniques previously developed. It is expected that the synergis-

tic use of SAIP and existing NHD-like techniques will result in improved adaptive radar performance in target-rich and other heterogeneous environments. The specific contribution of SAIP to overall adaptive radar performance is its ability to “convert” (to some degree) heterogeneous clutter data into a more homogeneous state, resulting in a net increase in clutter quality and quantity, the latter being realized upon the common application of NHD to a more homogeneous set of training data.

6.2 *Research Contribution Summary*

This research characterizes performance improvements which may be obtained by incorporating transmit/illumination pattern adaptivity into the cadre of existing radar signal processing techniques. For demonstration purposes, STAP receiver processing is used to characterize the benefits of employing AIP. AIP is applied to address two of STAP’s biggest challenges: 1) poor training data quality, and 2) limited training data quantity. These challenges are addressed either through using SAIP to mitigate training data contamination which occurs in dense target environments, or by using STIP to reduce the quantity of training data required in the classic side-looking linear array STAP scenarios (both of which are applicable to GMTI applications). Figure 6.1 provides the organizational research structure which is divided into three basic areas: 1) Extensions to existing radar models that incorporate Adaptive Illumination Patterns-Transmit Interpulse Pattern Diversity (AIP-TIPD), 2) Development and application of Space Time Illumination Patterns (STIP), and 3) Development and application of knowledge aided Scene Adaptive Illumination Patterns (SAIP).

Research contributions are summarized as follows:

1. Development of Adaptive Transmit Pattern Model: Extended previous radar model of [61, 99] to incorporate effect of adaptive transmit pattern on target and clutter responses [24].
 - Incorporates arbitrary spatial transmit weights for a planar Array (3D STAP).

Adaptive Illumination Patterns (AIP)

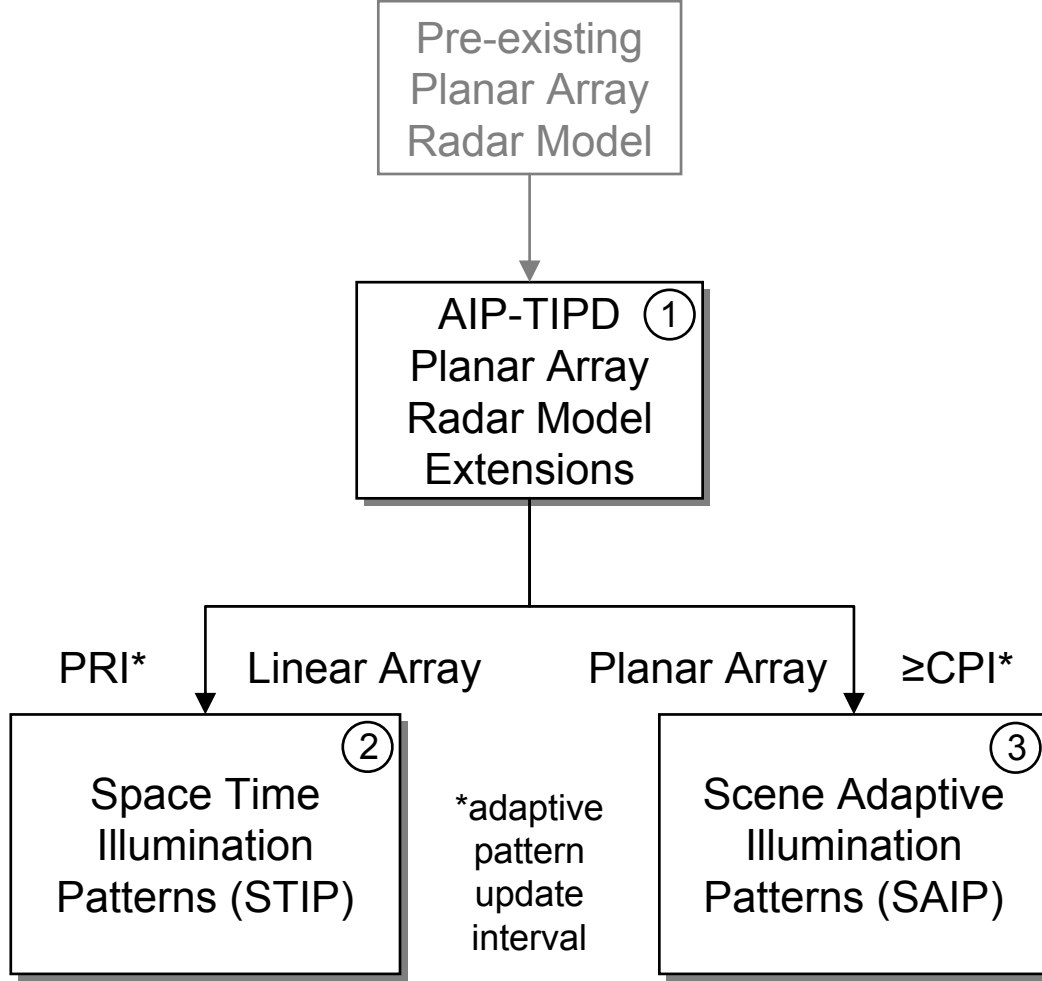


Figure 6.1: Summary of research structure and technical contribution areas, including 1) Incorporation of Adaptive Illumination Pattern-Transmit Inter-pulse Pattern Diversity (AIP-TIPD) extensions into pre-existing radar models, 2) development and application of Space Time Illumination Patterns (STIP) to pre-shape (re-distribute) clutter power such that STAP processing performs better with less Training Data, and 3) development and application of knowledge aided Scene Adaptive Illumination Patterns (SAIP) to minimize heterogeneous clutter effects in target saturated environments.

- Incorporates arbitrary pulse-varying set of transmit weights using a planar Array.

- Proved that the clairvoyant clutter covariance matrix incorporating TIPD is valid for *any* arbitrary statistical distribution *and/or* deterministic clutter reflectivity.
 - Incorporated analytic modeling of subarrays in the clutter covariance model which reduces computational load, memory requirements, and decreases modeling and simulation time.
 - Modified clutter snapshot model for range bin-by-range bin generation of clutter incorporating TIPD planar array (elevation dependent) illumination patterns.
2. Space Time Illumination Patterns (STIP): Introduced and developed the concept of STIP to accomplish space-time beamforming for simplified receiver processing [27]
- Extended linear array radar model of [61, 99] to incorporate Transmit Interpulse Pattern Diversity (TIPD) functionality.
 - Demonstrated performance matching that of an optimum filter using optimum TIPD weights with simplified Doppler receive filtering. Processing burden shifted from receiver to transmitter.
 - Developed understanding of the nature of joint space-time beamforming, detailing the differences between illumination and filtering.
3. Scene Adaptive Illumination Patterns (SAIP): Introduced and developed the concept of SAIP to improve STAP performance in dense target environments [25].
- Uses knowledge-aided technique to synthesize transmit patterns (adapt scene illumination) based on known road locations. Removal of mobile scatterer responses from road locations effectively “cleans up” training data.
 - Demonstrated performance improvement for planar array using SAIP with STAP receiver processing for close-in sensing applications.

6.3 *Future Research*

It is hoped that the active use of AIP within the larger context of Fully Adaptive Radar (FAR) will grow into a well-established area of research. This hope is based on 1) a recognition of the relative maturity of key enabling technologies, including the AESA, embedded processors, phase shifters, amplifiers, etc., 2) a fundamental belief in the new found potential of adaptive illumination when *combined with* existing adaptive receiver processing, and 3) the momentum behind knowledge aided, adaptive transmit and Bayesian approaches to emerging radar architectures. As such, there are many potential areas for future research. A few are listed here.

6.3.1 Radar Modeling Research. One possible criticism of STIP is the ability to synthesize usable space-time patterns without the aid of clairvoyant data. The ability to quantify the extent to which this is possible relies heavily on developing more detailed STAP models that incorporate such things as: Digital Terrain Elevation Data (DTED) data models, reflectivity models, scattering models, signal masking models, and array error models. Without the aid of measured datasets (since simulated data has to be reactive to synthesized antenna patterns), the aging of past CPI data must be modeled to determine the legitimacy and/or restrictions of this approach to STIP weight synthesis. Further, in depth modeling of real-world array errors and inter-channel biases would be useful in determining the potential for using knowledge-aided clutter model approaches to STIP weight synthesis.

6.3.2 Space Time Illumination Patterns. There are many knowledge-aided, model-based, and expert reasoning based strategies developed for STAP that are immediately applicable to STIP weight generation. The investigation of each technology as well as the combination of multiple technologies is viewed as a ripe area of further research, and one critical to the long-term success of STIP technology. The tremendous growth and successful contributions of knowledge-based/knowledge-aided processing directly support the future realization of practical STIP implementation. Another interesting area would be to apply STIP to 3D (azimuth, elevation, and

Doppler) scenarios to investigate the capability of the technique to counter and/or compensate for elevation-dependent effects.

In understanding the differences and tradeoffs between AIP and STAP, there may be important phenomenological effects due to the fundamental difference between the use of real antenna patterns on transmit and synthesized illumination patterns on receive. For example, some artifacts known to occur in signal processing may not appear when using AIP. Conversely, the precision of AIP may be much less than that afforded by STAP due to limited hardware precision. Such effects could be investigated, tested and/or quantified.

As mentioned in Chapter I, AIP has no impact on signal-independent sources in the scene, such as jammers or terrain scattered interference (a.k.a., hot clutter) [95,96]. However, it may be worth exploring the ability of AIP to alleviate some of the “cold” clutter processing burden from the receiver, potentially making more receive DOF available for mitigating the signal-independent interference.

6.3.3 Scene Adaptive Illumination Patterns. In synthesizing SAIP patterns, road segment selection when forming \mathbf{R}_{tx} is critical to proper performance and remains an area for future optimization. For example, the relationship between the locus of road samples (constraints) in the azimuth-elevation space and the resultant rank of the covariance matrix has not been related analytically. Such a derivation is difficult to synthesize due to the widely varying shape of projected road segments, sampling density, and locations. However, such a derivation is necessary for real-world deployment of the system so that the adaptive pattern is not over-specified by the null constraints.

6.4 Closing Thoughts

The future of AIP as part of a FAR architecture seems secure. As AESAs become more capable through faster phase shifters and more powerful T/R modules, the potential for AIP to make big contributions to radar performance only increases.

With the plethora of ongoing STAP research, especially in the areas of waveform diversity, knowledge-aided processing, and fully adaptive radar, more DOF will be the norm. The potential for larger arrays also increases the achievable spatial resolution in complex radar scenarios. Such increases in spatial resolution will further benefit AIP techniques, as more DOFs will be available for adapting illumination patterns to the scene. It is hoped that the application of AIP to adaptive radar will continue with great fervency, and that the men and women of the U.S. military will be safer and more capable because of it.

Bibliography

1. *2004 Tiger/Line File Technical Documentation*, Prepared by the Bureau of the Census, Washington D.C. 2004. [Www.census.gov/geo/www/tiger](http://www.census.gov/geo/www/tiger).
2. Adve, Raviraj S., Todd B. Hale, and Michael C. Wicks. "Practical Joint Domain Localised Adaptive Processing in Homogeneous and Nonhomogeneous Environments, Part 2: Nonhomogeneous Environments". *IEE Proceedings - Radar, Sonar, and Navigation*, 147(2):66–74, April 2000.
3. Adve, Raviraj S., M.C. Wicks, T.B. Hale, and P. Antonik. "Ground Moving Target Indication Using Knowledge Based Space-Time Adaptive Processing". *Record of the 2000 IEEE International Radar Conference*, 735–740. May 2000.
4. Adve, R.S., M.C. Wicks, T.B. Hale, and P. Antonik. "Ground moving target indication using knowledge based space time adaptive processing". *Radar Conference, 2000. The Record of the IEEE 2000 International*, 735–740. 2000.
5. Antonik, P., R. Bonneau, R. Brown, S. Ertan, V. Vannicola, D. Weiner, and M. Wicks. "Bistatic radar denial/embedded communications via waveform diversity". *Radar Conference, 2001. Proceedings of the 2001 IEEE*, 41–45. 2001.
6. Antonik, P., H. Schuman, P. Li, W. Melvin, and M. Wicks. "Knowledge-based space-time adaptive processing". *Radar Conference, 1997., IEEE National*, 372–377. 1997.
7. Antonik, P., H.K. Schuman, W.L. Melvin, and M.C. Wicks. "Implementation of knowledge-based control for space-time adaptive processing". *Radar 97 (Conf. Publ. No. 449)*, 478–482. 1997.
8. Antonik, Paul, Harvey K. Schuman, William L. Melvin, and Michael C. Wicks. "Implementation of Knowledge Based Control for Space-Time Adaptive Processing". *Proceedings of the 1997 International Radar Conference*. October 1997. Edinburgh, UK.
9. Armistead, Edwin Leigh. *AWACS and Hawkeyes*. MBI Publishing Company, MBI Publishing Company, Galtier Plaza, Suite 200, 380 Jackson Street, St. Paul, MN 55101-3885, 1st edition, 2002. ISBN 0-7603-1140-4. Hardback.
10. Balanis, Constantine. *Antenna Theory*. John Wiley & Sons, Inc., New York, NY, second edition, 1997.
11. Banister, B.C. and J.R. Zeidler. "Transmission subspace tracking for MIMO communications systems". *Global Telecommunications Conference, 2001. GLOBECOM '01. IEEE*, volume 1, 161–165 vol.1. 2001.
12. Bergin, J.S., P.M. Techau, W.L. Melvin, and J.R. Guerci. "GMTI STAP in target-rich environments: site-specific analysis". *Radar Conference, 2002. Proceedings of the IEEE*, 391–396. 2002. ISSN 1097-5659.

13. Bergin, J.S., C.M. Teixeira, P.M. Techau, and J.R. Guerci. "STAP with knowledge-aided data pre-whitening". *Radar Conference, 2004. Proceedings of the IEEE*, 289–294. 2004.
14. Billingsley, J. B. *Low Angle Radar Land Clutter*. SciTech, 2002.
15. Blunt, S.D., K. Gerlach, and M. Rangaswamy. "The enhanced FRACTA algorithm with knowledge-aided covariance estimation". *Sensor Array and Multichannel Signal Processing Workshop Proceedings, 2004*, 638–642. 2004.
16. Borsari, Geordi K. "Mitigating Effects on STAP Processing Caused by an Inclined Array". *Proceedings of the 1998 IEEE Radar Conference*, 135–140. 1998.
17. Brennan, L. E. and F. M. Staudaher. *Subclutter Visibility Demonstration*. Technical Report RL-TR-92-21, Adaptive Sensors Incorporated, March 1992.
18. Brennan, L.E. and I.S. Reed. "Theory of Adaptive Radar". *IEEE Transactions on Aerospace and Electronic Systems*, AES-9(2):237–252, March 1973.
19. Brooks, Lowell S. and Irving S. Reed. "Equivalence of the Likelihood Ratio Processor, the Maximum Signal-to-Noise Ratio Filter, and the Wiener Filter". *IEEE Transactions on Aerospace and Electronic Systems*, 690–692, September 1972. Correspondence.
20. Caldwell, James T. *Forward Looking Radar: Interference Modelling, Characterization, and Suppression*. Thesis, School of Engineering and Management, Air Force Institute of Technology (AETC), 2950 Hobson Way, Bldg 640, Wright-Patterson AFB, OH 45433-7765, March 2004. AFIT/GE/ENG/04-02.
21. Capraro, C.T., G.T. Capraro, D.D. Weiner, M.C. Wicks, and W.J. Baldygo. "Improved STAP performance using knowledge-aided secondary data selection". *Radar Conference, 2004. Proceedings of the IEEE*, 361–365. 2004. ISSN 1097-5659.
22. Carlson, Blair D. "Covariance Matrix Estimation Errors and Diagonal Loading in Adaptive Arrays". *IEEE Transactions on Aerospace and Electronic Systems*, 24(4):397–401, July 1988.
23. Conte, E., M. Longo, and M. Lops. "Modelling and simulation of non-Rayleigh radar clutter". *Radar and Signal Processing, IEE Proceedings F*, 138(2):121–130, 1991. ISSN 0956-375X.
24. Corbell, Phillip M., Michael A. Temple, Todd B. Hale, and Muralidhar Rangaswamy. "Transmit Interpulse Pattern Diversity (TIPD) For Fully Adaptive Radar (FAR)", September 2005. Submitted to IEEE Transactions on Aerospace and Electronic Systems, Received September 8th, 2005, Paper No. TAES-200501646, Under Review.
25. Corbell, Phillip M., Michael A. Temple, Todd B. Hale, and Muralidhar Rangaswamy. "Improving STAP Performance in Target Rich Environments Through

Adaptive Illumination”. *2006 International Conference on Waveform Diversity and Design*. 2006.

26. Corbell, P.M. and T.B. Hale. “3-dimensional STAP performance analysis using the cross-spectral metric”. *Radar Conference, 2004. Proceedings of the IEEE*, 610–615. 2004.
27. Corbell, P.M., M.A. Temple, T.B. Hale, W.P. Baker, and M. Rangaswamy. “Performance improvement using interpulse pattern diversity with space-time adaptive processing”. *Radar Conference, 2005 IEEE International*, 55–60. 2005.
28. Dybdal, R.B. and S.J. Curry. “Adaptive transmit antenna”. *Antennas and Propagation Society International Symposium, 1997. IEEE., 1997 Digest*, volume 4, 2410–2413 vol.4. 1997.
29. Entzminger, Jr., J.N., C.A. Fowler, and W.J. Kenneally. “JointSTARS and GMTI: past, present and future”. *Aerospace and Electronic Systems, IEEE Transactions on*, 35(2):748–761, 1999. ISSN 0018-9251.
30. Ertan, S., H.D. Griffiths, M.C. Wicks, P. Antonik, D. Weiner, R. Adve, and I. Fotinopoulos. “Bistatic radar denial by spatial waveform diversity”. *RADAR 2002*, 17–21. 2002.
31. French, M.C., Jinwoo Suh, J. Damoulakis, and S.P. Crago. “Novel signal processing architectures for knowledge-based STAP algorithms [radar SIGPRO]”. *Radar Conference, 2004. Proceedings of the IEEE*, 382–387. 2004.
32. Garren, D.A., A.C. Odom, M.K. Osborn, J.S. Goldstein, S.U. Pillai, and J.R. Guerci. “Full-polarization matched-illumination for target detection and identification”. *Aerospace and Electronic Systems, IEEE Transactions on*, 38(3):824–837, 2002.
33. Garren, D.A., M.K. Osborn, A.C. Odom, J.S. Goldstein, S. Unnikrishna Pillai, and J.R. Guerci. “Optimization of single transmit pulse shape to maximize detection and identification of ground mobile targets”. *Signals, Systems and Computers, 2000. Conference Record of the Thirty-Fourth Asilomar Conference on*, volume 2, 1535–1539 vol.2. 2000.
34. Garren, D.A., M.K. Osborn, A.C. Odom, J.S. Goldstein, S.U. Pillai, and J.R. Guerci. “Enhanced target detection and identification via optimised radar transmission pulse shape”. *Radar, Sonar and Navigation, IEE Proceedings -*, 148(3):130–138, 2001.
35. Garren, D.A., M.K. Osborn, A.C. Odom, J.S. Goldstein, S.U. Pillai, and J.R. Guerci. “Optimal transmission pulse shape for detection and identification with uncertain target aspect”. *Radar Conference, 2001. Proceedings of the 2001 IEEE*, 123–128. 2001.

36. Gerlach, D. and A. Paulraj. "Adaptive transmitting antenna methods for multipath environments". *Global Telecommunications Conference, 1994. GLOBECOM '94. 'Communications: The Global Bridge', IEEE*, 425–429 vol.1. 1994.
37. Gerlach, K., S.D. Blunt, and M.L. Picciolo. "Robust adaptive matched filtering using the FRACTA algorithm". *Aerospace and Electronic Systems, IEEE Transactions on*, 40(3):929–945, 2004. ISSN 0018-9251.
38. Goldstein, J.S., I.S. Reed, and L.L. Scharf. "A multistage representation of the Wiener filter based on orthogonal projections". *Information Theory, IEEE Transactions on*, 44(7):2943–2959, 1998. ISSN 0018-9448.
39. Goldstein, J.S., I.S. Reed, L.L. Scharf, and J.A. Tague. "A low-complexity implementation of adaptive Wiener filters". *Signals, Systems & Computers, 1997. Conference Record of the Thirty-First Asilomar Conference on*, volume 1, 770–774 vol.1. 1997.
40. Goldstein, J.S., P.A. Zulch, and I.S. Reed. "Reduced rank space-time adaptive radar processing". *Acoustics, Speech, and Signal Processing, 1996. ICASSP-96. Conference Proceedings., 1996 IEEE International Conference on*, volume 2, 1173–1176 vol. 2. 1996.
41. Goodman, N.A. and P.R. Gurram. "STAP training through knowledge-aided predictive modeling [radar signal processing]". *Radar Conference, 2004. Proceedings of the IEEE*, 388–393. 2004.
42. Graham, Alexander. *Kronecker Products and Matrix Calculus with Applications*. Ellis Horwood: Mathematics and its Applications. Ellis Horwood Limited, Market Cross House, Cooper Street, Chichester, West Sussex, PO19 1EB, England, 1981.
43. Guerri, J. R. *Space-Time Adaptive Processing for Radar*. Artech House, Incorporated, January 2003.
44. Guerri, J. R. "Knowledge-Aided Adaptive Waveform Design". Second Tri-Service Waveform Diversity Workshop, February 2004. Verona, NY.
45. Guerri, Joseph R. "KASSPER Overview". Technical Workshop Presentation, April 2002. Available at http://sunrise.deepthought.rl.af.mil/kassper_html/kassper.html.
46. Guerri, Joseph R. "Personnal E-mail Correspondance", February 26, 2006. Director, Special Projects Office (SPO), DARPA.
47. Guerri, Joseph R. and Edward J. Baranoski. "KASSPER Homepage". World Wide Web, February 2006. <Http://www.darpa.mil/spo/programs/kassper.htm>.
48. Guerri, J.R. and S.U. Pillai. "Adaptive transmission radar: the next Wave". *National Aerospace and Electronics Conference, 2000. NAECON 2000. Proceedings of the IEEE 2000*, 779–786. 2000.

49. Guerci, J.R. and S.U. Pillai. "Theory and application of optimum transmit-receive radar". *Radar Conference, 2000. The Record of the IEEE 2000 International*, 705–710. 2000.
50. Hale, T. B., M.A. Temple, and M.C. Wicks. "Clutter Suppression Using Elevation Interferometry Fused with Space-Time Adaptive Processing". *IEE Electronics Letters*, 37(12):793–794, June 2001.
51. Hale, T. B., M.A. Temple, M.C. Wicks, J.F. Raquet, and M.O. Oxley. "Performance Characterization of a Hybrid STAP Architecture Incorporating Elevation Interferometry". *IEE Proceedings - Radar, Sonar and Navigation*, 149(2):77–82, April 2002.
52. Hale, Todd B. *Airborne Radar Interference Suppression Using Adaptive Three-Dimensional Techniques*. Dissertation, School of Engineering and Management, Air Force Institute of Technology (AETC), 2950 P Street, Bldg 640, Wright-Patterson AFB, OH 45433-7765, June 2002. AFIT/DS/ENG/02-02.
53. Hale, Todd B., Michael A. Temple, John F. Raquet, Mark E. Oxley, and Michael C. Wicks. "Localised Three-Dimensional Adaptive Spatial-Temporal Processing for Airborne Radar". *IEE Proceedings - Radar, Sonar and Navigation*, 150(1):18–22, February 2003. Invited publication.
54. Hale, Todd B., Michael A. Temple, and Michael C. Wicks. "Target Detection in Heterogeneous Airborne Radar Interference Using 3D STAP". *Proceedings of IEEE 2003 Radar Conference*, 252–257. Institution of Electrical and Electronics Engineers, IEEE Aerospace and Electronic Systems Society, Huntsville, AL, May 2003.
55. Hale, Todd B., Michael A. Temple, Michael C. Wicks, John F. Raquet, and Mark E. Oxley. "Elevation Interferometric STAP Using a Thinned Planar Array". *Proceedings of IEEE 2002 Radar Conference*, 408–414. Institution of Electrical and Electronics Engineers, IEEE Aerospace and Electronic Systems Society, Long Beach, CA, April 2002.
56. Hale, Todd B., Michael A. Temple, Michael C. Wicks, John F. Raquet, and Mark E. Oxley. "Localized Three-Dimensional Adaptive Spatial-Temporal Processing for Airborne Radar". *Proceedings of the 2002 IEE International Radar Conference*, 191–195. Institution of Electrical Engineers, Robin Mellors-Bourne, Savoy Place, London WC2R 0BL, United Kingdom, October 2002. Best paper.
57. Harris, Fredric J. "On the Use of Windows for Harmonic Analysis with the Discrete Fourier Transform". *Proceedings of the IEEE*, volume 66, No. 1, 51–83. January 1978.
58. Hiemstra, J.D. "Colored diagonal loading". *Radar Conference, 2002. Proceedings of the IEEE*, 386–390. 2002. ISSN 1097-5659.

59. Hiemstra, J.D., M.D. Zoltowski, and J.S. Goldstein. "Recursive and knowledge-aided implementations of the multistage Wiener filter". *Radar Conference, 2003. Proceedings of the 2003 IEEE*, 46–50. 2003. ISSN 1097-5659.
60. Honig, M.L. and J.S. Goldstein. "Adaptive reduced-rank interference suppression based on the multistage Wiener filter". *Communications, IEEE Transactions on*, 50(6):986–994, 2002. ISSN 0090-6778.
61. Jaffer, A.G., M.H. Baker, W.P. Ballance, and J.R. Staub. *Adaptive Space-Time Processing Techniques for Airborne Radars*. Contract F30602-89-D-0028, Hughes Aircraft Company, Fullerton, CA 92634, July 1991.
62. Klemm, Richard. *Principles of Space-Time Adaptive Processing*, volume 12 of *IEE Radar, Sonar, Navigation and Avionics Series*. The Institution of Electrical Engineers, Michael Faraday House, Six Hills Way, Stevenage, Herts. SG1 2AY, United Kingdom, 2002. ISBN 0852961723.
63. Klemm, Richard. *Applications of Space-Time Adaptive Processing*. IEE, June 2004.
64. Kreithen, D.E., N.B. Pulsone, C.M. Rader, and G.E. Schrader. "The MIT Lincoln Laboratory KASSPER algorithm testbed and baseline algorithm suite". *Sensor Array and Multichannel Signal Processing Workshop Proceedings, 2002*, 38–42. 2002.
65. Liang, Jen-Wei and A.J. Paulraj. "Forward link antenna diversity using feedback for indoor communication systems". *Acoustics, Speech, and Signal Processing, 1995. ICASSP-95., 1995 International Conference on*, volume 3, 1753–1755 vol.3. 1995.
66. Lo, T. "Adaptive space-time transmission with side information". *Wireless Communications and Networking, 2003. WCNC 2003. 2003 IEEE*, volume 1, 601–606 vol.1. 2003.
67. Long, M. W. *Radar reflectivity of land and sea*. Artech House, 3rd edition, 2001.
68. Melvin, W., M. Wicks, P. Antonik, Y. Salama, Ping Li, and H. Schuman. "Knowledge-based space-time adaptive processing for airborne early warning radar". *Aerospace and Electronic Systems Magazine, IEEE*, 13(4):37–42, 1998.
69. Melvin, William, Paul Antonik, Ping Li, Harvey Schuman, and Michael Wicks. "Knowledge-Based Space-Time Adaptive Processing for Airborne Early Warning Radar". *IEEE AES Systems Magazine*, 13(4):37–42, April 1998.
70. Melvin, W.L. "Space-time adaptive radar performance in heterogeneous clutter". *Aerospace and Electronic Systems, IEEE Transactions on*, 36(2):621–633, 2000.
71. Melvin, W.L. "A STAP overview". *Aerospace and Electronic Systems Magazine, IEEE*, 19(1):19–35, 2004.

72. Melvin, W.L. and J.R. Guerci. "Adaptive detection in dense target environments". *Radar Conference, 2001. Proceedings of the 2001 IEEE*, 187–192. 2001.
73. Melvin, W.L., G.A. Showman, and J.R. Guerci. "A knowledge-aided GMTI detection architecture [radar signal processing]". *Radar Conference, 2004. Proceedings of the IEEE*, 301–306. 2004.
74. Michels, James H., Muralidhar Rangaswamy, and Braham Himed. "Performance of Parametric and Covariance Based STAP Tests in Compound-Gaussian Clutter". *Digital Signal Processing*, 12(2-3):307–328, 2002.
75. Page, D., S. Scarborough, and S. Crooks. "Improving knowledge-aided STAP performance using past CPI data [radar signal processing]". *Radar Conference, 2004. Proceedings of the IEEE*, 295–300. 2004.
76. Pillai, S.U., J.R. Guerci, and S.R. Pillai. "Joint optimal Tx-Rx design for multiple target identification problem". *Sensor Array and Multichannel Signal Processing Workshop Proceedings, 2002*, 553–556. 2002.
77. Pillai, S.U., H.S. Oh, and J.R. Guerci. "Multichannel matched transmit-receiver design in presence of signal-dependent interference and noise". *Sensor Array and Multichannel Signal Processing Workshop. 2000. Proceedings of the 2000 IEEE*, 385–389. 2000.
78. Pillai, S.U., H.S. Oh, D.C. Youla, and J.R. Guerci. "Optimal transmit-receiver design in the presence of signal-dependent interference and channel noise". *Information Theory, IEEE Transactions on*, 46(2):577–584, 2000.
79. Pillai, S.U., D.C. Youla, H.S. Oh, and J.R. Guerci. "Optimum transmit-receiver design in the presence of signal-dependent interference and channel noise". *Signals, Systems, and Computers, 1999. Conference Record of the Thirty-Third Asilomar Conference on*, volume 2, 870–875 vol.2. 1999.
80. Raleigh, G.G., S.N. Diggavi, V.K. Jones, and A. Paulraj. "A blind adaptive transmit antenna algorithm for wireless communication". *Communications, 1995. ICC 95 Seattle, Gateway to Globalization, 1995 IEEE International Conference on*, volume 3, 1494–1499 vol.3. 1995.
81. Rangaswamy, M. "An overview of space-time adaptive processing for radar". *Radar Conference, 2003. Proceedings of the International*, 45–50. 2003.
82. Rangaswamy, M., Pinyen Chen, J.H. Michels, and B. Himed. "A comparison of two non-homogeneity detection methods for space-time adaptive processing". *Sensor Array and Multichannel Signal Processing Workshop Proceedings, 2002*, 355–359. 2002.
83. Rangaswamy, M., B. Himed, and J.H. Michels. "Statistical analysis of the nonhomogeneity detector". *Signals, Systems and Computers, 2000. Conference Record of the Thirty-Fourth Asilomar Conference on*, volume 2, 1117–1121 vol.2. 2000.

84. Rangaswamy, M., D. Weiner, and A. Ozturk. "Computer generation of correlated non-Gaussian radar clutter". *Aerospace and Electronic Systems, IEEE Transactions on*, 31(1):106–116, 1995. ISSN 0018-9251.
85. Rangaswamy, Muralidhar, James H. Michels, and Braham Himed. "Statistical analysis of the non-homogeneity detector for STAP applications". *Digital Signal Processing*, 14(3):253–267, 2004.
86. Reed, Irving S., J.D. Mallett, and L.E. Brennan. "Rapid Convergence Rate in Adaptive Arrays". *IEEE Transactions on Aerospace and Electronic Systems*, AES-10, No. 6:853–863, November 1974.
87. Robey, Frank C., Daniel R. Fuhrmann, Edward J. Kelly, and Ramon Nitzberg. "A CFAR Adaptive Matched Filter Detector". *IEEE Transactions on Aerospace and Electronic Systems*, 28(1):208–216, January 1992.
88. Schindler, J.K. and H. Steyskal. "Transmit Beamforming and Waveforms for Random, Sparse Array Radar". *Proc. of International Waveform Diversity and Design, Edinburgh, Scotland*. Nov 8-10 2004.
89. Schrader, G.E. "The knowledge aided sensor signal processing and expert reasoning (KASSPER) real-time signal processing architecture [radar signal processing]". *Radar Conference, 2004. Proceedings of the IEEE*, 394–397. 2004.
90. Skolnik, Merrill I. *Introduction to Radar Systems*. McGraw-Hill, Inc., 1221 Avenue of the Americas, New York, NY 10020, third edition, 2001. ISBN: 0072909803.
91. Sowelam, S.M. and A.H. Tewfik. "Waveform selection in radar target classification". *Information Theory, IEEE Transactions on*, 46(3):1014–1029, 2000.
92. Steiner, Todd D. and Paul H. Merritt. "Airborne Laser Advanced Technology". *Proceedings of SPIE 1998*, volume 3381, 1–306. Orlando, FL, 1998.
93. Steinhardt, A. and J. Guerci. "STAP for RADAR: what works, what doesn't, and what's in store. IEEE radar conference, 2004". *Radar Conference, 2004. Proceedings of the IEEE*, 469–473. 2004.
94. Stimson, George W. *Introduction to Airborne Radar*. SciTech Publishing, Inc., Mendham, NJ, second edition, 1998.
95. Techau, P.M., J.R. Guerci, T.H. Slocumb, and L.J. Griffiths. "Performance bounds for hot and cold clutter mitigation". *Aerospace and Electronic Systems, IEEE Transactions on*, 35(4):1253–1265, 1999.
96. Techau, P.M., J.R. Guerci, T.H. Slocumb, and L.J. Griffiths. "Performance bounds for interference mitigation in radar systems". *Radar Conference, 1999. The Record of the 1999 IEEE*, 12–17. 1999.
97. Titi, G.W. and D.F. Marshall. "The ARPA/NAVY Mountaintop Program: adaptive signal processing for airborne early warning radar". *Acoustics, Speech*,

- and Signal Processing, 1996. ICASSP-96. Conference Proceedings., 1996 IEEE International Conference on*, volume 2, 1165–1168 vol. 2. 1996.
98. Ulaby, F. T. and M. C. Dobson. *Handbook of Radar Scattering Statistics for Terrain*. Artech House, 685 Canton Street, Norwood, MA 02062, 1989.
 99. Ward, James. *Space-Time Adaptive Processing for Airborne Radar*. Contract F19628-95-C-0002, Lincoln Laboratory, Massachusetts Institute of Technology, Lexington, Massachusetts, December 1994.
 100. Weippert, M.E., J.D. Hiemstra, J.S. Goldstein, and D.A. Garren. “Efficient implementation of the multistage Wiener filter for multiple beam applications”. *Phased Array Systems and Technology, 2003. IEEE International Symposium on*, 152–157. 2003.
 101. Zywicki, D.J., W.L. Melvin, G.A. Showman, and J.R. Guerci. “Stap performance in site-specific clutter environments”. *Aerospace Conference, 2003. Proceedings. 2003 IEEE*, volume 4, 2005–2020. 2003. ISSN 1095-323X.

REPORT DOCUMENTATION PAGE					<i>Form Approved</i> OMB No. 0704-0188							
The public reporting burden for this collection of information is estimated to average 1 hour per response, including the time for reviewing instructions, searching existing data sources, gathering and maintaining the data needed, and completing and reviewing the collection of information. Send comments regarding this burden estimate or any other aspect of this collection of information, including suggestions for reducing this burden to Department of Defense, Washington Headquarters Services, Directorate for Information Operations and Reports (0704-0188), 1215 Jefferson Davis Highway, Suite 1204, Arlington, VA 22202-4302. Respondents should be aware that notwithstanding any other provision of law, no person shall be subject to any penalty for failing to comply with a collection of information if it does not display a currently valid OMB control number. PLEASE DO NOT RETURN YOUR FORM TO THE ABOVE ADDRESS.												
1. REPORT DATE (DD-MM-YYYY) 23-03-2006		2. REPORT TYPE Doctoral Dissertation			3. DATES COVERED (From — To) Sept 2002 — Mar 2006							
4. TITLE AND SUBTITLE <div style="text-align: center;">Adaptive Illumination Patterns for Radar Applications</div>					5a. CONTRACT NUMBER 5b. GRANT NUMBER 5c. PROGRAM ELEMENT NUMBER 5d. PROJECT NUMBER 5e. TASK NUMBER 5f. WORK UNIT NUMBER 							
6. AUTHOR(S) Phillip M. Corbell, Capt, USAF					8. PERFORMING ORGANIZATION REPORT NUMBER AFIT/DS/ENG/06-02							
7. PERFORMING ORGANIZATION NAME(S) AND ADDRESS(ES) Air Force Institute of Technology Graduate School of Engineering and Management 2950 Hobson Way WPAFB OH 45433-7765					10. SPONSOR/MONITOR'S ACRONYM(S) 11. SPONSOR/MONITOR'S REPORT NUMBER(S) 							
9. SPONSORING / MONITORING AGENCY NAME(S) AND ADDRESS(ES) Dr. Muralidhar Rangaswamy, Senior Electronics Engineer, AFRL/SNHE 80 Scott Drive, Hanscom Air Force Base, MA 01731-2909, (781) 377-3446					12. DISTRIBUTION / AVAILABILITY STATEMENT Approved for Public Release; Distribution Is Unlimited.							
13. SUPPLEMENTARY NOTES 												
14. ABSTRACT The fundamental goal of Fully Adaptive Radar (FAR) involves full exploitation of the joint, synergistic adaptivity of the radar's transmitter and receiver. Little work has been done to exploit the joint space time Degrees-of-Freedom (DOF) available via an Active Electronically Steered Array (AESA) during the radar's transmit illumination cycle. This research introduces Adaptive Illumination Patterns (AIP) as a means for exploiting this previously untapped transmit DOF. This research investigates ways to mitigate clutter interference effects by adapting the illumination pattern on transmit. Two types of illumination pattern adaptivity were explored, termed Space Time Illumination Patterns (STIP) and Scene Adaptive Illumination Patterns (SAIP). Using clairvoyant knowledge, STIP demonstrates the ability to remove sidelobe clutter at user specified Doppler frequencies, resulting in optimum receiver performance using a non-adaptive receive processor. Using available database knowledge, SAIP demonstrated the ability to reduce training data heterogeneity in dense target environments, thereby greatly improving the minimum discernable velocity achieved through STAP processing.												
15. SUBJECT TERMS STAP, FAR, TIPD, Knowledge-Aided, Knowledge-Based, Adaptive Illumination, AESA, radar												
16. SECURITY CLASSIFICATION OF: <table border="1" style="width: 100%; border-collapse: collapse; font-size: x-small;"> <tr> <td style="width: 33%; padding: 2px;">a. REPORT</td> <td style="width: 33%; padding: 2px;">b. ABSTRACT</td> <td style="width: 33%; padding: 2px;">c. THIS PAGE</td> </tr> <tr> <td style="text-align: center; padding: 2px;">U</td> <td style="text-align: center; padding: 2px;">U</td> <td style="text-align: center; padding: 2px;">U</td> </tr> </table>			a. REPORT	b. ABSTRACT	c. THIS PAGE	U	U	U	17. LIMITATION OF ABSTRACT <div style="text-align: center;">UU</div>		18. NUMBER OF PAGES <div style="text-align: center;">166</div>	
a. REPORT	b. ABSTRACT	c. THIS PAGE										
U	U	U										
19a. NAME OF RESPONSIBLE PERSON Dr. Michael A. Temple			19b. TELEPHONE NUMBER (include area code) (937) 255-3636, ext 4279									